University of Twente

Master's Thesis

Towards an integrated Microbiome-gut-brain axis-on-chip platform.

Mariana Garcia-Corral

TNW faculty - Applied Stem-cell Technologies

Exam committee:
Dr. Kerensa Broersen (chairman)
Lena Sohpie Koch MSc (daily supervisor)
Prof. Dr. Loes Segerink (external supervisor)

October 20, 2020

Abstract

Recently, the close and constant dialogue between the brain, gastrointestinal tract, and bacteria residing within it, known as the microbiome-gut-brain axis (MGBA), has been highlighted for its role modulating homeostasis. Animal models are far too complex to accurately analyze the effects of individual MGBA components, whereas current in-vitro models achieve physiologically relevant complexity but still face challenges regarding manipulability and analysis. The main objectives for this master's thesis report were to design and develop a microfluidic platform that enables the compartmentalized culture of various MGBA components ensuring their fluidic communication and recapitulation of the axis' essential elements. Moreover, it was aimed to differentiate enteric nervous system neurons from human embryonic stem cells by adapting and optimizing a previously established protocol. The results obtained in the duration of this thesis include a prototype of the MGBA-on-chip platform which can achieve mechanical deformation, cellular compartmentalization and fluidic communication. Additionally, embryonic stem cells were successfully differentiated into immature enteric neurons responsive to extracellular environment changes. Notwithstanding, further optimization of the microfluidic platform is required to ensure its proper functioning as is further optimization of the embryonic stem cell differentiation protocol to increase induction efficiency. Future work on this project would include full characterization of the microfluidic platform and further maturation and subtype determination for the obtained neurons. The results obtained during this thesis lay the groundwork for subsequent versions of the MGBA on chip platform.

Acknowledgements

Definitely the work in this thesis report could not be accomplished on my own. I would like to thank all the people involved in helping to make this project happen. Firstly, I would like to thank Loes Segerink for finding a project that matched my interest and Kerensa Broersen for giving me the opportunity to work at her lab. Kerensa really made me feel welcome and that I was an important member of the lab. You went out of your way to help in every way and I really appreciate it. My direct supervisor, Lena Koch took the time to teach me step by step at the beginning but also gave me the freedom to make my own decisions during experiments which really gave me the opportunity to grow as a scientist. I really enjoyed being your student and getting to work with you! I would like to thank Pien Goldstein for letting me tag along and learn the ENS induction protocol from her. Also, thanks to Carla Cofiño who taught me how to do flow cytometry and analyze the data. Chip development was really a joint effort with people from BIOS, especially thanks to Elsbeth Bossink who took the time to teach me various protocols, mill early designs for me, and was overall always available. Thanks also to Johan Bomer who was behind the mask and SU-8 mold fabrication for the chips and Masha Zakharova who provided clean room PDMS membranes and bonded them to the chip. I would also like to thank Carlo Paggi for his advice regarding design and mechanical deformation and helping run mechanical deformation tests. These are only a handfull of people that really made a difference during my thesis assignment but there are many more people from AST that helped me out in different occasions. I really loved the environment at AST and feel lucky that I had the opportunity to work among a great group of people. Finally, I would like to thank David for his support and feedback in all stages and taking care of everything else when I was writing non-stop for days.

INDEX

Chapter 1: Introduction to the Microbiome-Gut-Brain Axis

The human gastrointestinal (GI) tract is home to more than 100 million bacteria which are often referred to as microbiota.[1] Despite their large numbers, even small reductions in bacterial diversity (dysbiosis) can alter intestinal or cognitive function.[2] In turn, the central nervous system (CNS) can closely regulate GI function, consequently affecting microbiota homeostasis.[3,4] This mutual relationship and multifaceted communication between the microbiota, the GI tract, and the CNS is recognized as the microbiota-gut-brain axis (MGBA). Due to the complexity of the MGBA, most of its communication mechanisms have only recently begun to be uncovered. Said communication pathways include the autonomic nervous system (ANS), the enteric nervous system (ENS), the neuroimmune system, the neuroendocrine system, and bacterial-derived molecules (Fig. 1).[5,6] This chapter briefly describes each of these communication pathways along with key examples of how they facilitate modulation of the MGBA components.

The ANS consists of enteric, vagal, and spinal nerves to transmit efferent signals from the CNS to the gut and afferent signals from the GI lumen to the brain. Vagal and spinal afferents innervate the GI muscularis and mucosal layers sensing pain, intestinal stretch and luminal nutrients (Fig. 1.1).[7–9] Owing to their lack of direct contact with the intestinal lumen, vagal afferents are considered second-order chemosensory neurons usually relaying signals from the ENS (the GI's intrinsic nervous system) or sensing diffused molecules released from secretory enteric cells.[10] There is ample evidence of the ANS facilitating communication from the gut to the brain resulting in modulation of CNS functions. For instance, vagal γ-aminobutyric acid (GABA) and noradrenaline signaling are triggered by probiotic treatments leading to anxiety and depression-reducing effects.[11] Vagal afferent neuron activity can be increased by some microbiota-derived metabolites[9], whereas dysbiosis can decrease their sensitivity and reduce innervation in the GI epithelium[12] thus hindering ANS-mediated gut-to-brain signaling.

Brain-to-gut signaling takes place through vagal efferent nerves which regulate multiple GI functions such as peristalsis, mucus secretion, epithelial cell proliferation and absorption, using acetylcholine as a neurotransmitter.[13] Vagal efferent signals can have a protective role in the gut against bacterial infections by inducing anti-inflammatory responses and reinforcing tight junctions in the intestinal epithelium.[14] However, stress-induced vagal signaling has also been associated to multiple GI disorders and thought to alter gut motility and induce dysbiosis.[3]

The ENS is also part of the ANS, however it is considered a separate entity owing to its capacity to coordinate with CNS while also being able to act autonomously from any CNS signals to accurately modulate GI function.[15] The ENS is a neuronal and glial network which intimately interacts with the GI epithelium to control exocrine and endocrine secretions, motility and microcirculation.[16] It can be sub-divided into two plexi: the Myenteric and submucosal plexus. These two plexi can interconnect between each other, with extrinsic nervous fibers and with other non-neuronal targets. Myenteric plexus ganglia (Fig. 1.2) are located between the circular and longitudinal muscle layers and coordinate gut motility. Whereas, the submucosal plexus controls the absorptive and secretory functions of the GI and its ganglia are located closest to the mucosa.[17] Even without direct contact, the ENS can also exert modulatory effects on gut microbiota. For instance, changes in host serotoninergic (5-HT) signaling during metabolic syndrome resulted in dysbiosis and changes in bacterial lipid metabolism.[18] Besides its autonomous functions, the ENS can closely interact with the CNS as is in the case in Parkinson's Disease (PD) where GI dysfunction has been shown to precede PD motor symptoms by decades.[19] Animal models have documented profound ENS dysfunction and α-synuclein aggregates (a PD hallmark) before evidence of any other symptoms.[20]

Given the continuous presence of microbiota in the gut lumen, the immune system is essential to establish immune balance for tolerance of commensal bacteria and to protect the body from pathogenic or foreign material invasion.[21] This function is mainly performed by gut-associated lymphoid tissues (GALT), organized collections of immune cells, such as Peyer's patches or isolated lymphoid follicles, consisting of microfold (M) cells, enteric glial cells, macrophages, dendritic cells, T cells, B cells, plasma cells, and mast cells (Fig. 1.3).[22] Neuroimmune crosstalk between GALT and the CNS is largely mediated through neurotransmitters, cytokines and chemokines secreted by immune cells, ENS glia/neurons, or enteric cells in response to inflammatory triggers.[23] In physiological conditions, muscularis macrophages constitutively secrete bone morphogenetic protein 2 which activates enteric neurons to regulate GI motility.[24] In return, enteric, vagal and dorsal root neurons actively modulate macrophages and Peyer's patches in order to limit bacterial invasion and dissemination.[8] On the other hand, bacterial-mediated immune activation in the gut can increase circulating cytokine/chemokine levels and vagal tone resulting in immune cell infiltration into the brain[25] and CNS microglial activation[26]. In situations with constant GI inflammation and dysbiosis, such as

irritable bowel disorders (IBD), there are clear effects on the CNS such as 5-HT imbalances leading to anxiety and depression.[27] In turn, psychological and environmental stressors can also trigger the immune system resulting in IBD-like symptoms and GI inflammation which can alter microbiota composition.[3,28]

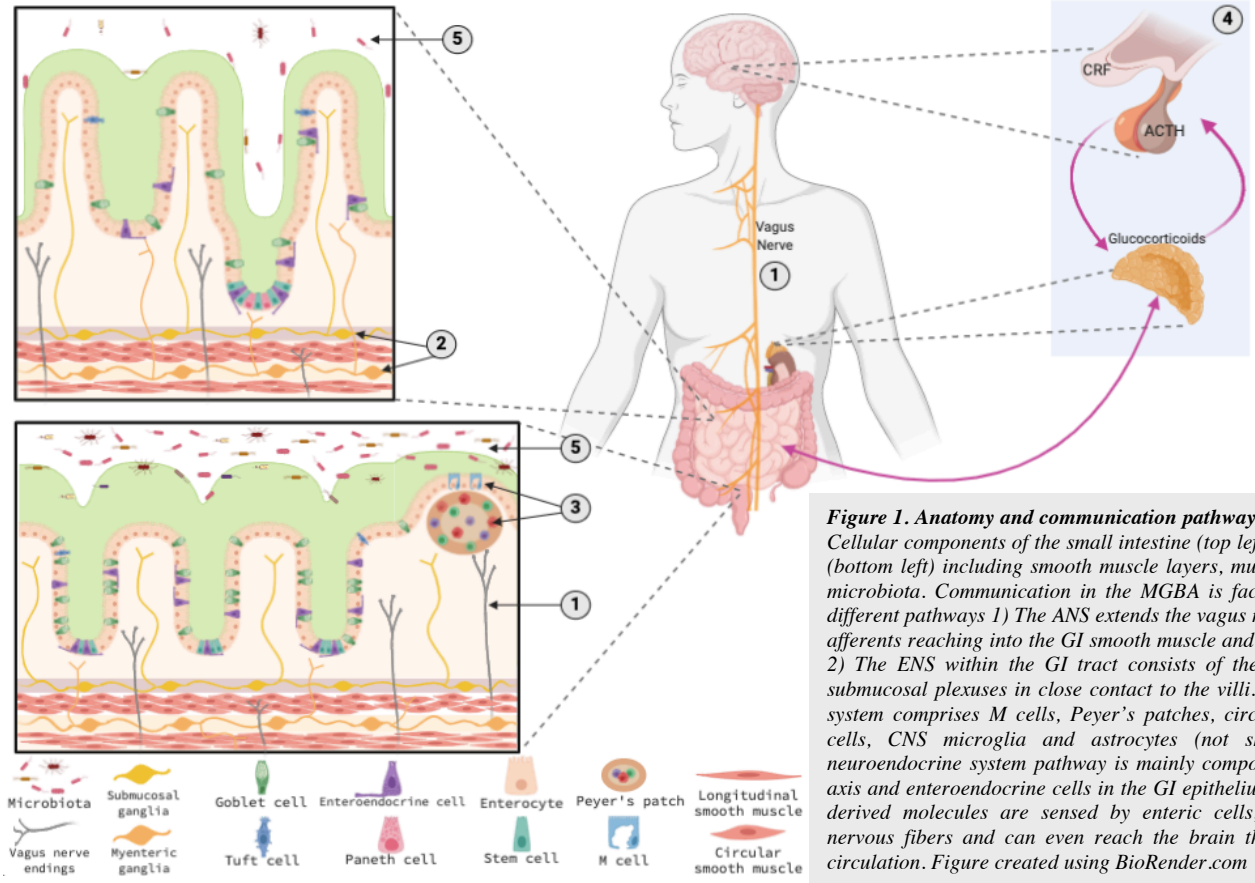

Figure 1. Anatomy and communication pathways of the MGBA. *Cellular components of the small intestine (top left) and the colon (bottom left) including smooth muscle layers, mucus (green) and microbiota. Communication in the MGBA is facilitated through different pathways 1) The ANS extends the vagus nerve and spinal afferents reaching into the GI smooth muscle and mucosal layers. 2) The ENS within the GI tract consists of the myenteric and submucosal plexuses in close contact to the villi. 3) The immune system comprises M cells, Peyer's patches, circulating immune cells, CNS microglia and astrocytes (not shown). 4) The neuroendocrine system pathway is mainly composed of the HPA axis and enteroendocrine cells in the GI epithelium. 5) Bacterial-derived molecules are sensed by enteric cells, immune cells, nervous fibers and can even reach the brain through systemic circulation. Figure created using BioRender.com*

As hinted above, stress modulates the function of different MGBA components and pathways through pro-inflammatory cytokines (IL-6, TNF-α, IL-1β)[28], neurotransmitters (5-HT, GABA, glutamate), and neuropepetides (peptide YY, glucagon-like peptide-1 (GLP-1))[29,30]. These effects of stress are mediated by the main neuroendocrine regulator of the body's response to stress: the hypothalamic– pituitary–adrenal (HPA) axis (Fig. 1.4).[31] In response to stress, the HPA axis produces and secretes corticotropin-releasing factor (CRF) from the hypothalamus which induces the systemic release of adrenocorticotropic hormone (ACTH). Upon reaching the adrenal cortex, ACTH induces the secretion of glucocorticoids, most importantly adrenaline, which reach and modulate different tissues and signal back to the brain in a negative feedback loop inhibiting

CRF and ACTH production.[32] Chronic glucocorticoid receptor (GR) activation in the gut can affect microbiota composition, alter enteroendocrine cell secretions, weaken the intestinal barrier, and cause cortisol resistance in immune cells further exacerbating inflammation and HPA axis activation.[3,33–35] On the other hand, the gut microbiota can shape the neuroendocrine system and is able to acutely activate it. Proof of this was found on mice devoid of any microorganisms (germ-free mice) which upon exposure to stress demonstrated increased CRF expression, elevated ACTH and corticosterone plasma levels, and decreased GR expression in the cortex.[36,37] This exacerbated HPA axis activity could be rescued by colonizing the mice with non-pathogenic bacterial strains.[36]

Enteroendocrine cells (EECs), specialized chemosensory epithelial cells, are the main component of the endocrine system in the GI tract and can be classified into at least eight cellular subsets[38]. EECs directly sense luminal contents and release up to 20 neuropeptides to neighboring or distant targets to modulate their function correspondingly.[39] Importantly, EECs produce 95% of the total 5-HT[39] which is crucially dependent on tryptophan availability. Moreover, specific bacterial metabolites can signal EECs to stimulate or inhibit 5-HT synthesis.[40] Bacterial-infections can disrupt the interplay between different EEC subpopulations and their abundance leading to dysregulation of gastric acid secretion and bacterial-derived gastritis.[41,42] In contrast, EECs can also protect the intestinal mucosa from bacterial inflammation and induce NO production in enteric neurons through GLP-1 secretion.[43,44] Interestingly, in animal models a specific set of ileum bacteria can impair GLP-1-activated gut-brain-mediated control of insulin secretion thus creating a state of GLP-1 resistance.[44] Fast (millisecond) signaling from the gut lumen to the brainstem was discovered through Neuropods, EEC subpopulations that form direct synapse-like connections with vagal afferents.[45] Neuropods can sense luminal sugar and release glutamate into the synapses with vagal neurons to reach the brain in a single synapse.[46]

Finally, the gut microbiota produces a wide range of bacterial metabolites which exert their effects on the various pathways of the MGBA described above, in turn, bacterial activity is responsive to signals conveyed from said pathways (Fig. 1.5).[4] Short-chain fatty acids (SCFAs), bacterial metabolites obtained by dietary fiber fermentation in the GI lumen, are the main molecules involved in microbiota-gut-brain crosstalk.[47,48] SCFAs have been associated with modulation of the different levels of the MGBA: the GI tract (gut motility, mucus secretion, tight junction expression), the immune system (anti-inflammatory cytokine production, CNS microglia maturation), the neuroendocrine system (neuropeptide secretion by enteroendocrine cells, stress

response coordination), and the CNS (satiety, behavior, and psychological state regulation through vagal and spinal pathways). As mentioned above, the gut microbiota can produce a range of neurotransmitters or neuroactive compounds including GABA[11], dopamine, acetylcholine and 5-HT.[4,13] Particularly, tryptophan metabolism and its product, 5-HT, are directly regulated by various bacterial strains.[49,50] Consequently, ENS and CNS development have been intimately related to microbiota composition in early life.[51,52] Dysbiosis-mediated changes in 5-HT signaling have been implicated in irritable bowel syndrome[53], depression[54], metabolic syndrome[18], and autism spectrum disorders[55].

The complex dialogue within the MGBA, the common pathways, and messengers responsible for coordinating organ function and host response have been highlighted throughout this introduction. Current studies that keep finding new cell subtypes, cellular interactions and communication pathways emphasize how much is left to understand about the MGBA and its functionality and show the further need for its study. It is no doubt that new tools and new techniques will be fundamental drivers for research to reach a better understanding of the MGBA in physiology and disease. What is more, the combination of said tools with the acquired knowledge may provide novel therapeutic targets or strategies for disease prevention.

1.1 Thesis framework and outline

The work presented in this master's thesis is focused on the fabrication and validation of a microbiome-gut-brain axis (MGBA)-on-chip platform. Device fabrication was carried out at the BIOS Lab on a Chip group while validation and cell culture experiments were carried out at the Applied Stem-Cell Technologies group, both at the University of Twente in the Netherlands.

Following through this manuscript, Chapter 2 provides an overview of the existing in-vitro MGBA models identifying their main advantages and limitations. Chapter 2 also describes a number of approaches used to functionally characterize in-vitro MGBA models and their various components. Subsequently, Chapter 3 introduces the proposed MGBA-on-chip platform and the limitations it aims to address. It delves on the rationale behind the chip design, fabrication methods and the resulting platform characterization tests. Chapter 4 investigates a different aspect required to achieve an MGBA-on-chip platform: the generation of enteric nervous system-derived neurons

from embryonic stem cells. After a brief introduction of the embryonic ENS development, it discusses the adaptation and optimization of a previously published protocol along with characterization of the obtained cells. Finally, Chapter 5 gives a brief conclusion about the work presented in this report.

Chapter 2. In-vitro MGBA models

The interaction between the components of the MGBA through the different pathways has become more and more evident, however the specific mechanisms that enable this communication remain to be elucidated. Given the multifaceted crosstalk between MGBA components, isolating and identifying specific molecules and pathways becomes highly challenging using animal models. In-vitro approaches have been used as an alternative for decades, owing to their simplified setup, reproducibility, and ease of manipulation.[56] This section delves into the various in-vitro approaches that have been used to model the GI tract and the MGBA, emphasizing organoid and organ-on-chip models.

Transwell® systems (Figure 2.1) are the most widely used setup to model the intestinal barrier. They consist of two stacked chambers (apical and basolateral) separated by a semipermeable membrane that can serve as a culture scaffold for intestinal epithelial cells (IECs) and allows for co-culture of other cell types on the basolateral chamber. Transwell®-based models have contributed invaluably to research regarding intestinal absorption, intercellular crosstalk between MGBA components[57], and pharmacokinetics of drugs[58]. The human cancer-derived Caco-2[56] and HT29-MTX[59] cell lines, used as proxies for absorptive and goblet-like IECs, respectively, are among the best characterized cells used for these system and are often cultured together.[60–62] Despite convenience and robustness of cell lines, they can't faithfully represent the diverse cell composition of the GI tract and the MGBA. To partially address this limitation, co-culture of IECs with other cell types (immune[56,63–65], mesenchymal[66], neuronal[64,67]) and single bacterial strains[68,69] has been implemented and allowed a better understanding of intercellular interactions (Figure 2.1). Primary animal[64] or human[70] cells are also alternatives that provide closer resemblance to in-vivo MGBA cell types, however they are not as easily accessible and expansion and long-term culture remain a challenge.[71] The discovery that LGR5+ stem cells (SCs) could be differentiated into all intestinal epithelial cell types[72] and the successful reprogramming of fibroblasts into induced pluripotent stem cells (iPSCs) with SC-like properties[73] were game-changing tools that made the use of intestinal stem cells (ISCs) more appealing and widespread.

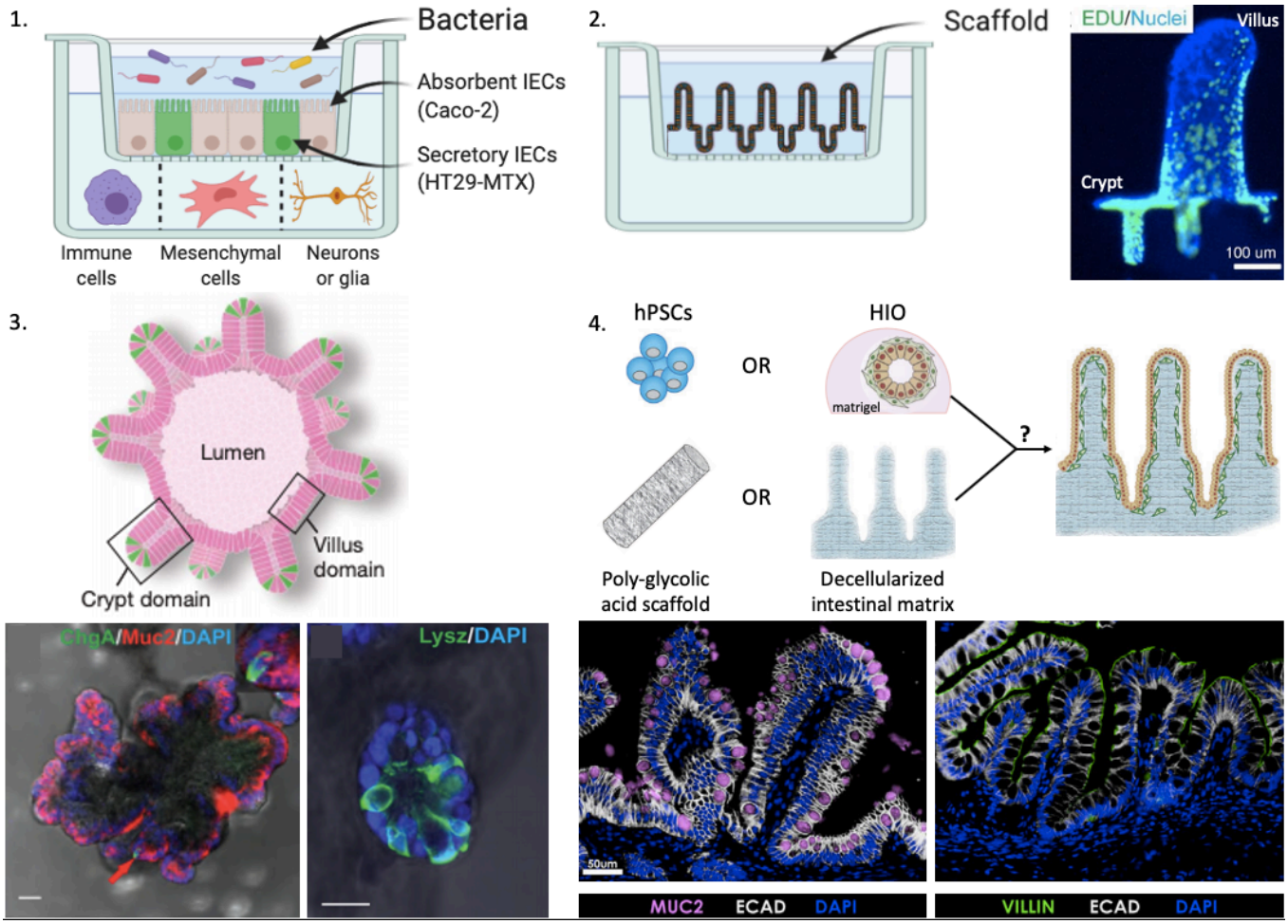

Figure 2. In-vitro models of the MGBA. ***1.*** *Models using Transwell inserts are separated into two chambers facilitating co-culture of IECs with other cell types and bacterial strains.* ***2.*** *Seeding IECs on microfabricated villi scaffolds mounted on Transwell inserts is a way of replicating the 3D topology of the intestinal epithelium and inducing physiological functions closer to the in-vivo gut such as proliferative cells located in the crypts (EDU).*[70] ***3.*** *Intestinal organoids with crypt and villus-like domains can be obtained from animal and human stem cells and express markers for different intestinal cell types such as neuroendocrine cells (ChgA), goblet cells (Muc2), and Paneth cells (Lysz).*[74,75] ***4.*** *Matrices of different origins (synthetic or biologic) have been tested for their ability to sustain and be reseeded by human pluripotent stem cells (hPSCs) or HIO-derived cells and for their capacity to aid them differentiate into an intestinal identity.*[76]

Another limitation of conventional 2D cell culture models is the lack of cellular structural organization, 3D topology of microvilli, or mechanical cues found in the human intestine. An approach to resolve this problem was to develop villi-like, micro-engineered scaffolds which could be seeded with IECs can be seeded and be placed on Transwell® inserts (Figure 2.2).[57,77] Alternatively, the use of ISCs and iPSCs prompted the generation of animal[75] and human[78] intestinal organoids (HIOs), self-organized 3D cellular structures that recapitulate major features of native intestinal epithelium (Figure 2.3).[71] HIOs offer a wide range of advantages such as the ability for self-renewal, expansion, and long-term culture[79], the recapitulation of different intestinal

cell types and villi structure[78], and the ability to use patient derived cells for personalized models[74]. HIOs are not without limitations, given their closed structure, access to the lumen is only available using microinjection needles and shear stress to the lumen cannot be applied.[80,81] Moreover, differentiation protocols yield heterogeneous organoids with medium-to-low efficiencies depending on the cell source and the obtained organoids more closely resemble an immature gut.[68,82] Incorporating HIO-derived intestinal epithelial cells into Transwells® has produced a model with similar cellular diversity to that found in-vivo but also with easy handling and lumen accessibility. Similarly, organoid-derived Transwell® models have been cultured using microengineered scaffolds[76] (Figure 2.4), co-cultured with single bacterial strains, immune cells[83], neurons[84], and myofibroblasts[84]. Further increases in the complexity of organoids by integrating bacteria into the lumen[69,82], adding ENS components[85–87] or reproducing contractility[87] have been accomplished and used to study their contributions on the MGBA. Importantly, robust protocols for obtaining iPSC-derived ENS precursors were published a few years ago[88,89], providing an alternative to the usual isolation of ENS cells from animals[90] and allowing the generation of all-human iPSC-derived HIOs with integrated ENS. Regardless of the advantages of HIOs and their co-culture capabilities, MGBA research still requires reliable and controllable tools to interrogate the function each of its components. To this end, bioengineering, microfluidic, and microfabrication technologies have been combined to create models which offer a controllable and physiologically relevant microenvironment.

Organ-on-chip (OoC) platforms are microfabricated microfluidic devices which aim to recapitulate the essential elements of an organ's functional unit in microscale. OoCs have emerged as the leading alternative to mimic the complex MGBA microenvironment by facilitating luminal access and a finer control of specific parameters such as spatial cellular arrangement[91–93], presence of bacteria[91,94–96], fluid flow[91–93,95,97–101], shear stress[93,97,98,100,101], cyclic strain[95,97–99,101], and oxygen[91,94,96] and molecular gradients[91,99]. Gut-on-chip designs generally consist of media-perfused chambers separated into apical and basolateral compartments by a semipermeable membrane (Figure 3); sometimes they can also include ports to control cyclic strain[95,97–99,101] (Figure 3.1) and even sensors for functional readouts[91,96,102,103] (Figure 3, 2-3). Leveraging the advantages of HIO-derived cells by dissociating them and culturing them in OoC platforms, studies have shown that cells within chips can spontaneously develop into microvilli-like folds[97,99,101], can produce a mucus layer with thickness and bilayer structure[100], and can sustain a complex anaerobe human

microbiome on their surface[96]. Other microfluidic platforms have opted on using synthetic microvilli scaffolds onto which cells are seeded in order to systematically study the contribution of 3D structure on gut cell function (Figure 3.4).[92,93]

Despite this, OoC platforms that incorporate and study the MGBA are still lacking. To our knowledge, there is only one published report of an OoC platform that has studied the gut-brain component of the MGBA.[104] This system modeled four organs- intestine, liver, brain, and kidney in distinct compartments of a chip which were connected by a microfluidic network. While the combination of four organs on chip is a great achievement, the research purpose of the chip was to investigate compound kinetics, as such intercellular communication was limited to paracrine signaling and no other types of stimuli were exerted onto the cells. Accurately replicating the complexity and diversity of the gut microbiota in-vitro remains a great challenge, resulting in models that only co-culture IECs with specifically chosen bacterial strains or isolates from stool samples.[94] A higher degree of microenvironment control (mucus secretion, oxygen & pH gradient, bacterial proliferation, IEC stability) has to be achieved for OoC devices to achieve a diverse bacterial-IEC co-culture. Thus, for studying the role of microbiota in the MGBA, animal-models are still the option of choice.

On the other hand, we have not found any published intestine- or gut-on-chip platform which has included the ENS component of the MGBA. External to OoC platforms, a bioengineered hollow lumen silk scaffolds were first used to create a robust 3D functional human intestinal epithelium[105,106] (Figure 3.5) , and then to create a 3D human-innervated intestine tissue model[107] (Figure 3.6). Despite the inclusion of ENS neurons, this model is comparable to organoids in that it does not allow precise fluidic and mechanical control.

There are currently two proposed OoC projects that include the ENS or the brain: a forum article describing the MINERVA platform[5,108] (http://www.minerva.polimi.it/) and an undergraduate proceedings poster validating enteroendocrine-ENS culture on chip (https://www.northeastern.edu/rise/presentations/gut-brain-axis-on-a-chip-a-microfluidic-model-of-the-enteroendocrine-enteric-nervous-system-interface/). The goal of MINERVA is to develop a multi-organ platform that recreates individual components of the MGBA in-vitro (microbiota, gut, immune system, blood brain barrier, and brain), fluidically interconnects them, and validates oxygen and mass transport among each other. Whereas the proceedings poster aims to model the

interface between an enteroendocrine cell-line and primary ENS-derived neurons in a compartmentalized microfluidic chip.

It is also important to consider the substrate the OoC platforms are made of given that its properties also determine the functionality of the platform. A number of OoC models have made poly-dymethilsyloxane (PDMS) their material of choice for chip fabrication owing to its flexibility, its fast prototyping potential, and accessible microfabrication. However, PDMS can entail limitations when using it to fabricate semipermeable membranes. Commercially available OoC chips use PDMS membranes that are ~10μm thick[109,110] while the in-vivo intestinal basement membrane is in the range of 10's of nm. This discrepancy motivated efforts to fabricate ultrathin PDMS membranes that reach down to 2nm thicknesses.[111,112] However, due to material properties, PDMS films below the μm range are very fragile and usually collapse under the weight of cells.[113] Other materials such as silicon nitride[114] and silicon dioxide (SiO_2)[113] have been used to fabricate ultrathin membranes of just 100 nm thick. However, these stiffer materials hinder peristalsis-like mechanical deformation, which is reportedly essential for proper ISC and microbiota function.[95,98] When choosing membrane materials there is a tradeoff between optical transparency, flexibility, or thickness that has to be considered based on the research question.

Performing live, non-invasive functional readouts in OoCs is feasible using electrodes. In some chips wire electrode probes are manually inserted into the inlet and outlet of the chamber that contains the cells or substance of interest. Although they do not obstruct visualization of the culture surface with optical imaging, the user has to insert and remove the probes every time a measurement is performed, introducing small placement variations that cause noise in the readouts. Alternatively, several OoC designs have integrated sensors into their platforms for in-situ functional readouts. Sensor integration allows continuous and reproducible data collection without inserting foreign objects or manipulating the cells in culture. However, popular electrode materials for OoC platforms with integrated sensors are gold, silver, or platinum alloys which are not optically transparent and wind up blocking the cells for optical imaging.[103] To overcome this issue optically transparent[115] or thin film electrodes[116] have been developed and successfully integrated into OoC devices. Having integrated sensors may open many testing possibilities, however, fabrication of such sensors into the chips often requires clean room facilities, making the process more costly and labor intensive.

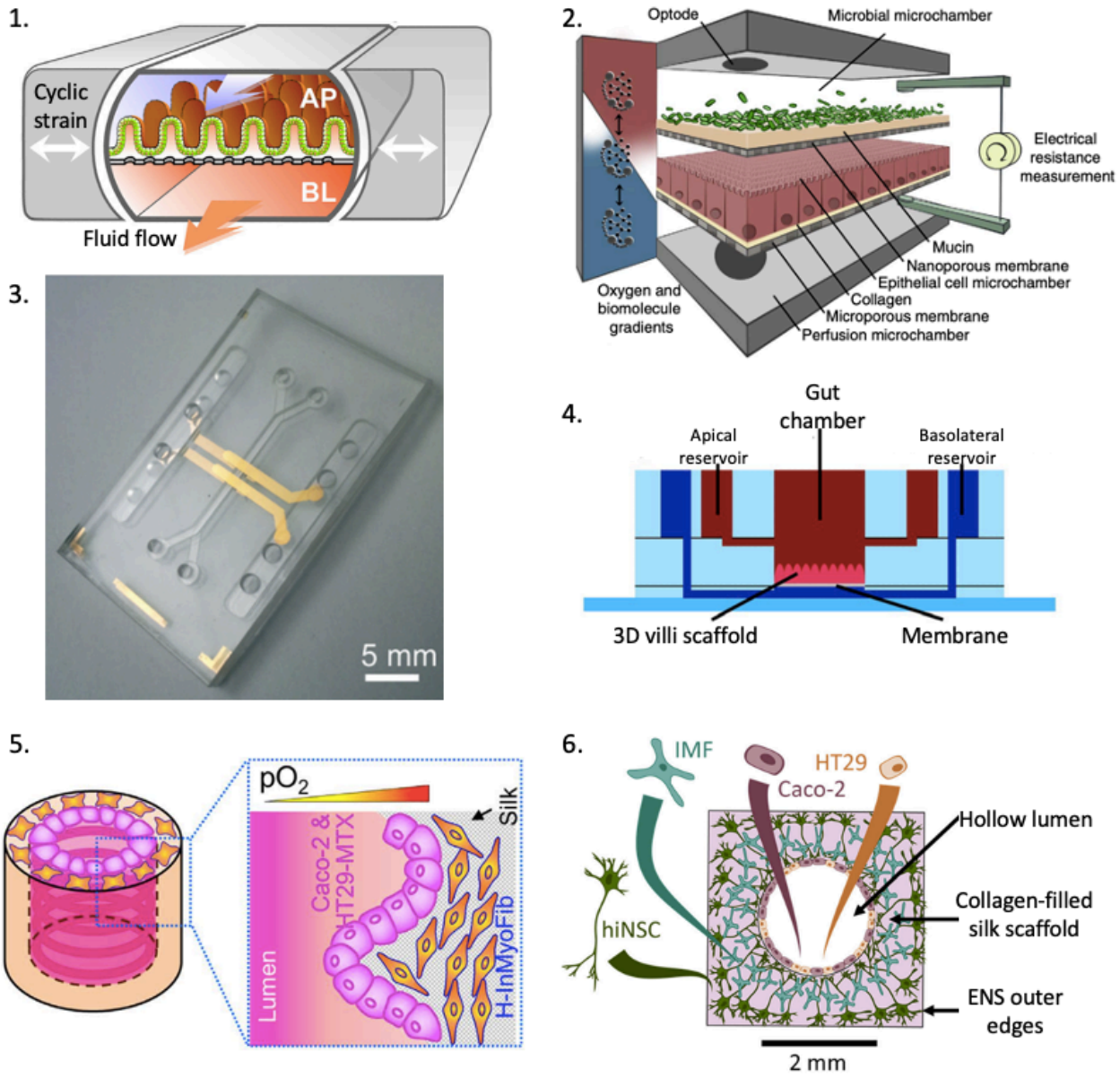

Figure 3. Gut-on chip models and 3D bioengineered intestinal tissue scaffolds. 1. *A microfluidic gut-on-a-chip that enables control of fluid flow, exposure of cells to cyclic strain, generation of molecular gradients, and recapitulates villi-like morphology.*[99] ***2.*** *The HuMiX is a modular microfluidic platform that facilitates the co-culture of bacteria and human intestinal cells while replicating representative oxygen conditions in the human gut.*[91] *It also has integrated optical sensors to measure oxygen concentration and dedicated apertures for chopstick electrodes to measure trans endothelial electrical resistance.* ***3.*** *A similar microfluidic gut-on-a-chip as seen on 1. with integrated thin film titanium-gold electrodes for non-invasive sensing of transepithelial barrier function via impedance spectroscopy.*[103] ***4.*** *A two-chambered microfluidic device that also incorporated a 3D collagen scaffold to mimic human intestinal morphology to systematically test the effects of fluidic shear and 3D topology affect cell function.*[92] ***5****. Bioengineered 3D silk scaffolds with hollow lumen been used as alternatives to OoCs to create functional intestinal epithelium that also mimics in-vivo oxygen conditions.*[105] ***6.*** *Follow-up work on the silk scaffolds involved creating a bioengineered enteric nervous system comprising IECs, intestinal myofibroblasts (IMF) and human induced neural stem cells.*[107]

There are clearly still many challenges to overcome to fully recapitulate the MGBA in-vitro. Thankfully, OoC, bioengineering, and microfabrication fields are still in their early stages and development is fast paced. We hope that, through the use and combination of these technologies, the intricate mechanisms of the MGBA can be better modeled and understood.

2.1 Characterizing the functionality of in-vitro MGBA models

Given the variety of in-vitro MGBA models and their different characteristics, it is important to determine which aspects of the MGBA each platform can recapitulate, to what extent, and how useful it is. The strategies used to qualitatively and quantitatively characterize cellular function within in-vitro MGBA models have been adapted from earlier experimental models, often in-vivo models. This section gives a brief overview of important MGBA characteristics and functions that can be measured in-vitro along with the common assays/technologies which are used to measure them.

Cell differentiation and maturation

As mentioned in previous sections, using ISCs or iPSCs to generate HIOs and obtain ENS-derived neurons allows researchers to recapitulate the cellular diversity of the human intestinal epithelium as depicted in Figure 1. Importantly, HIOs and ENS neurons derived from ISCs or iPSCs are more phenotypically similar to the embryonic intestine rather than the adult one. Consequently, various methods have been attempted to increase HIO maturation such as in-vivo transplantation[117], co-culture with other cell types[86] or continuous passaging[74,78]. Therefore, when using ISCs or iPSCs it is essential to confirm that cells have correctly differentiated into the desired cell type and to determine their maturation stage. A widespread approach is to fluorescently label the cells for specific proteins or genes using antibodies. Immunofluorescent labeling allows the observation of cellular morphology through optical imaging, cell counting using flow cytometry[118], or cell sorting using FACS[79,117,119] (fluorescence activated cell sorting). Figures 2.3 and 2.4 contain some examples of fluorescent images of the different intestinal cell types and structures achieved using HIOs and other platforms. In addition to the qualitative and semi-quantitative data obtained by optical imaging, flow cytometry and FACS provide valuable information regarding the number of total cells and the respective percentages of different cell

subtypes. Despite the widespread use of immunofluorescent labeling, the usefulness of these assays is affected by sample autofluorescence, unspecific antibody binding, leaking of light between fluorophore channels and other factors.[120,121]

Other high throughput assays offer a more comprehensive view of cell differentiation and maturation by evaluating differential gene expression between two or more conditions. Some of these techniques include quantitative reverse-transcription polymerase chain reaction (RT-qPCR)[76,87,105,117], RNA/DNA sequencing (RNA-seq)[88,96,97], and microarrays[73,91,95]. The accuracy and usability of the data obtained from these techniques is dependent on experimental design, appropriate use of controls, number of replicates, statistical algorithms and analysis techniques.[122]

Some of the common proteins and genetic markers used to determine a cell's maturation stage phenotype are shown on Table 1 in the Appendix. Through the combination of data obtained by immunolabeling and gene expression analysis it has become easier to determine the similarity between cells grown in in-vitro models to embryonic or adult intestinal tissue and even to classify them into specific intestinal regions such as the duodenum, ileum or colon.

Intestinal barrier integrity

The GI epithelium acts as a physical barrier to external microorganisms and pathogens, in consequence GI barrier integrity disruption is a key factor in many pathologies.[123,124] Therefore, to determine how closely an in-vitro model recapitulates GI barrier function, it is first necessary to characterize its integrity and its ability to act as a barrier. Labeling tight junction proteins of IEC monolayers using immunofluorescent markers is the standard approach to confirm their expression and visualize their subcellular localization. Appendix Table 1 also includes commonly targeted tight junction proteins of intestinal epithelial cells. Additionally, the strength of the intestinal barrier can be estimated by measuring the fluorescence intensity of the cells. However, the gold standards to quantitatively measure the tightness of intercellular junctions in a cell monolayer are transepithelial/endothelial resistance (TEER) and electric impedance spectroscopy (EIS).[125] TEER/EIS measures the electrical resistance and capacitance across a cell monolayer by using a pair of electrodes (one on each side of the membrane), applying a small, low-frequency alternate current, measuring the resulting voltage, and using Ohm's law to convert it to resistance. In Transwell models, this measurement can be done routinely and non-invasively using chopstick electrodes or commercially available insert adapters. However, as hinted above, performing TEER

readouts on HIOs or microfluidic models can be more challenging. Due to the closed configuration of HIOs, an electrode probe has to be inserted into the organoid to gain luminal access and measure TEER.[126] Alternatively, organoid derived cells are grown into monolayers in Transwells and used for representative TEER measurements.[118] In microfluidic platforms without integrated sensors, electrode probes, similar to those used in HIOs, are placed on each side of the membrane usually through the fluid ports or other adapters.[91,93] Several groups have successfully fabricated chips with embed TEER/EIS electrodes, allowing continuous TEER measurements which are compatible with the micro-meter dimensions of OOCs and their fluid perfusion capacity (Fig. 3).[102,103,127] Moreover, electrodes that measure EIS can be repurposed to monitor a wide variety of other parameters such as ion channel activity, gas concentration, and molecule specific permeability.[127] It is also common practice to observe the actual tight junctions in the intestinal epithelial layer to determine barrier integrity using immunofluorescent imaging.

Intestinal epithelium function

Additional to its barrier function, the GI epithelium also regulates the selective uptake and transport of nutrients and fluid into the body.[124] Thus, after determining intestinal barrier integrity, it is also important to characterize its functionality by measuring different parameters such as permeability, absorption, hormone secretion, and metabolic activity. Such studies are particularly important for drug screening models. The gold standard to measure apparent permeability, is to incubate/perfuse the luminal compartment with tracer molecules of varying molecular weights and then collect the supernatant/effluent of the basolateral compartment to measure the tracer's concentration. Specific transport routes can be examined depending on the molecular weight of the tagged particle. For instance,70 kDa-Dextran is transported via macropinocytosis, while 550 Da-Cascade blue exploits the paracellular pathway.[128] On the other hand, molecules, like Rhodamine 123, can be used to determine efflux permeability by adding them to the basolateral side and collecting from the luminal side.[92,102] A similar problem to TEER measurements is observed when measuring permeability with tagged tracers in HIOs given the lack of luminal access. Whereas in OOC platforms, the low volume requirements can create issues like decreased readout effectiveness due to insufficient volume sample.

Microvilli are an important functional and morphological feature of polarized IECs; they serve to increase cellular surface area, promote maturation, and enable structured organization of

the different IEC types. Optical, fluorescent and scanning electron microscopy are useful techniques to observe the 3D structure of microvilli including the polarized expression of transporters and membrane proteins on their surface.[97,100,117] It is also possible to quantify the relative expression of individual types of polarized transporters using RT-qPCR. Specific transporters largely responsible for nutrient absorption or drug efflux that are often studied using RT-qPCR include peptide transporter 1 (PEPT1)[87,97], glucose transporters SLC5A1 and GLUT-2[93], efflux transporter P-glycoprotein (P-gp)[97,117] and other ABC transporters[87]. Moreover, metabolic hormone[29,43,92,98,117,129], cytokine secretions[43,84,95,117,130,131], and antimicrobial peptides[81,82] of in-vitro MGBA models can be measured through a number of assays including enzyme-linked immunosorbent assay, electrochemiluminescence, bead-based immunoassays, and gene sequencing assays. Enzymatic activity is also often measured by adding the substrate of the enzyme of interest to the culture media in the luminal chamber and measuring the resulting metabolite concentrations.[67,92] Another way to observe the absorptive and secretory function of in-vitro MGBA models is through forskolin-induced swelling (FIS) which demonstrates the function of cystic fibrosis conductance regulator (CFTR), which is essential for fluid secretion in IECs.[87,132] Recently, an electrochemical method to measure permeability was proposed; it consists on integrating electrodes on the basolateral side of a cell monolayer and using them to detect electroactive tracers that have diffused through the monolayer.[116] Finally, RNA-seq[117,118,129] and DNA/RNA microarrays[101,106,117,119] combined with bioinformatic approaches are being used to better observe the differential expression of genes encoding intestinal enzymes and transporters by clustering them in groups with similar functions and expression patterns.

Mucus production by goblet cells is an essential function for MGBA homeostasis. Mucus provides an adhesive and nutritional environment for gut microbiome survival[133], protects the intestinal epithelium from bacteria and pathogens[57,133,134], enables immune crosstalk[21], among many other functions. Secreted mucus has been often observed by histological staining which can detect polysaccharides.[58,61,82,85,117,119,135,136] Recently, mucus accumulation on a colon on chip platform was deduced by observing the increasing opacity of the luminal channel through light microscopy. To confirm this hypothesis, researchers switched to darkfield microscopy, perfused fluorescent beads through the lumen and observed the accumulation of the beads on top of the mucus.[100] Changes in mucin gene and protein transcription levels are also measured[82], however some studies have found that increased mucin transcription did not correlate with increased mucin

protein levels[137,138]. Furthermore, changes in mucus composition and glycosylation in response to different conditions can also be tracked using western blot and anion- exchange chromatography.[137]

Nervous tissue function

The ENS and the Vagus have been previously established as key signaling pathways of the MGBA which can also alter its homeostasis. In-vitro MGBA models which have included nervous tissue have exploited a number of procedures to confirm their cellular identity and to characterize neuronal function. There are several genetic markers for nervous tissue at different maturation stages and even neuron subtype-specific markers[11] which can be measured through fluorescence microscopy, FACS, qRT-PCR, and RNA-sequencing[86,88,139] (Appendix Table 1). Besides genetic expression, the ability of neurons to produce action potentials in response to different stimuli and to communicate with other MGBA components is usually studied. Although the main ions contributing to neuronal action potentials are potassium and sodium, Ca^{2+} changes are also co-factors of membrane potential events.[85] Consequently, calcium imaging is a well-established non-invasive technique that allows the observation of intracellular calcium ion (Ca^{2+}) fluctuations with fluorescent indicators.[10,85] Moreover, excitability changes and neuron-derived intestinal function modulation can be observed through Ca^{2+} by exposing neurons to different stimuli like conditioned media[140], pharmacological agents[86–88], electrical current[86], and light[10,88]. Neuroscientists also measure neuronal activity using micro-electrode arrays (MEAs) which can non-invasively detect single-cell action potentials from a neuronal network with high spatiotemporal resolution. However, despite their commercial availability and widespread use in microfluidic models in neuroscience, MEAs have not yet been adapted into in-vitro MGBA models.[141]

Bacterial viability and function

The essential role that the microbiota plays in the MGBA is increasingly evident. Thus, characterizing bacterial growth, diversity and behavior within an in-vitro model is also fundamental for understanding their interaction with other MGBA components. Given that the vast majority of studies regarding microbiota are performed on animals, some bacterial characterization methods that are used animal models are also mentioned. A common and easy strategy to observe bacteria in a culture is to label them with green fluorescent protein (GFP) plasmids[57,81,82] or to

incorporate fluorescent amino acids into their surface molecules.[96,142] Besides constitutive fluorescence, scanning electron microscopy allows observation of bacteria in higher magnification.[57] Additionally, there are commercially available bacterial live/dead assays to assess viability of gram-negative and gram-positive bacteria.[94] In addition to establishing viability, the number of microorganisms in a region or chamber can be determined by collecting media samples or cell lysates and directly measuring their optical density or spreading them and culturing them on agar plates for subsequent counting of bacterial colonies using quantitative colony forming unit (CFU) analysis.[65,81] Using agar plates is also useful because it allows the identification of bacterial groups by colonial and cellular morphology, gram staining, spore formation, and aerobic and anaerobic growth.[41] Additionally, genetic sequencing techniques such as RT-qPCR[26,50] and 16S rRNA/DNA[2,40,55,96] are popular tools to study bacterial phylogeny and taxonomy and to study differences in microbial communities between experimental conditions. Testing for catalase, oxidase, and coagulase activities is also a useful and time efficient method for differentiating between bacterial strains and taxa compared to the previous agar plate and molecular genetic techniques.[143] Finally, it is also possible to determine bacterial metabolic and secretory activity such as enzymatic breakdown of known substrates[50,98], production of SCFAs, and secretion of endotoxins[64].

Microenvironment

Apart from all the cellular components, the microenvironment within the GI lumen is also crucial for ensuring MGBA homeostasis. A steep oxygen concentration gradient from the GI lumen to the epithelium enables survival of strict anaerobic bacteria on the lumen while also facilitating enterocyte survival on the epithelium. For this reason, several MGBA models have used implantable probes[82], microfluorometric nanoparticles[94], or integrated electrodes[96,106] to detect changes in oxygen concentration. There is also a gradual pH increase from the proximal to the distal end of the GI tract that influences bacterial and cellular function within the MGBA. Consequently, intracellular and luminal pH changes have been measured using electrodes[132] or pH-sensitive fluorescent molecules[144–147].

Overall, this section has reviewed fundamental components and functions within in-vitro MGBA models and the common strategies used to characterize and quantify them. Moreover, these

techniques are also helpful to study the interaction between MGBA components and their response to different stimuli. A more comprehensive understanding of how closely in-vitro MGBA models resemble in-vivo physiology will help identify areas of opportunity and unmet needs for in-vitro models.

Chapter 3. A novel MGBA-on-chip

Once the dynamic nature of the MGBA has been described and the state of the art for in-vitro MGBA models has been reviewed, we can introduce a novel platform that doesn't shy away from the complexity of the MGBA and addresses some of the limitations of current models. This chapter introduces the novel MGBA-on-chip platform. Ultimately, the goal of this microfluidic platform is to provide a robust and controllable environment that enables the simultaneous culture of various MGBA components and that facilitates the study of their interaction. Within this chapter, the design requirements, device materials, and fabrication methods will be discussed.

3.1 MGBA-on-chip design, material, and fabrication rationale

Considering the microenvironment of the MGBA and the constant interaction between all its components, a microfluidic platform for an in-vitro MGBA model should take into account the following design requirements:

- Employing a substrate that allows cell attachment.
- Providing adequate oxygenation, nutrient delivery, and waste removal.
- Sustaining long term culture of multiple cell types.
- Achieving cellular compartmentalization while ensuring intercellular crosstalk.
- Facilitating the localized delivery of (bio)chemical cues to cells within a determined compartment.
- Having dimensions that allow the organization of cells into 3D intestinal structures.
- Exerting physiologically relevant fluid shear stress and cyclical deformation.

The proposed MGBA-on-chip platform aims to reproduce the gut-brain communication pathway via the enteric nervous system. With this in mind, the platform contains three distinct and fluidically communicated compartments that help ensure the simultaneous and compartmentalized culture of IECs, ENS-derived neurons, and CNS-derived neurons (Figure 4). This chamber circuit is designed to allow individual nutrient perfusion to each chamber while ensuring intercellular communication between chambers. The gut and ENS compartments are stacked upon each other, separated by a thin and porous PDMS membrane that allows paracellular communication and ENS

axon infiltration into the gut epithelial layer (Figures 4.1-4.4). The CNS compartment, located at the center of the chip, is linked to the ENS compartment by a microchannel array. The microchannels facilitate synapse formation between neurons in both chambers (ENS & CNS) by guiding axonal growth while keeping out the neuron's soma.

In addition, the MGBA-on-chip aims to recapitulate the cyclical mechanical stress exerted on IECs in-vivo and to achieve a uniform stress distribution on the cells. The design features that ensure this result include a flexible substrate, the overall circular design of the chip, and the two curved vacuum chambers at the outer edges of the chip in close contact with the main channel (Figure 4.4). When activated, the vacuum chambers pull on the exterior wall of the gut and ENS chambers to exert radial mechanical stress. This is particularly different to other gut-on-chip designs with straight compartments (Figure 3.1) that only exert uniaxial stress.

Within the MGBA, the different components experience varying amounts of shear stress: IECs experience the most stress due to the transport of liquids and fecal matter whereas the ENS and the brain only experience minimal shear stress due to interstitial flow. To ensure that the brain compartment receives the least amount of shear stress, it is separated by membrane to the fluid perfusion channel. Due to the large diameter of the brain chamber it was necessary to add micropillars to ensure the structural support of the membrane and prevent it from collapsing. Moreover, fluid shear stress can also be controlled by tuning the microchannel dimensions, this will be discussed in more detail below.

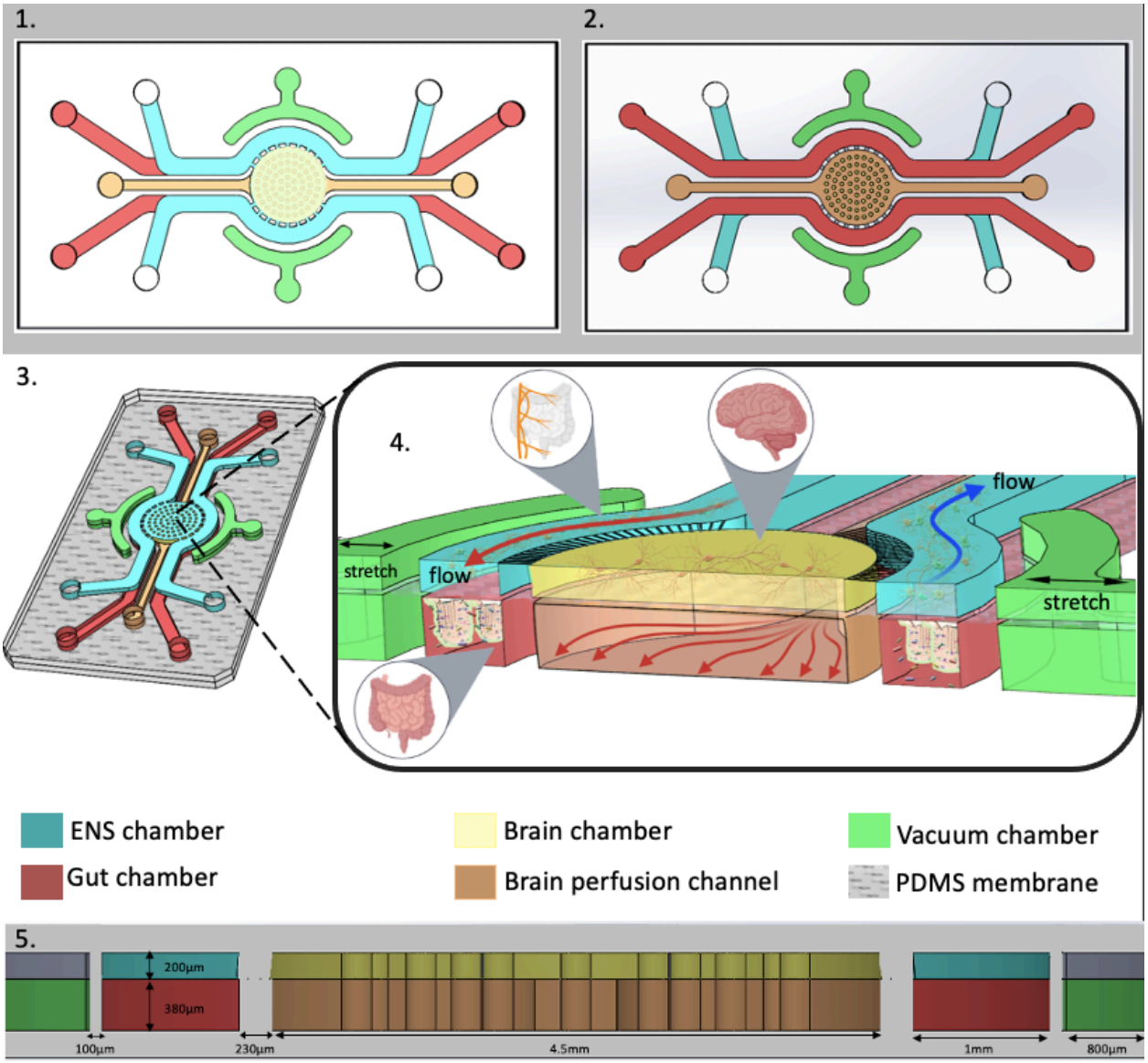

Figure 4. Novel MGBA-on-chip. ***1.*** *The top view of the MGBA-on-chip shows the ENS (blue) and Brain (yellow) chambers connected by microchannel arrays.* ***2.*** *The bottom view of the MGBA-on-chip shows the Gut chamber (pink) and the Brain perfusion channel (orange). The layers are separated by a porous PDMS membrane and their outer edges are surrounded by Vacuum chambers (green) which apply cyclic strain.* ***3.*** *Perspective view of the assembled chip.* ***4.*** *Schematic overview of the MGBA-on-chip including microvilli structures in the Gut chamber, ENS derived neurons and glia in the ENS chamber, and CNS neurons in the Brain chamber. The schematic shows a counter-flow perfusion where the gut channels are flowing in opposite directions to optimize inflow to the brain chamber through the microchannels. 5. Cross section at the center of the MGBA chip demonstrating the most relevant dimensions of the chip.*

Once the general chip layout and design requirements are taken into account, it is time to consider the chip's material and fabrication techniques. According to the dimensions and complexity of the chip design, there will be a more suitable fabrication method. Likewise, the

fabrication method will also impose design restrictions depending on its resolution capabilities. Moreover, the physical properties of the chosen material can entail thickness limitations and help determine the proper fabrication techniques. Taking all these factors into consideration, the design of the chip was done using SolidWorks software (Dassault Systèmes SOLIDWORKS Corp.) and a combination of fabrication techniques were chosen to create the MGBA-on-chip platform. Detailed schematics of the chip designs with dimensions can be found on Figures 1 and 2 of the Appendix.

The material of choice for the MGBA-on-chip is PDMS. This material is optically transparent, which facilitates in-situ imaging; flexible, enabling peristalsis-like movement; highly biocompatible, ensuring cell survival; and is versatile to different microfabrication techniques. Some alternative materials which can also be used for these types of platforms are Cyclic olefin copolymer (COC), Poly(methyl methacrylate) (PMMA), or Polycarbonate (PC). However, for the purpose of our chip these materials are too stiff to apply cyclic strain using a vacuum pump.

To fabricate PDMS chips using soft lithography, it is first necessary to make master molds with the positive stamp of the channel designs. The following sections describe two different approaches to fabricate the master molds: one that is fast and clean room-free, and another that requires clean room facilities and consequently is more costly and time consuming.

3.2 Master mold fabrication

Micromilling

Micromilling was used to create chip master molds that did not require clean room facilities. Using SolidWorks software, a milling path is programmed to reproduce a positive channel topography of the chip's CAD design. Then, a 200μm drill bit mills PMMA slabs to obtain the top and bottom master molds.

SU-8 wafer fabrication

Fabrication of the master molds on a silicon (Si) wafer with positive channel topographies was done by photolithography, as illustrated in Figure 5. Briefly for the top layer, silicon wafers were primed with hexamethyldisilazane (HMDS) to create a hydrophobic surface followed by spin-coating a layer of positive photoresist AZ® 40XT at a layer thickness of 3 μm (Figure 5.1). Then, the wafer was soft baked at 126ºC for 7 minutes. The Si wafer was exposed trough a high-

resolution transparency mask containing the microchannel array pattern and alignment marks for 30 s at 200 W (Figure 5.2). Subsequently the wafer was developed with PGMEA (photoresist developer) for 30 s, followed by two or three more washes with fresh PGMEA solution (Figure 5.3). After drying with inert pressurized gas, a second layer of photoresist was spin coated onto the wafer with a layer thickness of 200 µm (Figure 5.4). Then, the wafer was soft baked again at 126ºC for 7 minutes. A high-resolution transparency mask containing the larger channel and chamber pattern was aligned to the microchannels patterned to the wafer. Next, the wafer was exposed for 2 min at 200 W (Figure 5.5) and baked for 5 min at 90ºC. The wafer was developed with PGMEA for 5-10 min, rinsed three times with fresh developer and dried using pressurized inert gas (Figure 5.6). A similar process was followed for the fabrication of the bottom master mold excluding the first patterning step for the microchannels. Both SU-8 master molds were treated with FDTS for anti-stiction purposes.

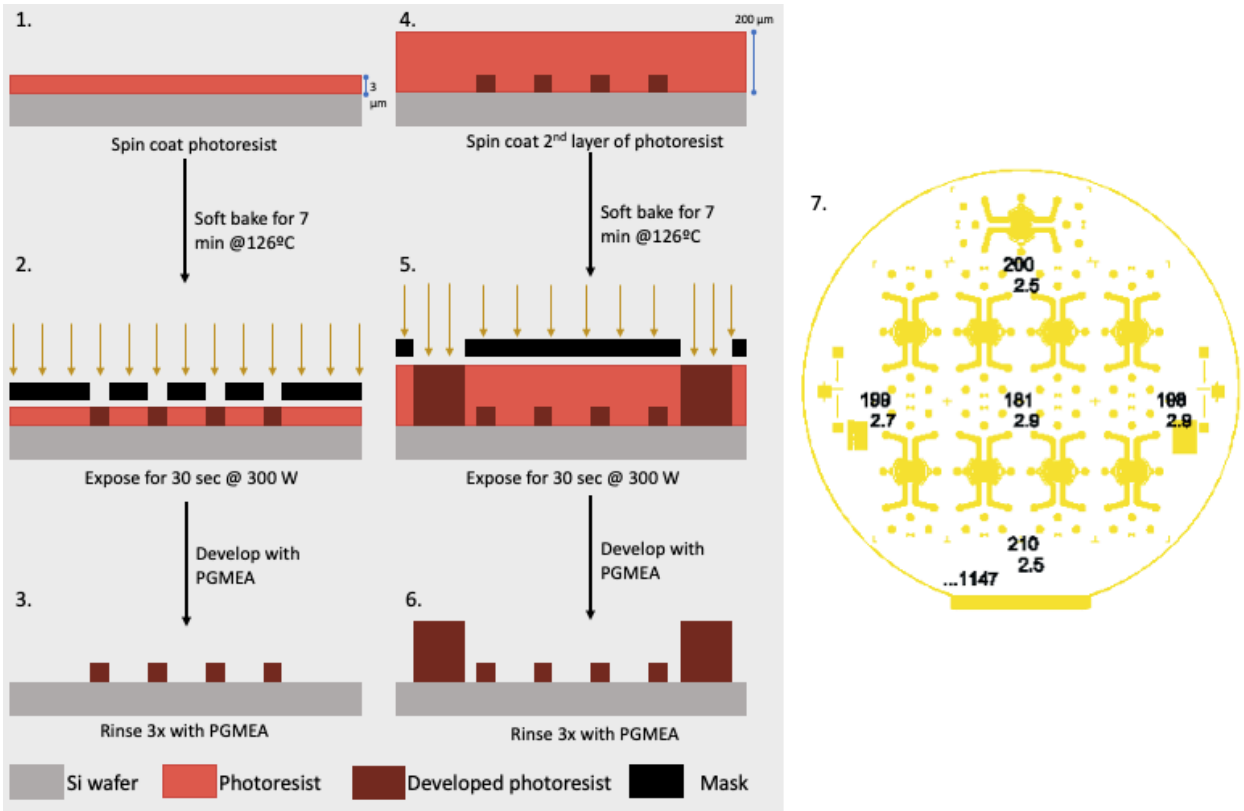

Figure 5. *Fabrication process of SU-8 master molds. A 3µm thick photoresist (PR) layer is spin coated onto an Si wafer* ***(1.)*** *followed by a brief UV-light exposure through a mask* ***(2.)*** *and resulting in a microchannel pattern after development* ***(3.)****. A thicker 200µm layer of PR is spin coated on the patterned Si wafer* ***(4.)****, subsequently exposed again to UV-light through a different mask* ***(5.)*** *and developed to finally reveal the top layer chip layout* ***(6.)****.* ***7.*** *Actual heights of both layers of the fabricated SU-8 top master mold.*

3.3 Membrane fabrication

Regarding fabrication of the PDMS membrane, the BIOS lab-on-a-chip group has previously developed and optimized different methods to produce molds for these membranes. These methods will be briefly described below but more information about their fabrication process can be found elsewhere.[148]

SmoothCast membrane

PDMS membranes were fabricated using a SmoothCast master mold patterned with micropillars 10µm in diameter and 30µm in height (Figure 6). First, a solution of 8% polyvinyl alcohol (PVA) was spin coated onto a thick (5mm) cured 15:1 PDMS slab and briefly baked at 120ºC. Freshly prepared uncured 10:1 PDMS was spin coated on top of the PVA, aligned with the SmoothCast master mold, pressed together with 1-3 kg weights, degassed, and cured for 1 h in a 60ºC oven. Once cured, the SmoothCast mold with the PDMS membrane and the PDMS slab were separated by placing under running DI water to dissolve the PVA and drying with nitrogen gas. This yielded a SmoothCast with a PDMS membrane that was ready to be plasma treated for integration into a chip.

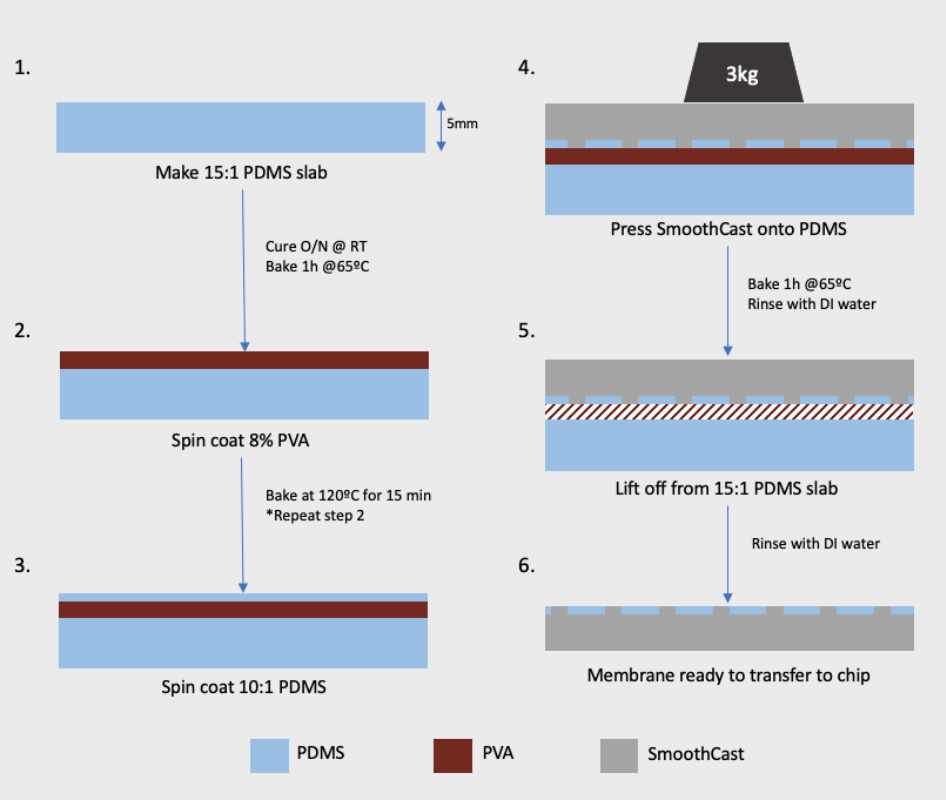

Figure 6. *Fabrication process of a PDMS membrane using SmoothCast molds. A 5mm thick 15:1 PDMS slab is prepared and cured* ***(1.)*** *A thin layer of 8% PVA is spin coated on it and baked, this process is repeated once more* ***(2.)****. Freshly prepared 10:1*

PDMS is spin coated on the slab ***(3.)*** *and the SmoothCast is aligned and pressed onto the PDMS* ***(4.)****. Once cured the PVA is rinsed off with DI water* ***(5.)*** *and the 15:1 PDMS slab can be lifted off leaving the SmoothCast with the PDMS membrane ready to be transferred* ***(6.)****.*

Clean room membrane

Thin PDMS membranes with 5µm diameter pores were obtained from BIOS following the protocol published by BIOS[148] and summarized in Figure 7. Briefly, a positive photoresist (AZ9260) layer was spin coated on a Si wafer to a thickness of 10µm and soft baked for 2 min at 110ºC. Next, a mask containing an array of 5µm pores was aligned on top of the wafer and exposed to UV light at 12 mW/cm^2 for 17 seconds. Wafers were left to rest for an hour posterior to exposure to reduce bubble formation. Once this incubation time was over, the wafers were soft backed at 120ºC for 2 min followed by PR development for 6 min resulting in a mold with micropillars. Next, a solution of PDMS at a 10:1 ratio was diluted with hexane at a 2:5 (PDMS:hexane) ratio to achieve a lower viscosity. This solution was spin coated onto the micropillar mold and baked at 60ºC for at least 3h. Finally, to ensure the porosity of the membrane, there is a final reactive-ion etching process of 2 min applied to the cured PDMS. This process results in a membrane that can be transferred to a PDMS chip by oxygen plasma treatment and later dissolving the sacrificial photoresist layer with acetone.

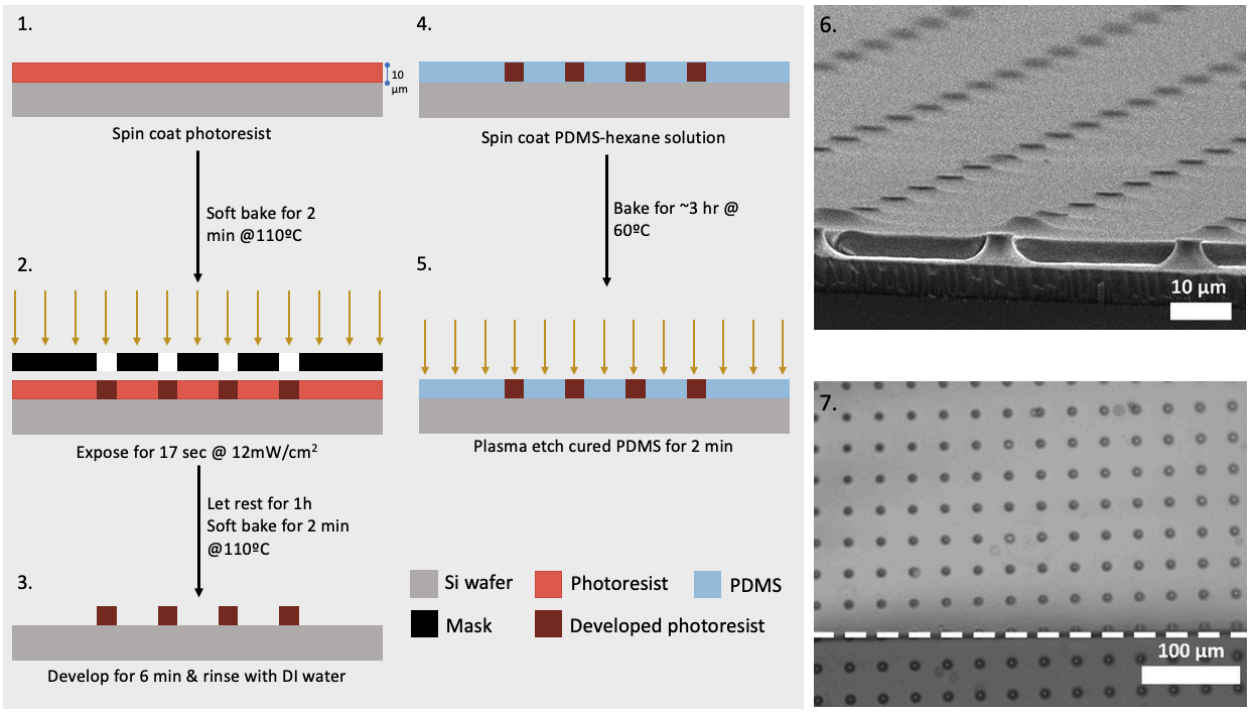

Figure 7. *Clean room fabrication process of PDMS membrane. A positive photoresist is spin coated on an Si wafer* ***(1.)*** *and subsequently exposed to UV-light through a patterned mask* ***(2.)****. The photoresist is then developed* ***(3.)****, a PDMS-hexane solution*

is spin coated on the wafer ***(4.)*** *and cured for 3 hours in the oven. Finally, to ensure porosity of the membrane, the cured PDMS is briefly plasma etched* ***(5.)*** *resulting in a membrane ready to be transferred onto a chip.* ***6.*** *A scanning electron micrograph of a PDMS coated photoresist column array. Reproduced from reference* [148] ***7.*** *A transferred membrane on a chip. Reproduced from reference* [148].

3.4 Chip casting and assembly

To produce the top and bottom layers of the chip that have high deformability, 20:1 PDMS was prepared, cast on the respective mold for each layer, degassed for at least 1h, baked at 65ºC for 1-2 hours (or overnight), and peeled off from the molds upon curing. The holes of inlets and outlets of the top and bottom layers were added using a 1mm hole puncher. For chip assembly, the top chip layer and either the SmoothCast or clean room PDMS membrane were treated with oxygen plasma for 40 seconds at 50W. Immediately after, the treated side of the device layer was placed on the PDMS membrane, pressed gently with a roller, and baked for 15-30 min in a 65ºC oven. Following this, the top layer with the integrated membrane was carefully peeled off and rinsed with acetone in the case of the clean room membrane. Subsequently, holes through the membrane were made for the bottom layer ports using a 1mm hole puncher. Finally, the top and bottom layers were treated with oxygen plasma for 60 seconds at 50W, aligned, pressed together with a roller, baked for 45 min at 65ºC, and examined under a microscope.

3.5 Mechanical and fluidic validation

Finite element modeling of fluid flow

Visualization of pressure and velocity within the different compartments chip is important to assess fluidic communication between the chambers and to determine the stresses cells will be exposed to. Given that the CAD design was made using Solidworks, it was convenient to also use its computational fluid dynamics package “Flow Simuation” to model the fluid distribution within the chip. For the simulation, fixed water density and viscosity values at 37ºC were selected and a both side channels were set to flow in the same direction. Gut inlets were established to have a constant mass flow rate of $1.096*10^{-8}$ Kg/s (60µL/h), ENS inlets were set at $8.23*10^{-9}$ Kg/s (30µL/h), the Brain perfusion channel was set at $5.49*10^{-9}$ Kg/s (20µL/h), and outlet ports were set at atmospheric pressure. Pressure, velocity and shear stress were then plotted.

Cell shear stress

As mentioned previously, cells within the MGBA are exposed to different magnitudes of shear stress, thus the MGBA-on-chip platform should also aim to recapitulate these conditions to achieve physiological relevance. To determine the wall shear stress in the different channels following equation can be used:

$$Eq.1 \qquad \tau_{wall} = \frac{6 * Q * \mu}{h^2 * w}$$

Where Q is the volumetric flow rate, μ is the viscosity of the medium, w is the width of the channel, and h is the height of the channel. Moreover, Gaver and Kute[149] previously determined the relationship between cells adhered to the bottom of the channel and wall shear stress to be approximated by:

$$Eq.2 \qquad \tau_{cell} = 3 * \tau_{wall}$$

Microchannel diffusion

Ensuring the diffusion of growth factors and other paracrine molecules between the ENS and brain chambers is also essential for cell interaction studies. Relevant growth factors that could be exchanged between the chambers, like GDNF and BDNF, are within the range of 10 to 140kDa, due to this 40kDa FITC-dextran was chosen as the paracellular diffusion marker. For better observation of diffusion between ENS and brain chambers, a top layer of the chip bonded to a glass coverslip was used for the experiment. Before adding the fluorescent molecule, all chambers were filled with PBS and a pre-cut 200μL pipette tip filled with approximately 20μL was inserted on the main ports. Next, 150μL of 40kDa FITC-dextran solution at a concentration of 1mg/mL (25mM) was added to one of the ENS inlet ports. Once the fluorescent solution was uniformly distributed in the channel images were taken every 10 seconds for 12 minutes. Fluorescence intensity of the brain compartment was measured using ImageJ software and normalized to the intensity measured on the ENS compartment. To obtain the flux of dextran into the brain chamber Fick's first law of diffusion was applied:

$$Eq.3 \qquad J = -D\frac{d\varphi}{dx} = -D * \left(\frac{c_1 - c_0}{x_1 - x_0}\right)$$

This equation postulates that flux (J) goes from regions of high concentration to those of low concentration at a rate dependent on the magnitude of the concentration gradient (dφ/dx) and

the molecule's diffusion coefficient (D). For flux calculations a diffusion coefficient of 44.7μm^2/s for 40 kDa FITC-dextran was considered.[150]

Mechanical deformation

Throughout chapters 1 and 2 the importance replicating the gut microenvironment, including peristalsis motion, was highlighted. Ensuring that the MGBA-on-chip can exert cyclic mechanical deformation is an important component to expose cells to peristalsis-like motion. Assembled chips were mounted on an inverted microscope, the vacuum chambers were connected to the Fluigent vacuum system, 300 mbar of vacuum were applied to either one or both vacuum chambers, and images were taken.

3.6 Chip fabrication and validation results and discussion

From the different fabrication methods, we obtained two versions of the MGBA-on-chip platform: a "rough" version that has larger than desired features (Figure 8), and a "clean" version that contains the dimensions according to the design requirements (Figure 10).

The "rough" MGBA chip was obtained by clean room-free methods which include casting PDMS onto the micro milled master molds (Figures 8.1 and 8.2) and transferring the thick SmoothCast PDMS membrane onto the chip (Figure 8.4). As mentioned above, each fabrication technique imposes different limitations on the design. One of the most notable limitations was the low resolution achieved by the 200μm drill. This can be appreciated by the large gaps replacing the microchannels that connect the ENS and brain chambers and the increased wall thickness between the gut chamber and the vacuum chamber (Figures 8.3 and 8.5).

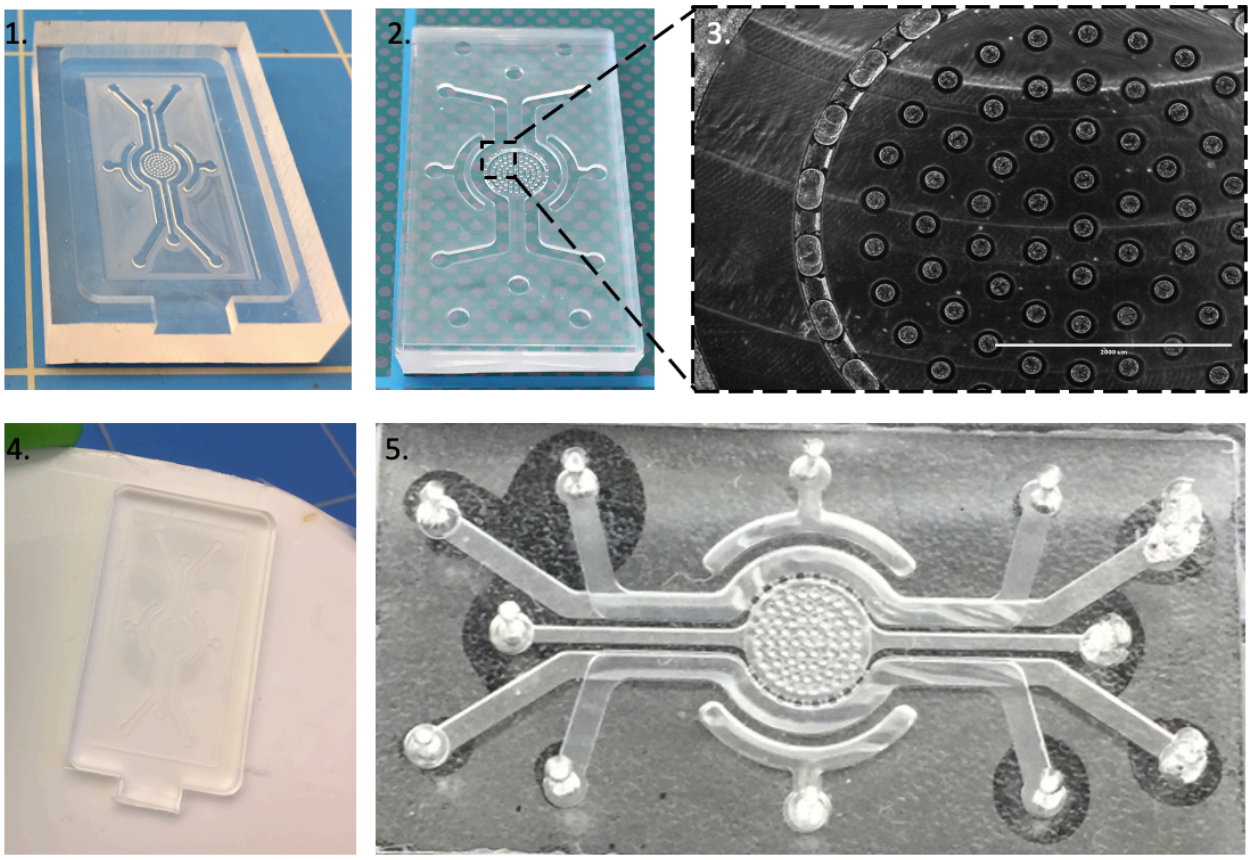

Figure 8. *Clean room-free MGBA-on-chip fabrication results.* ***1.*** *Micro-milled master mold of the bottom layer.* ***2.*** *Bottom layer of the chip made by soft lithography.* ***3****. Closeup of the top chip layer showing "channels" connecting the ENS and brain compartments that are approximately 200µm wide and not useful for cell isolation. Scale bar 2,000µm.* ***4.*** *Process of transferring the PDMS membrane from the SmoothCast mold onto the chip.* ***5.*** *Fully assembled chip showing an uneven membrane on the microchannels.*

The large dimensions of the channels connecting the ENS and brain compartment render their purpose obsolete given that they cannot isolate the two chambers. Fabrication of PDMS membranes with the SmoothCast also yielded sub-optimal results. Initial attempts to replicate the established protocol at AST facilities resulted in imperfect membranes that adhered more tightly to the SmoothCast than to the plasma treated chip and thus yielded chips without a membrane. Further attempts to make the membrane were performed at BIOS facilities under supervision of BIOS staff, however the problem of attachment to the SmoothCast persisted. There is, perhaps, a key step or technique in the protocol that has not yet been identified that could affect the outcome of the membrane and is affecting the replicability of membrane. Considering that the main issue is the surface attachment to the SmoothCast, it might be useful to test how environments with different humidity affect membrane transfer. Going forward in the project, the SmoothCast membrane was fabricated and transferred to the chips by BIOS staff. Thereon, membrane

transferer was successful, but membrane attachment to the SmoothCast persisted, producing microchannels with an uneven membrane (Figure 8.5). Surprisingly, notwithstanding the increased thickness between the vacuum chamber and the gut chambers (500μm), when vacuum was applied, deformation of the could still be observed (Figure 9). This can be attributed to the high deformability of the 20:1 PDMS chip and to the proper bonding of the top and bottom layers between the vacuum chambers. Unfortunately, quantification of the deformation could not be performed owing to the chip's rugged membrane. Applying vacuum did stretch the membrane, but not to a degree that the pores were significantly deformed.

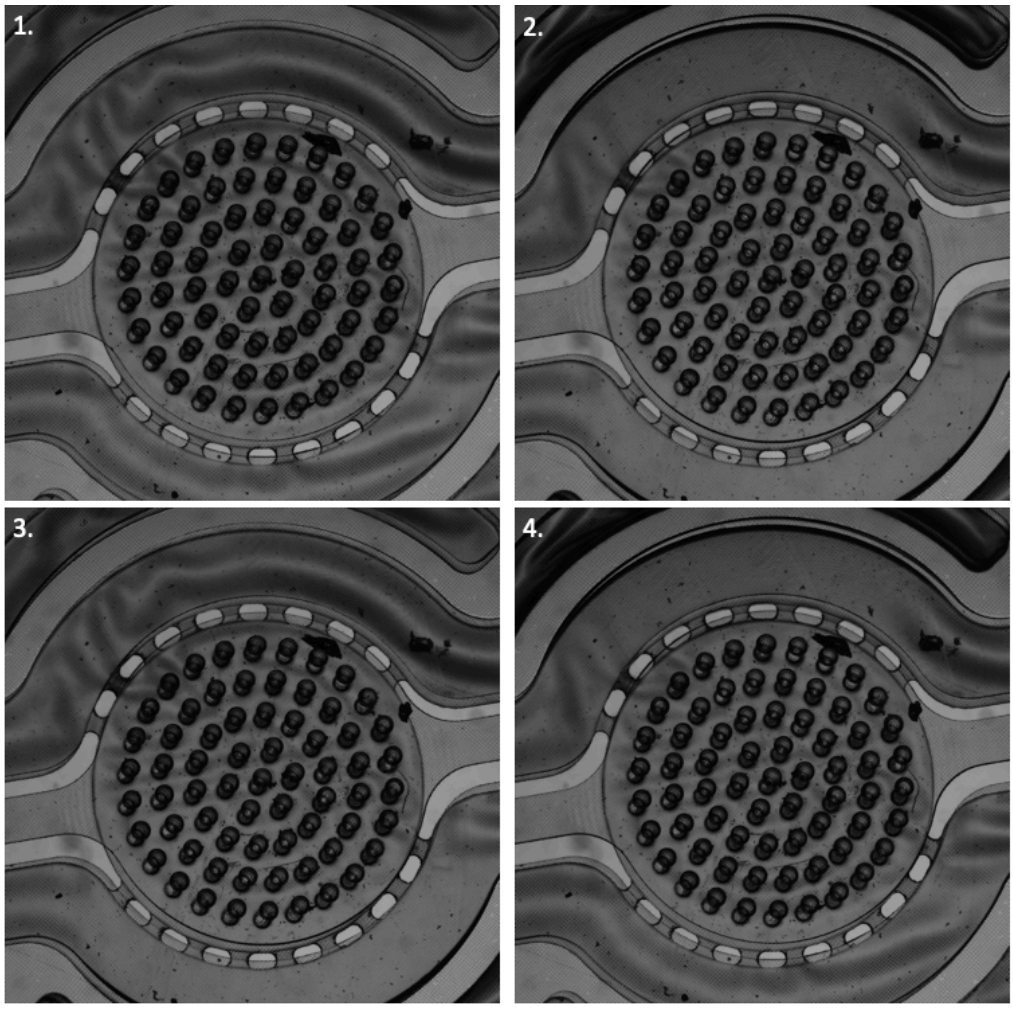

***Figure 9**. Mechanical deformation test on "rough" MGBA chip. **1**. View of the chip without any vacuum chamber activated. **2**.View of the chip with both vacuum chambers activated, a stretching of the membrane on both sides can be observed. **3.** View of the chip with the bottom vacuum chamber activated. **4.** View of the chip with the top vacuum chamber activated.*

The MGBA chip obtained from clean room fabrication techniques is shown in Figure 10. Clean room fabrication allows for small dimensions with high precision as can be observed from the microchannels connecting the ENS and brain compartments, the thin wall between the vacuum and gut chambers, and the thin PDMS membrane (Figures 10.2-10.4). It is important to note that all the clean room fabrication was performed by BIOS staff due to lab access restrictions. An advantage of having clean room fabricated PDMS membranes is that a 2μm thickness can be achieved. This effectively reduces the distance between IECs and ENS-derived cells which can improve intercellular communication and axonal infiltration into the gut channel. Nevertheless, there were occasional issues when transferring the PDMS membrane onto the chip where the membrane caved down and attached to the horizontal wall of the microchannel (Figure 10.4). PDMS membranes with 10μm thicknesses or less have lower structural stability due to the material's properties which makes them prone to collapsing in wide microchannels or due to the weight of the cells. Of the 5 chips that could be fabricated this way, n=2 had a partially collapsed membrane which affected the chip's perfusion functionalities. On the other hand, a couple of drawbacks that arise from having small wall spacing between chambers are the reduced surface area for the membrane to attach and the need of a much more precise alignment when bonding. A combination of these two issues can result in connected vacuum and gut chambers, making cyclical deformation impossible. Of the chips which did not have a collapsed membrane (n=3), only one of them had a proper alignment and bonding between the chambers that allowed observation of mechanical deformation of the membrane (Figure 11). On Figures 11.1 and 11.2 it can clearly be observed how the vacuum chamber compresses and the gut chamber is stretched out. Upon closer inspection in Figures 11.3 and 11.4, deformation of the pores can be appreciated compared to static conditions. By analyzing the image in ImageJ it could be determined that pore area was increased from 124 pixels up to 151 pixels resulting in an increase of 20%. On the other hand, spacing between pores was increased from 45 pixels to 61.5 pixels, consisting on a 36% increase on pore spacing. A zoomed-out view of the chip during the deformation test can be found on Appendix Figure 3.

Notably, by observing the membrane deformation tests of both chips we can make the assumption that having a wall spacing thickness within the range of 100μm to 250μm would still yield chips where cyclical deformation can be achieved. Finally, although clean room fabrication

yields master molds with high resolution, it is important to consider that fabrication time and cost also increase significantly, making it a less attractive option for prototyping.

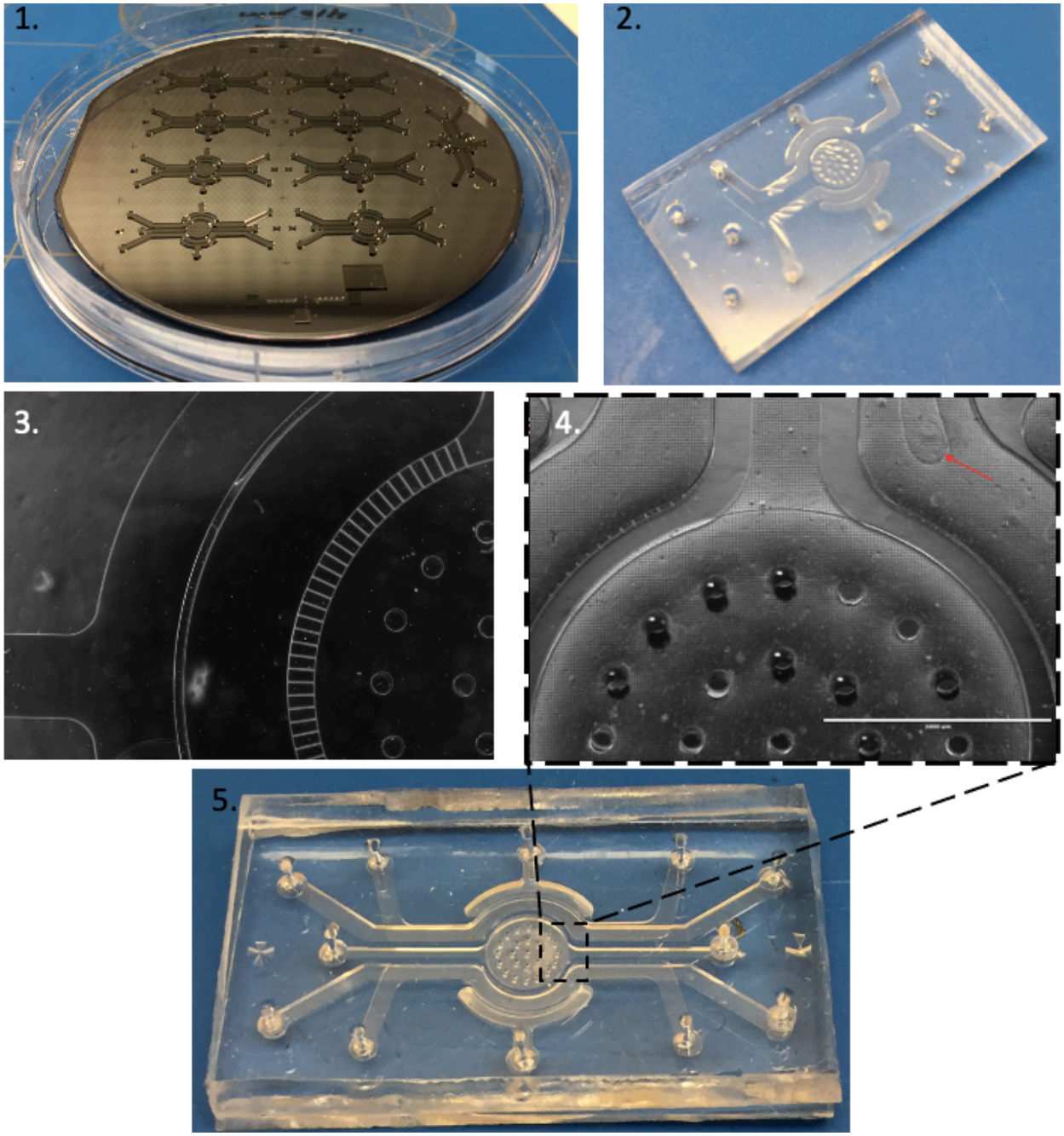

Figure 10. *Clean room MGBA-on-chip fabrication results.* ***1.*** *SU-8 bottom layer master mold on a Si.* ***2****.Top layer of the chip with transferred PDMS membrane.* ***3****. Closeup of the top chip layer showing a microchannel array connecting ENS and brain chambers and the thin wall spacing between the vacuum and ENS chamber.* ***4****. Closeup of the assembled chip showing a partially collapsed PDMS membrane (red arrow). Scale bar 2mm.* ***5****. Full view of the assembled MGBA-on-chip.*

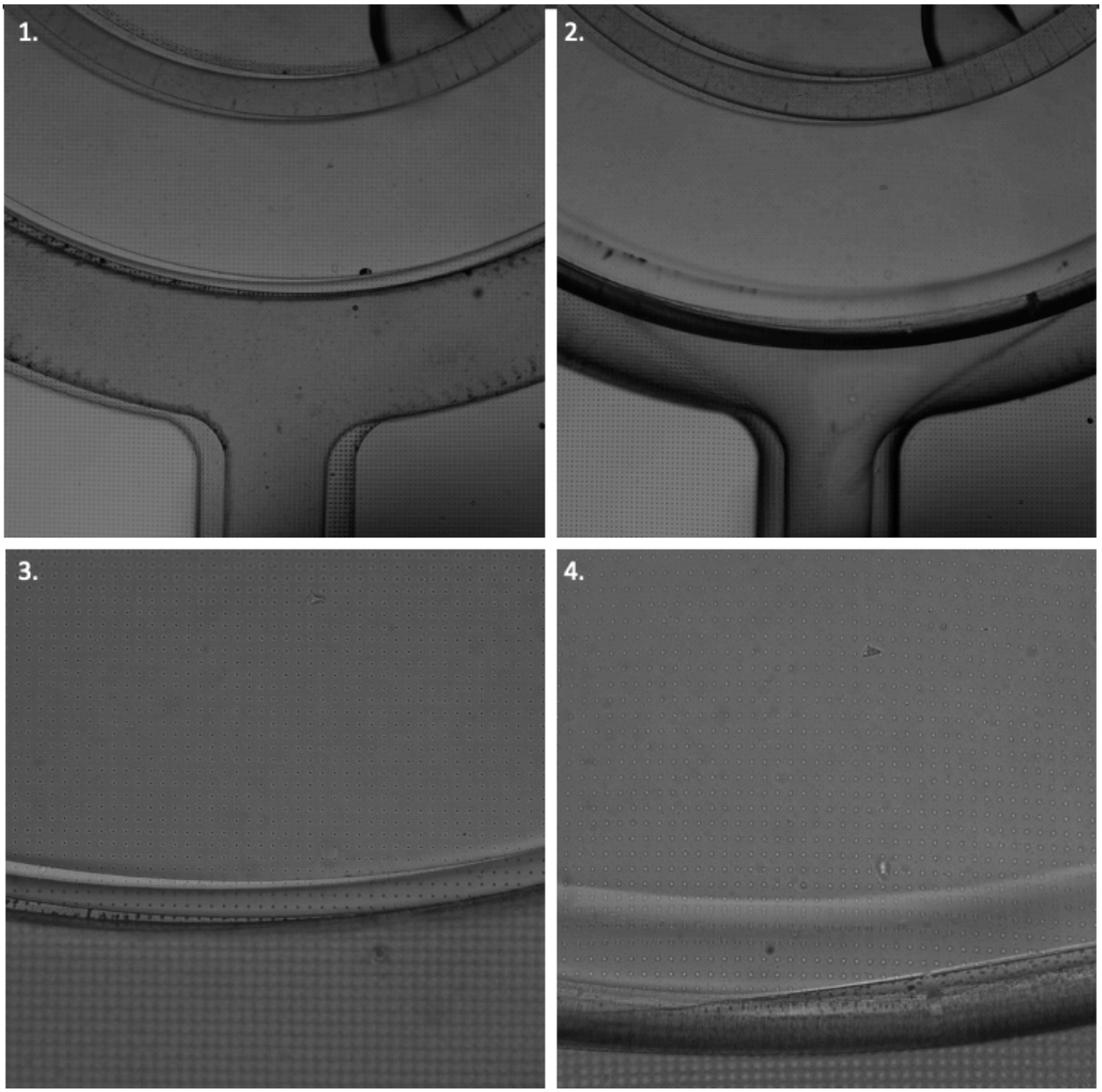

Figure 11. *Mechanical deformation test on clean room fabricated MGBA chip.* ***1-2.*** *View of the bottom chambers of the chip in static conditions and after vacuum chamber activation. 4x magnification.* ***3-4.*** *Closeup view of the bottom chambers of the chip under static conditions and after vacuum chamber activation. Note the increased area of the pores and the increased distance between pores. 10x magnification.*

Figure 12.1 shows the simulated velocity profile within the chip. Within the straight channels we can observe how velocity is at is maximum at the center of the channels and at its minimum at the walls which is consistent with a parabolic flow profile. On the other hand, once the liquid has reached the central brain chamber, we can observe a lower velocity profile caused by the widening of the chamber which can be further decreased by the micropillar structures. As

should be expected, the fluid inlets have the highest pressure while the outlets have the lowest. Within the center of the chip pressure has balanced to a middle range and is well distributed throughout. Shear stress for both layers is at the range of $1.75x10^{-11}$-$3.22x10^{-10}$ MPa (or $1.75x10^{-4}$ -$3.22x10^{-3}$ dyne/cm^2) which falls short from the reported physiological range of the gut epithelium. On the other hand, low shear stresses are required for the ENS and brain chamber, so values like the ones obtained in the simulation are desriable. However, considering that media, which is more viscous than water, will be perfused through the chip at the same flowrate we should expect the pressure to increase in a proportional manner to its viscosity and consequently the shear stress to also increase. Another factor to consider is that in the simulation, the PDMS membrane between both layers was not added. This might be affecting results in that fluid flow is distributed between top and bottom channels thus reducing the shear stress measurements.

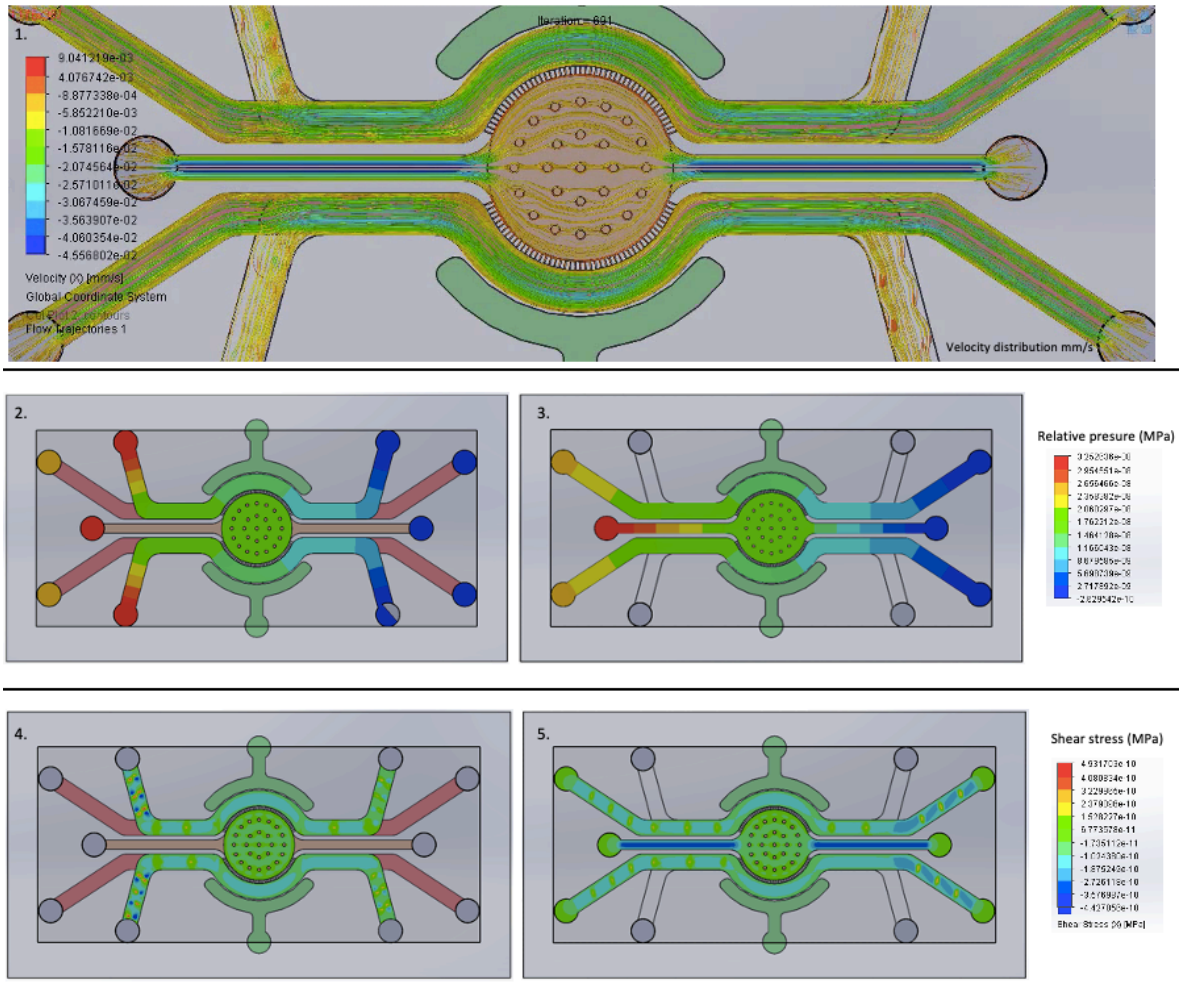

Figure 12. *Solid Works fluid simulation results.* ***1.*** *Simulated velocity distribution within the two layers of the chip.* ***2.*** *Pressure profile on the top part of the chip.* ***3.*** *Pressure profile at the bottom part of the chip.* ***4.*** *Shear stress at the surface of the top layer of the chip.* ***5.*** *Shear stress at the surface of the top layer of the chip.*

In order to better asses changes in wall shear stress of each chamber Eq. 1 was used to calculate an approximation of the wall shear stress at flow rates ranging from 80 to 10 µL/h. The viscosity of media was considered to be $9.4*10^{-4}$ Pa*s, the height of the Gut chamber as 400 µm and the height of the ENS chamber as 200 µm. The cell shear stress was then calculated following Eq.2 and plotted against flow rate as shown on Graph 2. Observing such values, the strong relationship between shear stress and channel dimensions can be observed. In the gut chamber, a cell shear stress of 0.002 to 0.08 dyne/cm^2 is desirable to replicate physiological conditions.[98] A cell shear stress within that range can be achieved at flow rates between 60 to 80 µL/h. In contrast, ENS neurons are not directly exposed to shear stress so it is desirable to have lower cell shear stress values. However, due to the reduced height of the ENS compartment, even flow rates as low as 30 µL/h already exert important stress. Graph 3 visualizes how cell shear stress would decrease if the dimensions of the ENS chamber were tuned. Importantly, the cell shear stress in the ENS compartment is almost reduced by 50% by just a 50µm height increase.

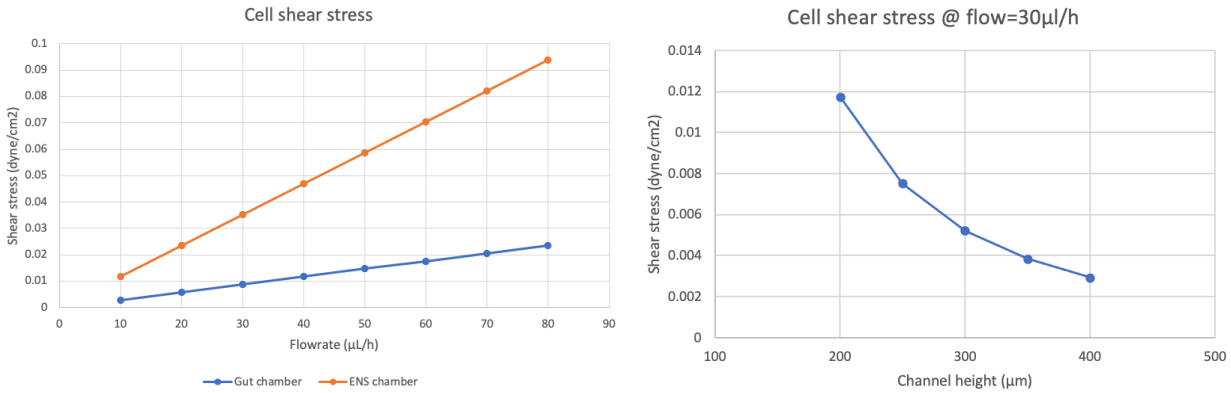

Graph 3. *Cell shear stress experienced in the Gut (blue) and the ENS (orange) compartments.* ***Graph 3****. Changes in cell shear stress due to different ENS channel heights.*

Results of the microchannel diffusion test can be observed in Figure 13, where the gradual fluorescence increase at different time points can be appreciated. Moreover, by zooming into the gap between both chambers and adjusting the brightness threshold, using ImageJ, the microchannels can be seen more clearly. The graph in Figure 13.5 shows the normalized 40 kDa FICT-dextran intensity profiles of both chambers throughout the duration of the experiment. FITC-dextran flux into the brain compartment can be calculated by considering the concentration gradient from ENS channel (25mM/mL) into the brain compartment (0mM/mL), the length of the microchannel (200µm), and the diffusion coefficient of 40 kDa FITC-dextran (44.7 µm^2/s), and solving Eq.1.

$$J = -D * \left(\frac{c_1 - c_0}{x_1 - x_0}\right) = -44.7\mu m^2 s^{-1} * \left(\frac{0\frac{M}{mL} - 25\frac{mM}{mL}}{200\mu m - 0\mu m}\right) = 5.5\frac{mM}{\mu m^2 * s}$$

This could be considered an ideal condition flux given that the experiment was performed with PBS and in the absence of cells. By performing the diffusion experiment only on the top layer of the chip with quasi-static conditions a few important factors were removed. 1. When the chip is being perfused, there are pressure differences between chambers that also contribute to mass transport. 2. While in a static model, the concentration gradient decreases until it reaches a balance, having chip perfusion constantly renews the gradient keeping a steady flux. 3. Considering an assembled chip, substances in the ENS compartment can also diffuse into the gut, which would decrease the overall flux into the brain chamber. Further experiments that introduce such factors increase the complexity of the analysis but can give helpful insigt depending on future research questions.

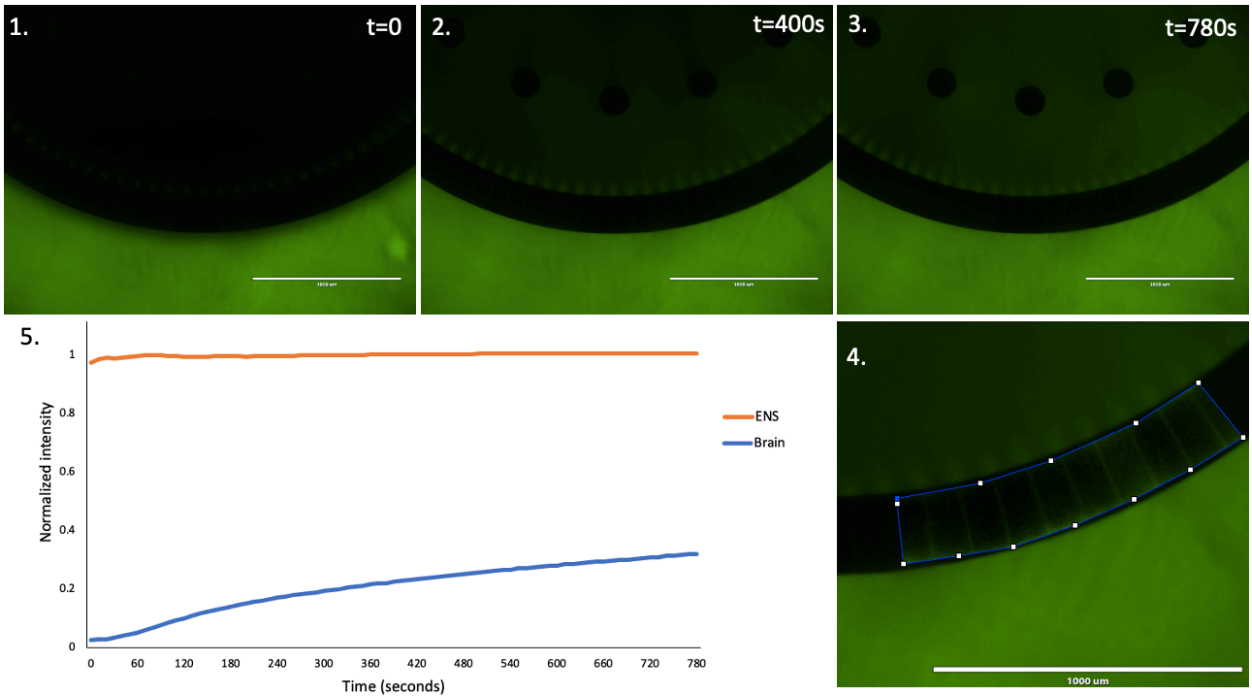

Figure 13. *Microchannel diffusion test. 40 kDa FITC-dextran solution was added to the ENS compartment (bottom) and left to diffuse into the brain compartment (top). Snapshots of both compartments at t=0* ***(1.)****, t=400s* ***(2.)****, and t=780s* ***(3.)****. Scale bar 1,000μm.* ***4.*** *A closeup of image 3 delineating the area where brightness thresholds were adjusted to show the interconnecting microchannels. Scale bar 1,000μm.* ***5.*** *Normalized intensity profiles of the ENS and brain compartments throughout the duration of the experiment.*

Taking the results of both chips into consideration a few fabrication and design adaptations and use suggestion can be proposed. Firstly, the uneven transfer of the SmoothCast PDMS membrane made its use on the chips less convenient. To improve membrane transfer outcomes some surface modifications can be made to the SmoothCast mold. FDTS (perfluorodecyltrichlorosilane) is a common chemical used to treat SU-8 wafers to reduce surface energy, consequently creating an anti-stiction effect on their surface.[151] Performing an FDTS treatment on the SmoothCast mold doesn't require clean room facilities but has the potential to drastically increase durability of the mold and improve the transfer of the membranes onto the chips. Other anti-stiction surface treatments commonly used for microelectromechanical systems (MEMS), such as organic self-assembled monolayers[152], could also be explored.

Additionally, achieving proper membrane transfer to chips would eliminate the requirement of clean room facilities for fabrication of the membrane, thus reducing fabrication time and costs. Membrane deformation results of "rough" chip suggest that even increased wall thicknesses can be deformed by the vacuum chamber considering the chip is made of highly deformable 20:1 PDMS. Thus, for increased chip bonding reproducibility and alignment a mechanical deformation compromise can be made by tuning the wall spacing between the vacuum and gut chamber to around 250µm and keeping the 20:1 PDMS ratio.

With the current design, there was no direct access to the brain culture chamber which caused air entrapment. Adding to this, the micropillar array that serves to prevent the PDMS membrane from collapsing increases surface area where bubbles can also be entrapped. Increasing the hydrophilicity of the surfaces of brain chamber and micropillar structures to prevent bubble formation could be a viable strategy. Moreover, a small access port could be added to the brain chamber with a hole puncher in order to provide direct access to the chamber and reduce bubble formation.

Regarding shear stress experienced by the cells within the MGBA chip, even at low perfusion rates there is a tendency to exert high shear stress in the ENS chamber. Considering that the neuronal microenvironment is not subject to a lot of direct shear stress, this is not a desirable feature. Fortunately, as seen on the equations above, cell shear stress can be decreased by almost half by increasing the ENS chamber height from 200µm to 250µm.

3.7 Conclusions and future outlook

The designs shown above underwent several optimization steps even before being fully assembled chips. For future design endeavors it is important to consider how all the desired functionalities of the chip can affect its dimensions and affect fabrication outcomes. Flow simulations and theoretical shear stress calculations are convenient tools that, if used right, can eliminate a few optimization steps before fabrication has even started.

The developed MGBA-on-chip platform is still in early prototype stages and a few more iterations can be expected to obtain a fully optimized chip. Further fluidic and mechanical characterization tests are required for the MGBA chip. In particular tests that involve perfusion at a constant rate on the completely assembled chip. For instance, membrane permeability measurements of the empty chip are necessary to calculate the actual permeability of the device when it has a cell monolayer. Furthermore, despite the shown preliminary mechanical deformation results, time constraints prevented further testing of the clean room MGBA chip which has an even membrane and thinner walls. It is expected that clean room fabricated MGBA chips which were bonded properly will show an increased mechanical deformation potential than the "rough" chips. However, due to the reduced surface area for bonding there is still a risk of chamber or membrane detachment once the vacuum pressure is applied. After mechanical deformation of the empty chip has been characterized the following step would be to determine the actual mechanical strain exerted on the cells.

Ideally, electrode integration into the MGBA-on-chip platform such as MEAs for the neuronal compartments and TEER electrodes for the gut compartment would also be desirable. This would facilitate measurements for barrier permeability and for neuronal activity. Several factors come into play for proper electrode integration ranging from the electrode material and its optical and conductive properties, to its fabrication method and placement on the chip. It will also be important to re-asses mechanical deformation capabilities of the chip after electrode integration. Incorporating sensors to measure other aspects of the MGBA microenvironment, such as pH and oxygen concentration, could also be considered. For this, are many available technologies (such as microbeads, engineered bacteria, etc.) mentioned in Chapter 2 that could be explored depending on the available resources.

Finally, establishing the actual MGBA in the chip will be an arduous task that will require tuning and optimization of multiple factors. A few of these factors include media composition, to

ensure the survival of the different cell types; seeding density of the different cell types, to prevent overgrowth or to achieve a stable monolayer; perfusion rate, to achieve a physiologically relevant shear stress on each of the chambers, and cyclic deformation frequency, to stimulate cells into villi formation.

Chapter 4. Generation of ENS neurons from embryonic stem cells

The Enteric nervous system (ENS) is a network of peripheral neurons and enteric glia that closely interacts with the gastrointestinal (GI) epithelium. The ENS is often considered a separate entity from the peripheral nervous system thanks to its capacity to coordinate with the central nervous system (CNS) but also to act autonomously from it to directly modulate GI exocrine and endocrine secretions, motility and microcirculation.[16] More details about the ENS and its role within the MGBA can be found on Chapter 1.

Recognizing the essential role that the ENS plays modulating gut and CNS homeostasis, its inclusion in in-vitro models becomes necessary to obtain physiologically relevant results. Having identified this need, intestinal organoid models, among others, have successfully integrated ENS neurons and glia to the point of obtaining self-contracting organoids (see Chapter 2 for more details).[85–87] However, OoC models are trailing behind where a platform that combines intestinal epithelial cells (IECs) and ENS neurons is yet to be found in literature.

The MGBA-on-chip proposed in the previous chapter addresses this need by providing a platform for the co-culture of IECs and ENS-derived cells. However, to accomplish this goal, it is first necessary to establish a model system to derive and isolate ENS precursors for their further differentiation into functional enteric neurons and integration on chip. Consequently, this chapter discusses the efforts to adapt and optimize an established protocol for neural crest (NC) induction and ENS differentiation[88] for H9 embryonic stem cells (ESCs) on our lab.

4.1 Embryonic origin of the ENS

During embryonic development, when the neural plate folds into itself to form the neural tube and the ectoderm converges forming a neuroepithelium, the neural crest is induced at the interface between them. This process is now known to occur thanks to a combination of bone morphogenic protein (BMP), fibroblast growth factor (FGF), and Wnt signaling activity.[153] During further development, neural crest progenitors migrate from the neural tube to distant locations within the body generating a wide array of cell lineages. Neural crest cells from vagal and sacral regions (HOXB3-HOXB5$^+$) migrate to extensively colonize the gut where they display an enteric neural crest identity (SOX10$^+$, PHOXB2$^+$, EDNRB$^+$) and finally commit to neuronal fates (TUJ1$^+$, TRKC$^+$).[154] This knowledge of embryonic development and its associated signaling pathways has

been essential to establish differentiation protocols that generate neural crest cells and enteric cell lineages.

4.2 Experimental methods

Culture of undifferentiated H9 human embryonic stem cells

Undifferentiated H9 human ESCs (obtained from the University of Leiden) were maintained on vitronectin XF™ coated (10 µg/mL) Non tissue culture-treated 6-well plates using complete TeSR™-E8™ culture medium supplemented with Penicillin-Streptomycin (1%) and without feeders. Daily media changes using complete TeSR™-E8™ were performed along with visual assessment of colony growth until the next passaging time. To maintain the undifferentiated culture, cells were detached once they reached 70-80% confluency (4-6 days) using ReLeSR™, an enzyme free reagent for dissociation of human ES, and passaged onto new vitronectin coated well plates using TeSR™-E8™ supplemented with Rock inhibitor (10µM) (TeSR-E8+rock$^-$).

Alternatively, H9 cells that had been passaged at least three times with the previous method were transferred into "single-cell" culture. This was done by detaching cells that had reached 70-80% confluency applying ethylenediaminetetraacetic acid (EDTA) at a concentration of 0.5mM for 4 minutes at room temperature. After the incubation period, the EDTA was aspirated and the cells were gently detached with a serological pipet tip using essential E8 medium supplemented with Rock inhibitor (10µM) (E8+rock$^-$). The cells were then centrifuged, resuspended in 1mL of E8+rock$^-$, counted, and seeded on a vitronectin coated (5 µg/mL) tissue culture-treated 6-well plate at densities ranging between $4x10^4$ and $8x10^4$ cells/well. The following day, media was replaced by essential E8 medium without Rock inhibitor. From that point onwards, cells were maintained on essential E8 medium and further passages were performed using EDTA and vitronectin coated plates.

Induction into enteric neural crest

The differentiation of human ES into enteric neural crest (ENC) cells was adapted from the protocol published by the Struder lab.[88] Upon reaching 70-80% confluency, H9 ES cells were detached with EDTA (0.5mM) for 3-4 min at room temperature and plated on Mat[88]rigel-coated tissue culture treated 6-well plates at a density of 150 K cells/well using E8+rock$^-$. Neural crest

induction was initiated when cells reached 60% confluence using KSR medium (knockout DMEM plus 15% KSR, Glutamax (1X), MEM NEAA (1X), and 2-mercaptoethanol (55 nM)) containing LDN193189 (100 nM) and SB431542 (10 μM). The KSR medium was gradually replaced with increasing amounts of N2 medium (DMEM/F-12 Hepes and N2 supplement) from day 4 to day 10. For ENC induction, cells were treated with 3 μM CHIR99021 in addition to LDN193189 and SB431542 from day 2 to day 11 and with 1 μM retinoic acid from day 6 to day 11.

Differentiation of ENCs to enteric neurons

On day 12, cells were detached using EDTA (0.5mM) for 5-15 min , spun down, resuspended in VP spheroid medium (Neurobasal® medium plus, FGF2 (10 ng/mL), CHIR 99021 (3 μM), N2 supplement (1X), B27 (1X), Glutamax(1X), and MEM NEAA(1X) and plated on Ultra Low Attachment 6-well plates at a 2:1 ratio to induce spheroid formation. VP spheroid media was replenished after a couple of days. Between day 15 or 16, VP spheroids were rinsed with PBS, dissociated using EDTA (0.5mM) for 10-15 min at 37ºC, spun down and resuspended in ENS medium (Neurobasal® medium plus, ascorbic acid (100μM), N2 supplement (1X), B27 (1X), MEM NAA(1X), Glutamax (1X), and GDNF (25 ng/mL). The dissociated cells were re-plated using a droplet method at a density of $3x10^4$ cells/well on 24-well plates coated with Poly-L-ornithine (PLO, 15 μg/mL), Fibronectin (FN, 2 μg/mL) and Laminin (Lam, 2 μg/mL) that had been previously left to dry out 15 min. Media was changed every couple of days for up to 20 days.

Immunofluorescence analysis

Cells at different time points were fixed with 4% formaldehyde for 10-15 min, for matured neurons this was substituted by adding 20 %(v/v) of 4% formaldehyde to the culture media already in the well and incubating for 10-15 min at 37ºC. Cells were then blocked and permeabilized using 1% bovine serum albumin (BSA) and 0.1% Triton X-100 and incubating for 40-60 min at room temperature. Next, cells were rinsed with PBS and incubated in primary antibody solutions (see Appendix Table 2) overnight at 4ºC. The following day cells were rinsed again with PBS and stained with fluorophore-conjugated secondary antibody solutions for 40 min at room temperature protected from light. Finally, the cells were counterstained with DAPI (1ng/mL) for 10 min and rinsed with PBS before imaging. Immunofluorescence analysis was performed using the EVOS FL Cell Imaging System.

Flow cytometry analysis

Cells at D12 of vagal precursor differentiation were dissociated for flow cytometry analysis using EDTA (0.5mM) and incubating for 10-15 min at 37ºC. Cells were then resuspended using a serological pipet, spun down and resuspended in 2mL of VP spheroid medium. 50µL of cell suspension were aliquoted into 4 round bottom test tubes, which were spun down and resuspended in 200µL of chilled PEB buffer (2mM EDTA, 0.5% BSA in PBS). The fluorophore-conjugated antibodies are added onto the respective test tube and incubated for 40 min at 4ºC protected from light (see Appendix Table 2 for antibodies). After incubation, the cells are spun down and resuspended in 400µL of fresh PEB buffer and add one droplet of NucBlue live ready probe to each test tube. Samples were analyzed in a MACSQuant flow cytometer and data was analyzed using FlowLogic software.

Live calcium imaging

Live calcium imaging was performed on ENS neurons that had been in maturation for 14 days or longer. To accomplish this, the media of the cells was replaced with ENS media supplemented with 1µM of the intracellular calcium indicator Fulo-4 AM and incubated for 30 minutes at 37ºC. Following the incubation period, the fluorescent solution was removed and fresh ENS media was added to the cells. Fluorescent image sequences were taken using the Nikon A1 confocal microscope at 2 frames per second for 5-10 minutes using the 10X objective at room temperature. After taking an image sequence without stimulation, cells were stimulated by adding 100µL of a 50mM KCl solution and subsequently imaged. Posterior to the analysis, cells were fixed for further immunofluorescent staining. Fluorescence intensity changes were measured using ImageJ software. First, average fluorescence intensity of the background in all frames was first determined. Next, a region of interest was selected, its fluorescence intensity determined, those values were normalized to background intensity using Eq. 4 and plotted using Excel.

$$Eq.4. \qquad ROI\ fluorescence\ Intensity = \frac{ROI\ integrated\ density}{Area\ of\ ROI * background\ fluorescence}$$

4.3 In-vitro derivation of ENS lineages results and discussion

The protocol we decided to follow was chosen due to the opportunity to learn it first-hand from researchers at the University of Groningen that had successfully implemented it with the same H9 embryonic cell line. This protocol (Figure 13.1) drives cells into the neuroectoderm pathway by dual SMAD inhibition achieved by LDN193189 and SB431542 which target BMP and TGF-β, respectively. Moreover, it exploits activation of canonical WNT signaling and retinoic acid to specify and posteriorize cells into neural crest (NC) lineage. Finally, it promotes commitment into enteric neurons by exposing cells to glial derived brain neurotrophic factor (GDNF) and other neural derived growth factors. This section demonstrates the results obtained from adapting and optimizing the protocol for use in our lab. Nonetheless, there are multiple other studies that have also demonstrated the ability to differentiate human pluripotent stem cells into ENCs that differ greatly regarding cellular origin, pathway activation, and culture environment, some of which will be discussed throughout this section.

Optimization of the protocol began by switching the maintenance of undifferentiated stem cells fromTesR-E8/Vitronectin-XF culture to culture with Essential E8/vitronectin. Both TeSR-E8 and Essential E8 are feeder-free and xeno-free chemically defined media based on the original formulation by Guokai Chen et al.[155] in the laboratory of James Thomson. Similarly, vitronectin-XF is a purified xeno-free cell culture matrix optimized for the growth and differentiation of human ESCs. This switch also entailed using different solutions, ReLeSR vs. EDTA, for dissociation and passaging of stem cells. The main difference being that ReLeSR is optimal for clump passaging of stem cells while EDTA is more convenient when single cell suspensions are desired. Upon trying both culture alternatives, it was easier to maintain a consistent culture by using the Essential E8/vitronectin alternative owing to the ability to better control seeding densities. On the other hand, using TeSR-E8/vitronectin for more than 3 passages often resulted sudden detachment of colonies and loss of the culture. Considering that within our lab Essential E8/vitronectin culture was already well-established and based on the previous outcomes, switching to Essential E8/vitronectin alternative for undifferentiated stem cell maintenance provided a more consistent, robust, and cost effective alternative.

Once a robust culture of ESCs was established, the following step required the transfer of ESCs into Matrigel to prime them for ENC induction. Following the protocol that was taught from our colleagues at the University of Groningen, this transfer of ESCs into a different substrate required an enzymatic dissociation step using Accutase. However, applying this step on our H9 cultures resulted in massive cell death after two days and the subsequent loss of the cultures. Due to this, it was decided to continue using EDTA to obtain a single cell suspension (Figure 13.2).

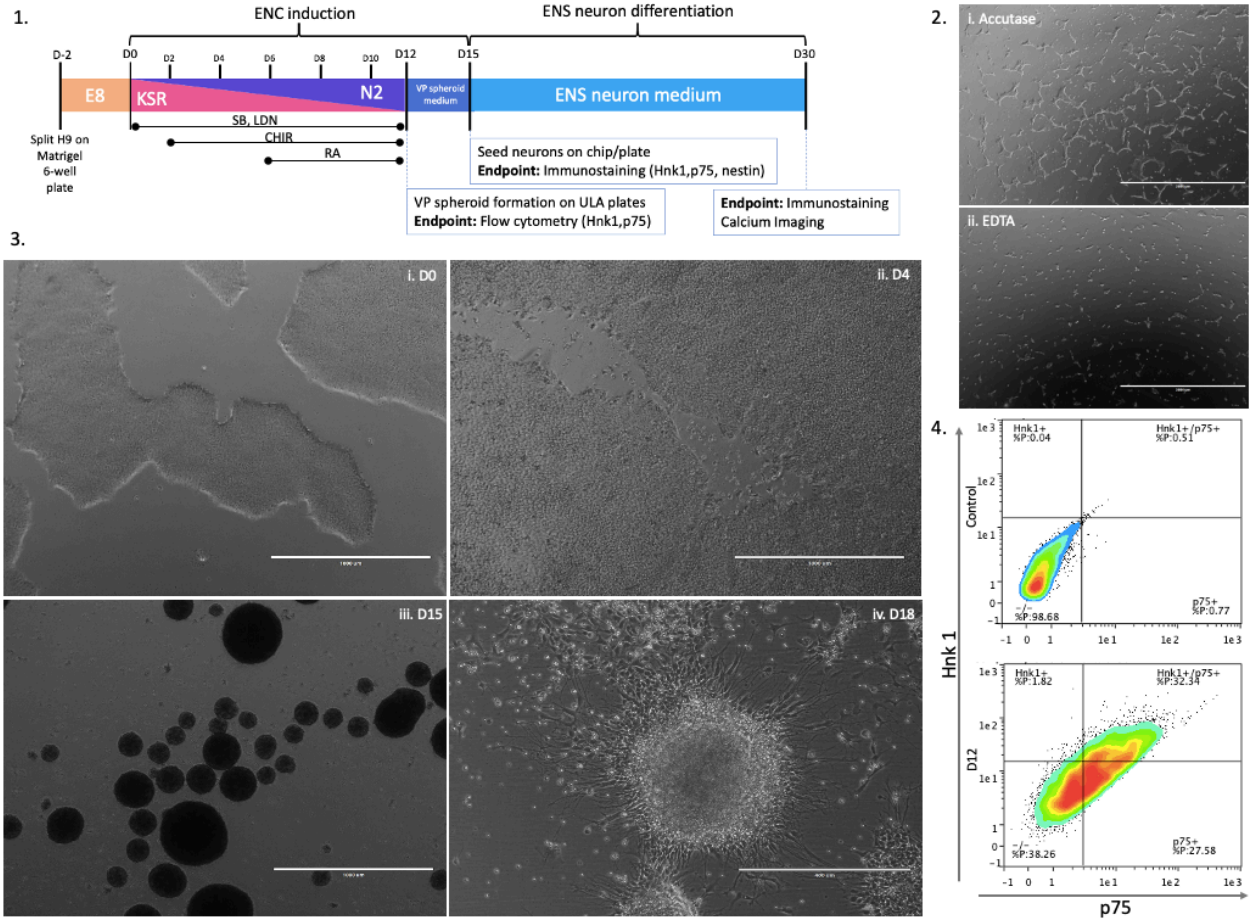

Figure 14. 1. *Overview of ENS lineage induction protocol.* ***2.*** *Cell culture the day after Accutase and EDTA treatment, when media was refreshed there was excessive cell detachment on the Accutase treated cells, while EDTA cells recovered and kept growing. Scale bar 2,000µm.* ***3. i.*** *Cells grown on Matrigel coated plates were grown to 60% confluency to begin NC induction. Scale bar 1,000µm.* ***ii.*** *Once NC induction has started, cells proliferate rapidly and by day 4 have already reached confluency. Scale bar 1,000µµ.* ***iii.*** *Dissociated cells are cultured in suspension to form neurospheroids which have clearly defined edges. Scale bar 1,000µm.* ***iv.*** *After 3-4 days in suspension culture, neurospheroids are dissociated and plated onto PLO/FN/Lam coated plates for further maturation into ENS neurons.* ***4.*** *Flow cytometry of ENCs for HNK1 and p75 at day 12 of induction.*

Importantly, the original protocol using Accutase required relatively high seeding densities, probably accounting for the expected massive cell death. In contrast, using EDTA did

not cause any significant cell death which allowed us to drastically reduce seeding concentration. When cells had reached approximately 60% confluency, media was switched to KSR and gradually changed to N2 medium up to day 10. This phase was characterized by very rapid proliferation, resulting in a confluent monolayer of cells between days 4-5 (Figure 13.3i-ii). After 12 days of induction, cells are dissociated and seeded in suspension well plates to induce spheroid formation. This 3D culture step is meant to enhance the purity of neural crest cells and neurons via neurospheroid formation.[154,156] However, additional enrichment for neural crest population can be achieved by isolating p75 and HNK1 double positive cells by FACS. p75 and HNK1, along with SOX10, PHOXB2, and EDNRB, are well known NC markers that have been widely used in previous studies to identify and isolate NC populations.[156–159] Other surface markers can also be used for NC population purification, for instance Fattahi et al., identified CD49D as a reliable early surface marker of SOX10+ NC lineages. After a couple of days spheroids should have well defined rounded shape (Figure 13.3iii).

Our approach was to determine induction efficiency through flow cytometry while relying on the 3D culture step to enhance neural crest purification. Flow cytometry analysis showed the portion of HNK1+/p75+ cells to be approximately 32% consistent among individual differentiations (n=4). Moreover, low grade noise on the HNK1 channel of the single stained p75 condition was also detected (Appendix Figure 4). Taking into consideration the combination of low signal expression and low-grade noise on other channels, determining a clear gate for HNK1 became difficult during analysis. The stark contrast between our induction efficiency and those reported by colleagues or in literature led us to believe that ENC induction was being affected by the use of expired reagents, however new inductions with fresh reagents yielded similar results. We then explored whether overnight antibody incubation would improve the signal resulting in a ~10% yield increase (Appendix Figure 5), which still meant a difference of around 55% efficiency from the expected results. Notwithstanding the low induction efficiencies, the 3D spheroidal cultures presented well defined rounded shapes.

To visualize HNK1, p75 expression patterns, D12 cells and D15 spheroids were fixed and stained with the same antibodies used for flow cytometry (Figure 14). To take HNK1 images from D12 cultures high laser intensity and long exposure times were required to obtain only a faint signal, whereas p75 was more easily detectable well distributed throughout the culture plate. Similar results were obtained by staining D15 spheroids where p75 was more easily detectable and

HNK1 required higher exposures. We found a close similarity between p75 expression on our spheroids and other reported neural crest spheroids (Figure 14. x-xi).[156,160] These images are consistent with flow cytometry results where only around 25% of cells were detected on the single stained HNK1 condition (Appendix Figure 4). Moreover, considering that p75 expression on flow cytometry was detected on 80-90% of the total cells, fluorescent expression at D12 and D15 also seems to be consistent with such results. Owing to the low HNK1 signal, Nestin expression, another neural stem cell marker, was also investigated on our spheroids (Figure 14. vii-ix). Indeed, our results show a clear and well-defined Nestin signal throughout the spheroids supporting the claim for their neural progenitor identity.

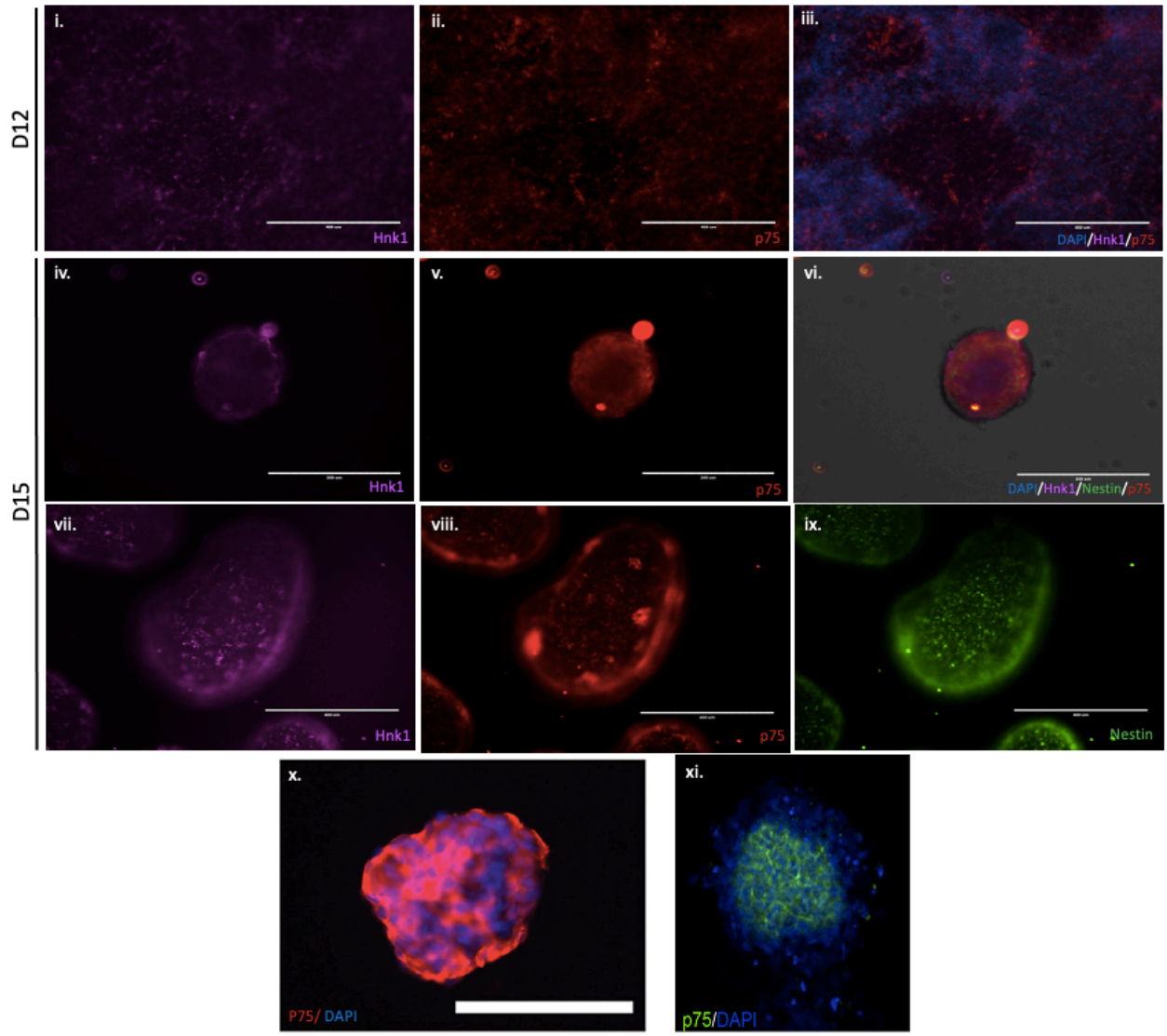

Figure 15. *NC immunofluorescence staining.* ***i-iii.*** *HNK1(magenta) and p75(red) counterstain on NCs at after 12 days of induction. Scale bar 400µm.* ***iv-ix.*** *Immunostaining of HNK1 (magenta), p75(red) and Nestin (green) on D15 neurospheroids. Scale bar 200µm*

from iv. to vi, and 400µm from viii. to ix. ***x.-xi.*** *p75 immunostaining of NC neurospheroids obtained from reference* [160] *(Scale bar 100µm) and form reference*[161].

The following step in the protocol, after completing neural induction, consists on dissociating the spheroids and seeding them on PLO/FN/Lam coated plates to grow as adherent cultures. Early maturation of neuronal cultures for 3 days can be observed in Figure 15.1 where dendrites reach out from the spheroid to sense their environment in the lookout for nearby spheroids. As maturation continues after 6 days (Figure 15.2), there is an increase of dendrites extending from the spheroids and there are a few spheroids that are networked. By day 15 post-reseeding (Figure 15.3) there is a potentiation of these connections into axons but there is also an increase in the density of the spheroids and a growing population of cells at their surroundings that don't seem to have neuronal lineage. At this stage cultures were fixed and stained for Nestin and β-III tubulin, a cytoskeletal marker for immature neurons. A few difficulties were encountered when performing these assays as cultures were fragile, detached easily and projections were not visible after fixation. Upon further inspection the most likely causes of these issues are a combination of low formaldehyde exposure and the use of PBS without ions which exerts osmotic pressure on the cells and causes them to lose their morphology. Regarding neuronal fixation, the original protocol called for 16% formaldehyde to be mixed into the media as opposed to the 4% formaldehyde solution that was used. Nevertheless, a few images were successfully obtained and are shown in Figure X. Unfortunately, both Nestin and β-III tubulin had the same host for the primary antibody which made counterstains impossible, thus impeding visualization of spatial expression of both proteins at the same time. Cultures were also stained for GFAP, a glial fibrillary protein found in astrocytes and enteric glia, however no positive signal was detected. The presence of both Nestin and β-III tubulin suggests an immature neuron phenotype (β-III tub) but also the presence of less differentiated neural progenitor cells (Nestin). The lack of GFAP expression is consistent with previous studies which report that GFAP is only be detected in cultures at later stages of maturation.[154] Interestingly, β-III tubulin filaments branch out from a cluster of cells which we could assume to be the center of the neurospheroid. On the other hand, Nestin+ cells seem to be well distributed, leading us to believe that these are the cells found in the surroundings of the neurosphere networks shown on Figure14.3. It would not be surprising to find that Nestin+ cells are also positive for cell proliferation markers, making them responsible for the increase in density of the neurospheroids and the proliferation of other surrounding cells within the culture.

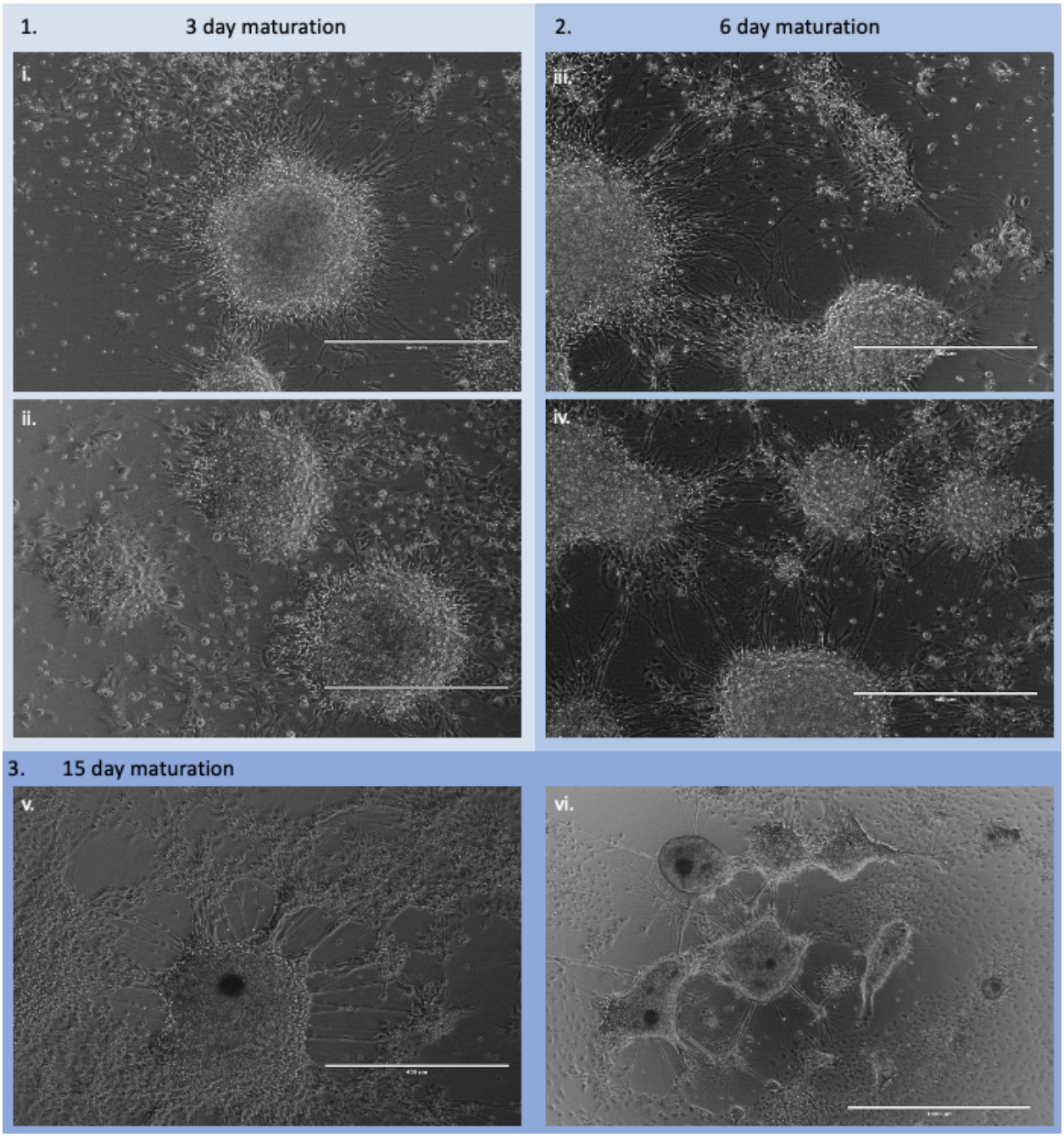

Figure 16. *ENS neuron maturation in plates.* ***1.*** *Maturation of seeded neurospheroids after 3 days of dissociation. Scale bar 400µm.* ***2.*** *ENS-derived neuron maturation 6 days post-dissociation. Scale bar 400µm.* ***3.*** *ENS-derived neuron maturation 15 days post-dissociation. Scale bar v. 400µm, vi. 1,000µm.*

To probe at the functionality of the neuronal cultures, cells were incubated with a fluorescent intracellular Ca^{2+} marker and changes in fluorescent intensity were recorded upon stimulation with KCl. This experiment revealed that cells are responsive to changes of extracellular

ion concentrations as determined by an increase in fluorescence intensity that translates to changes in intracellular calcium concentration (Figure 16). The images in Figure 16.1 and 16.2 depict the neural cell culture before and after the stimuli was delivered, respectively. For quantitative analysis, two regions of interest (ROI) were chosen: the center of a spheroid and one of the projecting axon bundles. Subsequently, fluorescence intensity within the ROI was measured for every frame of the image sequence, values were normalized with the average background intensity and plotted. The graph shown in Figure 16.3 describes the magnitude of change in fluorescence as a response to the KCl stimulus. Before the stimulus we observe a baseline fluorescence level that represents the intracellular Ca^{2+} concentration of the cells at rest. Following the KCl pulse, a steep rise on intracellular Ca^{2+} concentration can be observed as fluorescence increases in both ROIs. After the first KCl pulse, we probed the ability to trigger a second depolarization in the cells, however the effect was much more attenuated than in the first try. These results hint toward the right functionality of the differentiated cells, however the stimulus was delivered on a global level, thus it was impossible to determine the interconnectivity of the network. Moreover, it is also useful to determine if blocking sodium channel activity abolishes the response to the KCl impulse to confirm that the depolarization generated is voltage-gated channel dependent.

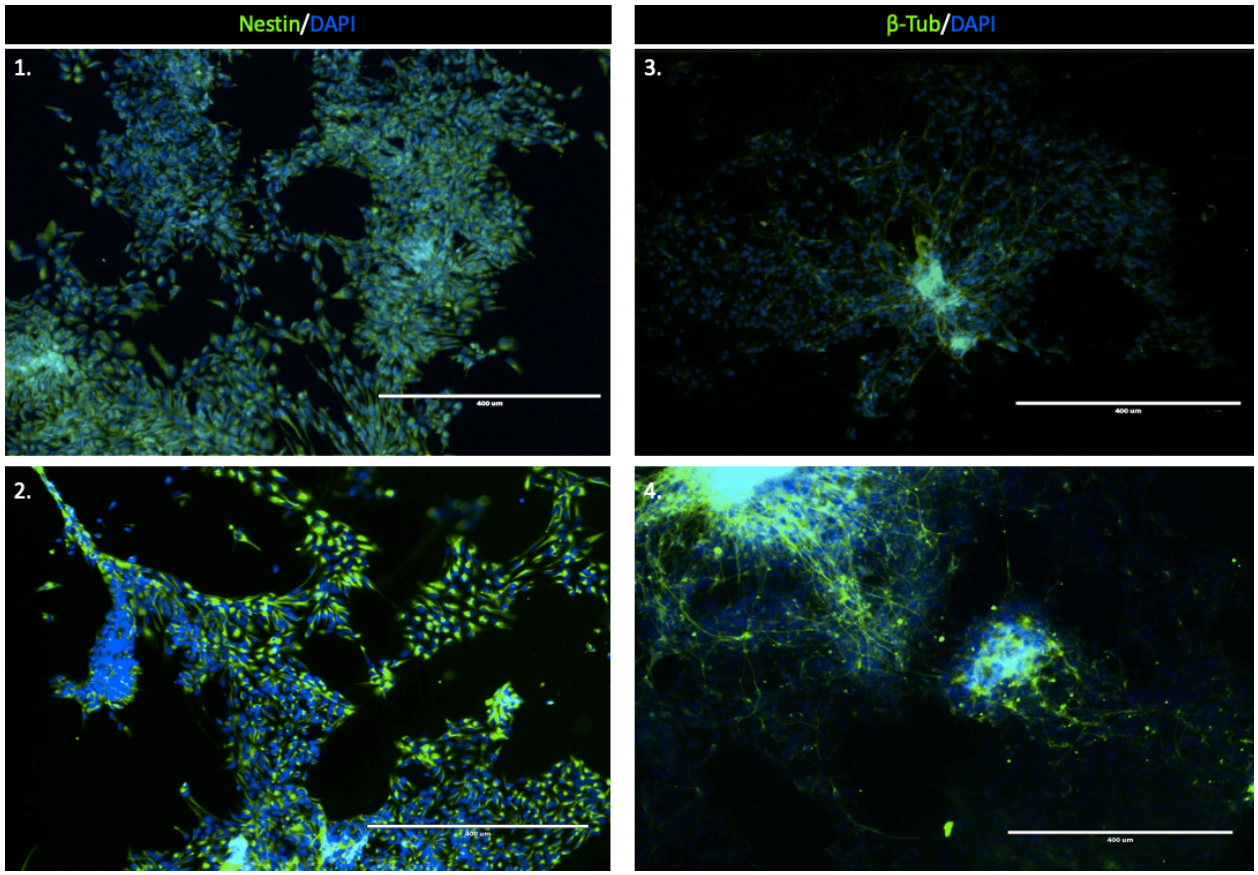

Figure 17. *Immunofluorescence images of neurons.* ***1-2.*** *Nestin (green) neuronal expression after 15 days of maturation, note the semi-dispersed distribution of cells. Scale bar 400µm.* ***3-4****. β-III tubulin (green) neuronal expression after 15 days of maturation, note the majority of projections stemming from a highly dense mass of cells. Scale bar 400µm.*

Interestingly, the original published protocol was intended for induction of feeder ESCs which require knockout serum replacement for their maintenance as an alternative to using FBS and is most likely the reason why it was used during the induction phase. However, our lab, as most other labs in the stem cell field, have migrated to the use of feeder-free cells. Such cells are commonly grown using more defined culture media, such as the ones discussed above, that no longer require serum replacement. Thus, by changing our stable ESC culture from Essential 8 medium to KSR medium we have inadvertently introduced a source for variation and inconsistency to our induction which could have been avoided. More recent protocols focused on vagal neural crest induction take this into account and propose the use of Essential 6 medium to perform the differentiation.[154] By adopting this alternative, the use of LDN is no longer required and there is the need for low-grade activation of SMAD signaling during early stages which can be achieved by addition of BMP4. This newer protocol resembles that published by the Dalton lab a few years

back which already used feeder-free stem cells and noted that low grade SMAD activity and activation of canonical WNT signaling are requirements for NC induction.[159]

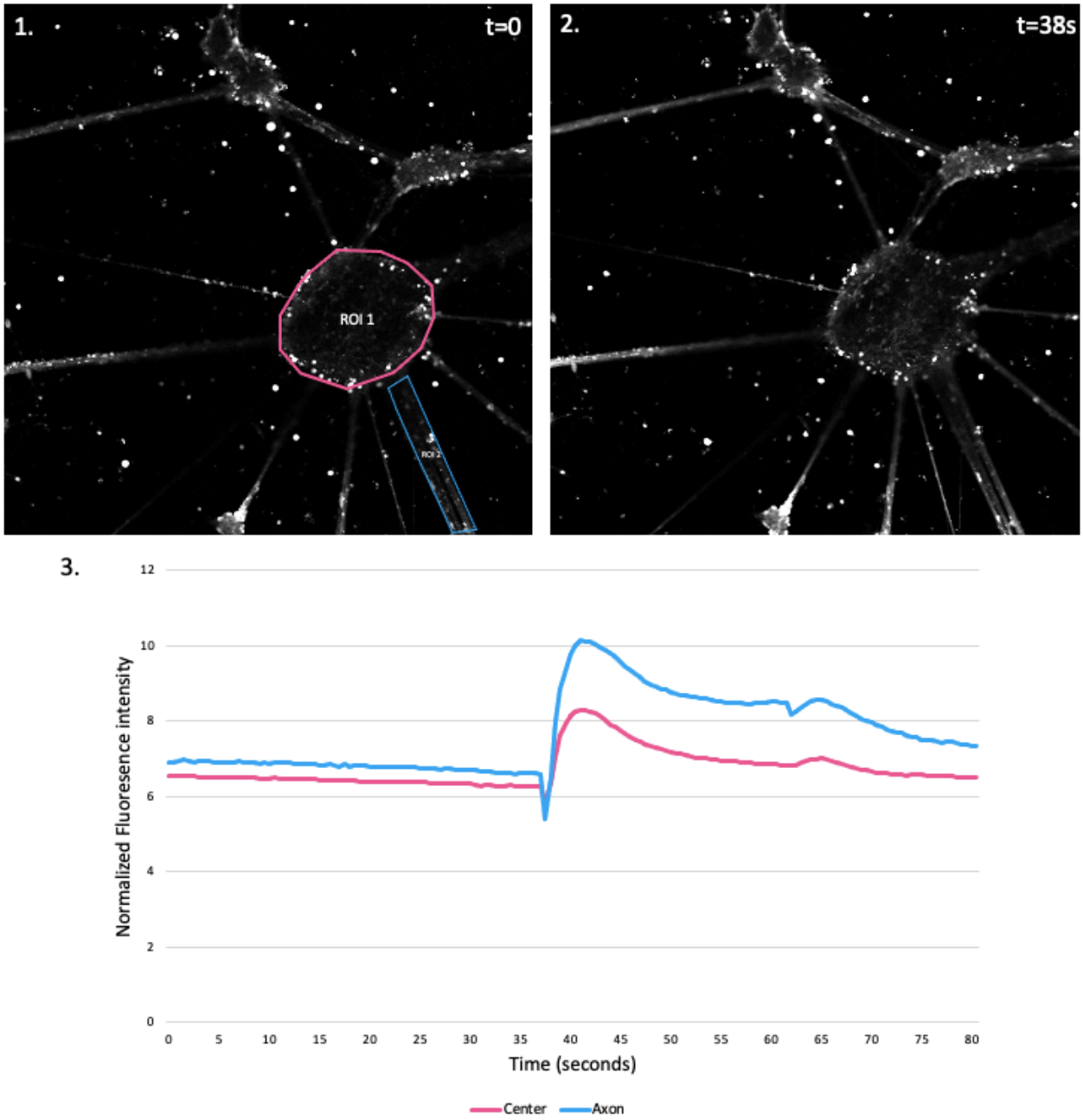

Figure 18. *Calcium imaging analysis.* ***1.*** *Snapshot of the neuronal culture at t=0 before KCl stimulation depicting the two regions of interest, one at the center of the neurospheroid (pink) and another at an axonal bundle (blue).* ***2.*** *Snapshot of the neuronal culture at t=38s right after the KCl pulse was applied. Note a slight increase in the visible neurons within the neural spheroid center.* ***3.*** *Graph of the normalized fluorescence intensity of both ROIs as a response to two different KCl pulses at t=38s and t=64s.*

4.4 Conclusions and future outlook

The work presented here describes a strategy to derive ENC precursors from embryonic stem cells. After several steps of optimization, we obtained what seem to be immature but functionally responsive enteric neurons. It has been recognized that this, and other ENC induction protocols, result in a varied population of neuronal subtypes and other ENC lineages.[88,159] Evidently, further optimization for the first NC induction stage of the protocol is required. A suggested pathway of action is adopting a more chemically defined medium that is better suited for feeder free stem cells and provides a more accurate control of their exposure to growth factors. The efficiency of adopting this method should be confirmed by flow cytometry analysis which would hopefully yield better results than the current method. On the other hand, if there is continued use of the current strategy, it would be suggested to explore new NC markers such as SOX10 or CD49D for flow cytometry and FACS. Exploring the addition of a FACS purification step for NC markers at day 12 before the formation of neurospheroids would also be recommended given the amount of contaminating non-neuronal cells found at the neuronal maturation stage.

The data obtained by immunofluorescence and calcium imaging analysis provides a first look into the morphology and functionality of the neurons obtained by the protocol. However, it is necessary to identify the neuronal subtype through marker expression or relative gene expression analysis. Moreover, further studies are required to determine if cells are spontaneously active, a sign of correct neuronal development, and to test network synchronization. For this, only preliminary attempts have been made to find the right seeding density to achieve MEA surface coverage by neurons. However, reducing the emergence of contaminating cells in neuronal cultures remains a challenge which would hopefully be reduced by the approaches mentioned above.

Finally, integration of neurons into the MGBA-on-chip platform would also entail optimization of seeding density, ensuring purity of the neuronal cultures, and confirming soma isolation by the microchannel arrays between chambers. A few initial attempts were made to culture neurons on 2-channel chips and in glass-bonded top layer MGBA chips however no notable progress was made in that respect (Appendix Figure 6).

Chapter 5. Conclusion

The objectives of this master's thesis were to design and develop a Microbiome-gut-brain axis-on-chip prototype which would enable the fluidically communicated co-culture of intestinal epithelial cells, ENS-derived neurons and CNS-derived neurons. The results displayed in this report are a first endeavor to achieve such a platform. The fabrication and initial characterization of the MGBA-on-chip platform have shown that mechanical deformation is achievable and fluidic communication of chambers through microchannel arrays is also feasible. Further design optimization is required to obtain a fully functioning chip, but hopefully with the data provided in this report, the next iterations are well guided.

Moreover, this thesis also aimed to adapt a protocol that would induce embryonic stem cells into enteric neural crest cells and then into enteric neurons. This task proved to require several optimization steps in different phases, some of which remain to be addressed. Notwithstanding, immature and stimuli responsive neurons were successfully obtained. Going forward with this work the few suggestions to tune the differentiation protocol for the specific needs of our embryonic stem cells should be considered for more efficient results.

Bibliography

1. Zhu, X. *et al.* Microbiota-gut-brain axis and the central nervous system. *Oncotarget* **8**, 53829–53838 (2017).
2. Fröhlich, E. E. *et al.* Cognitive impairment by antibiotic-induced gut dysbiosis: Analysis of gut microbiota-brain communication. *Brain. Behav. Immun.* **56**, 140–155 (2016).
3. Karl, J. P. *et al.* Effects of Psychological, Environmental and Physical Stressors on the Gut Microbiota. *Front. Microbiol.* **9**, (2018).
4. Kim, N., Yun, M., Oh, Y. J. & Choi, H.-J. Mind-altering with the gut: Modulation of the gut-brain axis with probiotics. *J. Microbiol.* **56**, 172–182 (2018).
5. Raimondi, I. *et al.* Organ-On-A-Chip in vitro Models of the Brain and the Blood-Brain Barrier and Their Value to Study the Microbiota-Gut-Brain Axis in Neurodegeneration. *Front. Bioeng. Biotechnol.* **7**, (2020).
6. Grenham, S., Clarke, G., Cryan, J. F. & Dinan, T. G. Brain-gut-microbe communication in health and disease. *Front. Physiol.* **2 DEC**, 94 (2011).
7. Egerod, K. L. *et al.* Profiling of G protein-coupled receptors in vagal afferents reveals novel gut-to-brain sensing mechanisms. *Mol. Metab.* **12**, 62–75 (2018).
8. Lai, N. Y. *et al.* Gut-innervating nociceptor neurons protect against enteric infection by modulating the microbiota and Peyer's patch microfold cells. *bioRxiv* 580555 (2019). doi:10.1101/580555
9. Wang, F.-B. & Powley, T. L. Vagal innervation of intestines: afferent pathways mapped with new en bloc horseradish peroxidase adaptation. *Cell Tissue Res.* **329**, 221–230 (2007).
10. Williams, E. K. *et al.* Sensory Neurons that Detect Stretch and Nutrients in the Digestive System. *Cell* **166**, 209–221 (2016).
11. Bravo, J. A. *et al.* Ingestion of Lactobacillus strain regulates emotional behavior and central GABA receptor expression in a mouse via the vagus nerve. *Proc. Natl. Acad. Sci. U. S. A.* **108**, 16050–16055 (2011).
12. Sen, T. *et al.* Diet-driven microbiota dysbiosis is associated with vagal remodeling and obesity. *Physiol. Behav.* **173**, 305–317 (2017).

13. Cox, L. M. & Weiner, H. L. Microbiota Signaling Pathways that Influence Neurologic Disease. *Neurotherapeutics* **15**, 135–145 (2018).
14. Bonaz, B., Bazin, T. & Pellissier, S. The Vagus Nerve at the Interface of the Microbiota-Gut-Brain Axis. *Front. Neurosci.* **12**, 49 (2018).
15. Hu, H. & Spencer, N. J. Enteric Nervous System Structure and Neurochemistry Related to Function and Neuropathology. in *Physiology of the Gastrointestinal Tract* **1**–**2**, 337–360 (Elsevier, 2018).
16. Cabarrocas, J., Savidge, T. C. & Liblau, R. S. Role of enteric glial cells in inflammatory bowel disease. *GLIA* **41**, 81–93 (2003).
17. Walsh, K. T. & Zemper, A. E. The Enteric Nervous System for Epithelial Researchers: Basic Anatomy, Techniques, and Interactions With the Epithelium. *Cell. Mol. Gastroenterol. Hepatol.* **8**, 369–378 (2019).
18. Singhal, M. *et al.* Serotonin Transporter Deficiency is Associated with Dysbiosis and Changes in Metabolic Function of the Mouse Intestinal Microbiome. *Sci. Rep.* **9**, 2138 (2019).
19. Ambrosini, Y. M. *et al.* The Gut-Brain Axis in Neurodegenerative Diseases and Relevance of the Canine Model: A Review. *Front. Aging Neurosci.* **11**, 130 (2019).
20. Kuo, Y.-M. *et al.* Extensive enteric nervous system abnormalities in mice transgenic for artificial chromosomes containing Parkinson disease-associated α-synuclein gene mutations precede central nervous system changes. *Hum. Mol. Genet.* **19**, 1633–1650 (2010).
21. Zhao, Q. & Elson, C. O. Adaptive immune education by gut microbiota antigens. *Immunology* **154**, 28–37 (2018).
22. Min, S., Kim, S. & Cho, S.-W. Gastrointestinal tract modeling using organoids engineered with cellular and microbiota niches. *Exp. Mol. Med.* **52**, 227–237 (2020).
23. Powell, N., Walker, M. M. & Talley, N. J. The mucosal immune system: Master regulator of bidirectional gut-brain communications. *Nature Reviews Gastroenterology and Hepatology* **14**, 143–159 (2017).
24. Muller, P. A. *et al.* Crosstalk between muscularis macrophages and enteric neurons regulates gastrointestinal motility. *Cell* **158**, 300–313 (2014).
25. Wallner, S. *et al.* The Granulocyte-colony stimulating factor has a dual role in neuronal

and vascular plasticity. *Front. Cell Dev. Biol.* **3**, 48 (2015).

26. Erny, D. *et al.* Host microbiota constantly control maturation and function of microglia in the CNS. *Nat. Neurosci.* **18**, 965–977 (2015).
27. Simpson, C. A., Mu, A., Haslam, N., Schwartz, O. S. & Simmons, J. G. Feeling down? A systematic review of the gut microbiota in anxiety/depression and irritable bowel syndrome. *Journal of Affective Disorders* **266**, 429–446 (2020).
28. Holzer, P. *et al.* Visceral Inflammation and Immune Activation Stress the Brain. *Front. Immunol.* **8**, (2017).
29. Lu, V. B. *et al.* Adenosine triphosphate is co-secreted with glucagon-like peptide-1 to modulate intestinal enterocytes and afferent neurons. *Nat. Commun.* **10**, 1029 (2019).
30. Lai, N. Y., Mills, K. & Chiu, I. M. Sensory neuron regulation of gastrointestinal inflammation and bacterial host defence. *J. Intern. Med.* **282**, 5–23 (2017).
31. Farzi, A., Fröhlich, E. E. & Holzer, P. Gut Microbiota and the Neuroendocrine System. *Neurotherapeutics* **15**, 5–22 (2018).
32. Cussotto, S., Sandhu, K. V., Dinan, T. G. & Cryan, J. F. The Neuroendocrinology of the Microbiota-Gut-Brain Axis: A Behavioural Perspective. *Front. Neuroendocrinol.* **51**, 80–101 (2018).
33. Weaver, I. C. G. *et al.* Epigenetic programming by maternal behavior. *Nat. Neurosci.* **7**, 847–854 (2004).
34. Klengel, T. *et al.* Allele-specific FKBP5 DNA demethylation mediates gene-childhood trauma interactions. *Nat. Neurosci.* **16**, 33–41 (2013).
35. De Punder, K. & Pruimboom, L. Stress induces endotoxemia and low-grade inflammation by increasing barrier permeability. *Front. Immunol.* **6**, 223 (2015).
36. Sudo, N. *et al.* Postnatal microbial colonization programs the hypothalamic-pituitary-adrenal system for stress response in mice. *J. Physiol.* **558**, 263–275 (2004).
37. Cohen, S. M., Tsien, R. W., Goff, D. C. & Halassa, M. M. The impact of NMDA receptor hypofunction on GABAergic neurons in the pathophysiology of schizophrenia. *Schizophr. Res.* **167**, 98–107 (2015).
38. Allaire, J. M. *et al.* The Intestinal Epithelium: Central Coordinator of Mucosal Immunity. *Trends Immunol.* **39**, 677–696 (2018).
39. Latorre, R., Sternini, C., De Giorgio, R. & Greenwood-Van Meerveld, B. Enteroendocrine

cells: a review of their role in brain-gut communication. *Neurogastroenterol. Motil.* **28**, 620–630 (2016).

40. Yano, J. M. *et al.* Indigenous Bacteria from the Gut Microbiota Regulate Host Serotonin Biosynthesis. *Cell* **161**, 264–276 (2015).
41. Liu, Y., Vosmaer, G. D. C., Tytgat, G. N. J., Xiao, S. D. & Ten Kate, F. J. W. Gastrin (G) cells and somatostatin (D) cells in patients with dyspeptic symptoms: Helicobacter pylori associated and non-associated gastritis. *J. Clin. Pathol.* **58**, 927–931 (2005).
42. Lomax, A. E., Linden, D. R., Mawe, G. M. & Sharkey, K. A. Effects of gastrointestinal inflammation on enteroendocrine cells and enteric neural reflex circuits. *Auton. Neurosci.* **126**–**127**, 250–257 (2006).
43. Lebrun, L. J. *et al.* Enteroendocrine L Cells Sense LPS after Gut Barrier Injury to Enhance GLP-1 Secretion. *Cell Rep.* **21**, 1160–1168 (2017).
44. Grasset, E. *et al.* A Specific Gut Microbiota Dysbiosis of Type 2 Diabetic Mice Induces GLP-1 Resistance through an Enteric NO-Dependent and Gut-Brain Axis Mechanism. *Cell Metab.* **25**, 1075-1090.e5 (2017).
45. Bohórquez, D. V. *et al.* An Enteroendocrine Cell – Enteric Glia Connection Revealed by 3D Electron Microscopy. *PLoS One* **9**, e89881 (2014).
46. Kaelberer, M. M. *et al.* A gut-brain neural circuit for nutrient sensory transduction. *Science (80-.).* **361**, eaat5236 (2018).
47. Dalile, B., Van Oudenhove, L., Vervliet, B. & Verbeke, K. The role of short-chain fatty acids in microbiota–gut–brain communication. *Nat. Rev. Gastroenterol. Hepatol.* **16**, 461–478 (2019).
48. Kayama, H., Okumura, R. & Takeda, K. Interaction Between the Microbiota, Epithelia, and Immune Cells in the Intestine. *IY38CH02_Takeda ARjats.cls April* **5**, (2020).
49. Desbonnet, L. *et al.* Effects of the probiotic Bifidobacterium infantis in the maternal separation model of depression. *Neuroscience* **170**, 1179–1188 (2010).
50. Jiménez, E. *et al.* Antibiotic resistance, virulence determinants and production of biogenic amines among enterococci from ovine, feline, canine, porcine and human milk. *BMC Microbiol.* **13**, 288 (2013).
51. Van De Wouw, M. *et al.* Host Microbiota Regulates Central Nervous System Serotonin Receptor 2C Editing in Rodents. *ACS Chem. Neurosci.* **10**, 3953–3960 (2019).

52. Clarke, G. *et al.* The microbiome-gut-brain axis during early life regulates the hippocampal serotonergic system in a sex-dependent manner. *Mol. Psychiatry* **18**, 666–673 (2013).
53. Stasi, C., Bellini, M., Bassotti, G., Blandizzi, C. & Milani, S. Serotonin receptors and their role in the pathophysiology and therapy of irritable bowel syndrome. *Tech. Coloproctol.* **18**, 613–621 (2014).
54. Valles-Colomer, M. *et al.* The neuroactive potential of the human gut microbiota in quality of life and depression. *Nat. Microbiol.* **4**, 623–632 (2019).
55. Golubeva, A. V. *et al.* Microbiota-related Changes in Bile Acid & Tryptophan Metabolism are Associated with Gastrointestinal Dysfunction in a Mouse Model of Autism. *EBioMedicine* **24**, 166–178 (2017).
56. Kämpfer, A. A. M. *et al.* Development of an in vitro co-culture model to mimic the human intestine in healthy and diseased state. *Toxicol. Vitr.* **45**, 31–43 (2017).
57. Kim, S. H. *et al.* Three-dimensional intestinal villi epithelium enhances protection of human intestinal cells from bacterial infection by inducing mucin expression. *Integr. Biol.* **6**, 1122–1131 (2014).
58. Antunes, F., Andrade, F., Araújo, F., Ferreira, D. & Sarmento, B. Establishment of a triple co-culture in vitro cell models to study intestinal absorption of peptide drugs. *Eur. J. Pharm. Biopharm.* **83**, 427–435 (2013).
59. Behrens, I., Stenberg, P., Artursson, P. & Kissel, T. Transport of lipophilic drug molecules in a new mucus-secreting cell culture model based on HT29-MTX cells. *Pharm. Res.* **18**, 1138–1145 (2001).
60. Chen, X.-M., Elisia, I. & Kitts, D. D. Defining conditions for the co-culture of Caco-2 and HT29-MTX cells using Taguchi design. *J. Pharmacol. Toxicol. Methods* **61**, 334–342 (2010).
61. Béduneau, A. *et al.* A tunable Caco-2/HT29-MTX co-culture model mimicking variable permeabilities of the human intestine obtained by an original seeding procedure. *Eur. J. Pharm. Biopharm.* **87**, 290–298 (2014).
62. Hilgendorf, C. *et al.* Caco-2 versus Caco-2/HT29-MTX Co-cultured Cell Lines: Permeabilities Via Diffusion, Inside- and Outside-Directed Carrier-Mediated Transport. *J. Pharm. Sci.* **89**, 63–75 (2000).

63. Tanoue, T., Nishitani, Y., Kanazawa, K., Hashimoto, T. & Mizuno, M. In vitro model to estimate gut inflammation using co-cultured Caco-2 and RAW264.7 cells. *Biochem. Biophys. Res. Commun.* **374**, 565–569 (2008).
64. Zoumpopoulou, G., Tsakalidou, E., Dewulf, J., Pot, B. & Grangette, C. Differential crosstalk between epithelial cells, dendritic cells and bacteria in a co-culture model. *Int. J. Food Microbiol.* **131**, 40–51 (2009).
65. Sawai, T., Goldstone, N., Drongowski, R. A., Coran, A. G. & Harmon, C. M. Effect of secretory immunoglobulin A on bacterial translocation in an enterocyte-lymphocyte co-culture model. *Pediatr. Surg. Int.* **17**, 275–279 (2001).
66. Seltana, A., Basora, N. & Beaulieu, J.-F. Intestinal epithelial wound healing assay in an epithelial-mesenchymal co-culture system. *Wound Repair Regen.* **18**, 114–122 (2010).
67. SATSU, H., YOKOYAMA, T., OGAWA, N., FUJIWARA-HATANO, Y. & SHIMIZU, M. Effect of Neuronal PC12 Cells on the Functional Properties of Intestinal Epithelial Caco-2 Cells. *Biosci. Biotechnol. Biochem.* **67**, 1312–1318 (2003).
68. Trapecar, M., Goropevsek, A., Gorenjak, M., Gradisnik, L. & Slak Rupnik, M. A Co-Culture Model of the Developing Small Intestine Offers New Insight in the Early Immunomodulation of Enterocytes and Macrophages by Lactobacillus spp. through STAT1 and NF-kB p65 Translocation. *PLoS One* **9**, e86297 (2014).
69. Pearce, S. C. *et al.* Intestinal in vitro and ex vivo models to study host-microbiome interactions and acute stressors. *Frontiers in Physiology* **9**, 1584 (2018).
70. Wang, Y. *et al.* A microengineered collagen scaffold for generating a polarized crypt-villus architecture of human small intestinal epithelium. *Biomaterials* **128**, 44–55 (2017).
71. Costa, J. & Ahluwalia, A. Advances and Current Challenges in Intestinal in vitro Model Engineering: A Digest. *Front. Bioeng. Biotechnol.* **7**, 144 (2019).
72. Barker, N. *et al.* Identification of stem cells in small intestine and colon by marker gene Lgr5. *Nature* **449**, 1003–1007 (2007).
73. Takahashi, K. *et al.* Induction of Pluripotent Stem Cells from Adult Human Fibroblasts by Defined Factors. *Cell* **131**, 861–872 (2007).
74. Sato, T. *et al.* Long-term expansion of epithelial organoids from human colon, adenoma, adenocarcinoma, and Barrett's epithelium. *Gastroenterology* **141**, 1762–1772 (2011).
75. Sato, T. *et al.* Single Lgr5 stem cells build crypt-villus structures in vitro without a

mesenchymal niche. *Nature* **459**, 262–265 (2009).

76. Finkbeiner, S. R. *et al.* Generation of tissue-engineered small intestine using embryonic stem cell-derived human intestinal organoids. *Biol. Open* **4**, 1462–1472 (2015).
77. Sung, J. H., Yu, J., Luo, D., Shuler, M. L. & March, J. C. Microscale 3-D hydrogel scaffold for biomimetic gastrointestinal (GI) tract model. *Lab Chip* **11**, 389–392 (2011).
78. Spence, J. R. *et al.* Directed differentiation of human pluripotent stem cells into intestinal tissue in vitro. *Nature* **470**, 105–109 (2011).
79. Barker, N. *et al.* Lgr5+ve Stem Cells Drive Self-Renewal in the Stomach and Build Long-Lived Gastric Units In Vitro. *Cell Stem Cell* **6**, 25–36 (2010).
80. Leslie, J. L. *et al.* Persistence and toxin production by Clostridium difficile within human intestinal organoids result in disruption of epithelial paracellular barrier function. *Infect. Immun.* **83**, 138–145 (2015).
81. Wilson, S. S., Tocchi, A., Holly, M. K., Parks, W. C. & Smith, J. G. A small intestinal organoid model of non-invasive enteric pathogen-epithelial cell interactions. *Mucosal Immunol.* **8**, 352–361 (2015).
82. Hill, D. R. *et al.* Bacterial colonization stimulates a complex physiological response in the immature human intestinal epithelium. *Elife* **6**, (2017).
83. Barnett, A. M., Roy, N. C., Cookson, A. L. & McNabb, W. C. Metabolism of caprine milk carbohydrates by probiotic bacteria and Caco-2:HT29–MTX epithelial co-cultures and their impact on intestinal barrier integrity. *Nutrients* **10**, (2018).
84. Puzan, M., Hosic, S., Ghio, C. & Koppes, A. Enteric Nervous System Regulation of Intestinal Stem Cell Differentiation and Epithelial Monolayer Function. *Sci. Rep.* **8**, (2018).
85. Pastuła, A. *et al.* Three-Dimensional Gastrointestinal Organoid Culture in Combination with Nerves or Fibroblasts: A Method to Characterize the Gastrointestinal Stem Cell Niche. *Stem Cells Int.* **2016**, 3710836 (2016).
86. Workman, M. J. *et al.* Engineered human pluripotent-stem-cell-derived intestinal tissues with a functional enteric nervous system. *Nat. Med.* **23**, 49–59 (2017).
87. Uchida, H. *et al.* A xenogeneic-free system generating functional human gut organoids from pluripotent stem cells. *JCI Insight* **2**, e86492 (2017).
88. Fattahi, F. *et al.* Deriving human ENS lineages for cell therapy and drug discovery in

Hirschsprung disease. *Nature* **531**, 105–109 (2016).

89. Menendez, L. *et al.* Directed differentiation of human pluripotent cells to neural crest stem cells. *Nat. Protoc.* **8**, 203–212 (2013).
90. Grundmann, D., Klotz, M., Rabe, H., Glanemann, M. & Schäfer, K.-H. Isolation of high-purity myenteric plexus from adult human and mouse gastrointestinal tract. *Sci. Rep.* **5**, 9226 (2015).
91. Shah, P. *et al.* A microfluidics-based in vitro model of the gastrointestinal human-microbe interface. *Nat. Commun.* **7**, 1–15 (2016).
92. Shim, K. Y. *et al.* Microfluidic gut-on-a-chip with three-dimensional villi structure. *Biomed. Microdevices* **19**, (2017).
93. Costello, C. M. *et al.* Microscale Bioreactors for in situ characterization of GI epithelial cell physiology. *Sci. Rep.* **7**, 1–10 (2017).
94. Shin, W. *et al.* A Robust Longitudinal Co-culture of Obligate Anaerobic Gut Microbiome With Human Intestinal Epithelium in an Anoxic-Oxic Interface-on-a-Chip. *Front. Bioeng. Biotechnol.* **7**, 13 (2019).
95. Kim, H. J., Li, H., Collins, J. J. & Ingber, D. E. Contributions of microbiome and mechanical deformation to intestinal bacterial overgrowth and inflammation in a human gut-on-a-chip. *Proc. Natl. Acad. Sci. U. S. A.* **113**, E7–E15 (2016).
96. Jalili-Firoozinezhad, S. *et al.* A complex human gut microbiome cultured in an anaerobic intestine-on-a-chip. *Nat. Biomed. Eng.* **3**, 520–531 (2019).
97. Kasendra, M. *et al.* Duodenum Intestine-Chip for preclinical drug assessment in a human relevant model. *Elife* (2020). doi:10.7554/eLife.50135
98. Kim, H. J., Huh, D., Hamilton, G. & Ingber, D. E. Human gut-on-a-chip inhabited by microbial flora that experiences intestinal peristalsis-like motions and flow. *Lab Chip* **12**, 2165–2174 (2012).
99. Shin, W., Hinojosa, C. D., Ingber, D. E. & Kim, H. J. Human Intestinal Morphogenesis Controlled by Transepithelial Morphogen Gradient and Flow-Dependent Physical Cues in a Microengineered Gut-on-a-Chip. *iScience* **15**, 391–406 (2019).
100. Sontheimer-Phelps, A. *et al.* Human Colon-on-a-Chip Enables Continuous In Vitro Analysis of Colon Mucus Layer Accumulation and Physiology. *CMGH* **9**, 507–526 (2020).

101. Kasendra, M. *et al.* Development of a primary human Small Intestine-on-a-Chip using biopsy-derived organoids. *Sci. Rep.* **8**, 1–14 (2018).
102. Tan, H.-Y. *et al.* A multi-chamber microfluidic intestinal barrier model using Caco-2 cells for drug transport studies. *PLoS One* **13**, e0197101 (2018).
103. van der Helm, M. W. *et al.* Non-invasive sensing of transepithelial barrier function and tissue differentiation in organs-on-chips using impedance spectroscopy. *Lab Chip* **19**, 452–463 (2019).
104. Ramme, A. P. *et al.* Autologous induced pluripotent stem cell-derived four-organ-chip. *Futur. Sci. OA* **5**, (2019).
105. Chen, Y. *et al.* Robust bioengineered 3D functional human intestinal epithelium. *Sci. Rep.* **5**, 1–11 (2015).
106. Chen, Y., Zhou, W., Roh, T., Estes, M. K. & Kaplan, D. L. In vitro enteroid-derived three-dimensional tissue model of human small intestinal epithelium with innate immune responses. *PLoS One* **12**, e0187880 (2017).
107. Manousiouthakis, E. *et al.* Bioengineered in vitro enteric nervous system. *J. Tissue Eng. Regen. Med.* **13**, 1712–1723 (2019).
108. Raimondi, M. T., Albani, D. & Giordano, C. An Organ-On-A-Chip Engineered Platform to Study the Microbiota–Gut–Brain Axis in Neurodegeneration. *Trends in Molecular Medicine* **25**, 737–740 (2019).
109. Huh, D. *et al.* Reconstituting organ-level lung functions on a chip. *Science (80-.).* **328**, 1662–1668 (2010).
110. Technology — Emulate. Available at: https://www.emulatebio.com/our-technology#chip-s1. (Accessed: 5th June 2020)
111. Quirós-Solano, W. F. *et al.* Microfabricated tuneable and transferable porous PDMS membranes for Organs-on-Chips. *Sci. Rep.* **8**, 1–11 (2018).
112. Bračič, M. *et al.* Preparation of PDMS ultrathin films and patterned surface modification with cellulose. *RSC Adv.* **4**, 11955–11961 (2014).
113. Carter, R. N. *et al.* Ultrathin transparent membranes for cellular barrier and co-culture models. *Biofabrication* **9**, 015019 (2017).
114. Salminen, A. T. *et al.* Ultrathin Dual-Scale Nano- and Microporous Membranes for Vascular Transmigration Models. *Small* **15**, 1804111 (2019).

115. Gillis, K. D., Liu, X. A., Marcantoni, A. & Carabelli, V. Electrochemical measurement of quantal exocytosis using microchips. *Pflugers Archiv European Journal of Physiology* **470**, 97–112 (2018).
116. Wong, J. F., Mohan, M. D., Young, E. W. K. & Simmons, C. A. Integrated electrochemical measurement of endothelial permeability in a 3D hydrogel-based microfluidic vascular model. *Biosens. Bioelectron.* **147**, 111757 (2020).
117. Jung, K. B. *et al.* Interleukin-2 induces the in vitro maturation of human pluripotent stem cell-derived intestinal organoids. *Nat. Commun.* **9**, 3039 (2018).
118. Freire, R. *et al.* Human gut derived-organoids provide model to study gluten response and effects of microbiota-derived molecules in celiac disease. *Sci. Rep.* **9**, (2019).
119. Montenegro-Miranda, P. S. *et al.* A Novel Organoid Model of Damage and Repair Identifies HNF4α as a Critical Regulator of Intestinal Epithelial Regeneration. *Cell. Mol. Gastroenterol. Hepatol.* (2020). doi:10.1016/j.jcmgh.2020.02.007
120. Francisco-Cruz, A., Parra, E. R., Tetzlaff, M. T. & Wistuba, I. I. Multiplex Immunofluorescence Assays. in *Methods in Molecular Biology* **2055**, 467–495 (Humana Press Inc., 2020).
121. Lee, C. W. *et al.* Multiplex immunofluorescence staining and image analysis assay for diffuse large B cell lymphoma. *J. Immunol. Methods* **478**, 112714 (2020).
122. Rapaport, F. *et al.* Comprehensive evaluation of differential gene expression analysis methods for RNA-seq data. *Genome Biol.* **14**, R95 (2013).
123. Henderson, P., Van Limbergen, J. E., Schwarze, J. & Wilson, D. C. Function of the intestinal epithelium and its dysregulation in inflammatory bowel disease. *Inflammatory Bowel Diseases* **17**, 382–395 (2011).
124. Ma, T. Y., Nighot, P. & Al-Sadi, R. Tight Junctions and the Intestinal Barrier. in *Physiology of the Gastrointestinal Tract: Sixth Edition* **1**–**2**, 587–639 (Elsevier Inc., 2018).
125. Arlk, Y. B. *et al.* Barriers-on-chips: Measurement of barrier function of tissues in organs-on-chips. *Biomicrofluidics* **12**, 042218 (2018).
126. Cakir, B. *et al.* Engineering of human brain organoids with a functional vascular-like system. *Nat. Methods* **16**, 1169–1175 (2019).
127. Henry, O. Y. F. *et al.* Organs-on-chips with integrated electrodes for trans-epithelial

electrical resistance (TEER) measurements of human epithelial barrier function. *Lab Chip* **17**, 2264–2271 (2017).

128. Ménard, S., Cerf-Bensussan, N. & Heyman, M. Multiple facets of intestinal permeability and epithelial handling of dietary antigens. *Mucosal Immunology* **3**, 247–259 (2010).
129. Chang-Graham, A. L. *et al.* Human Intestinal Enteroids With Inducible Neurogenin-3 Expression as a Novel Model of Gut Hormone Secretion. *Cell. Mol. Gastroenterol. Hepatol.* **8**, 209–229 (2019).
130. Noel, G. *et al.* A primary human macrophage-enteroid co-culture model to investigate mucosal gut physiology and host-pathogen interactions. *Sci. Rep.* **7**, 1–14 (2017).
131. Beaurivage, C. *et al.* Development of a gut-on-a-chip model for high throughput disease modeling and drug discovery. *Int. J. Mol. Sci.* **20**, (2019).
132. Kim, G. A., Ginga, N. J. & Takayama, S. Integration of Sensors in Gastrointestinal Organoid Culture for Biological Analysis. *CMGH* **6**, 123-131.e1 (2018).
133. Schroeder, B. O. Fight them or feed them: how the intestinal mucus layer manages the gut microbiota. *Gastroenterol. Rep.* **7**, 3–12 (2019).
134. He, J., Guo, H., Zheng, W. & Yao, W. Effects of Stress on the Mucus-microbial Interactions in the Gut. *Curr. Protein Pept. Sci.* **20**, 155–163 (2018).
135. Capeling, M. M. *et al.* Nonadhesive Alginate Hydrogels Support Growth of Pluripotent Stem Cell-Derived Intestinal Organoids. *Stem Cell Reports* **12**, 381–394 (2019).
136. Altay, G. *et al.* Self-organized intestinal epithelial monolayers in crypt and villus-like domains show effective barrier function. *Sci. Rep.* **9**, 1–14 (2019).
137. HASNAIN, S. Z., THORNTON, D. J. & GRENCIS, R. K. Changes in the mucosal barrier during acute and chronic Trichuris muris infection. *Parasite Immunol.* **33**, 45–55 (2011).
138. Dohrman, A. *et al.* Mucin gene (MUC 2 and MUC 5AC) upregulation by Gram-positive and Gram-negative bacteria. *Biochim. Biophys. Acta - Mol. Basis Dis.* **1406**, 251–259 (1998).
139. Bai, L. *et al.* Genetic Identification of Vagal Sensory Neurons That Control Feeding. *Cell* **179**, 1129-1143.e23 (2019).
140. Pradhananga, S., Tashtush, A. A., Allen-Vercoe, E., Petrof, E. O. & Lomax, A. E. Protease-dependent excitation of nodose ganglion neurons by commensal gut bacteria. *J. Physiol.* JP279075 (2020). doi:10.1113/JP279075

141. Hasan, M. & Berdichevsky, Y. Neural Circuits on a Chip. *Micromachines* **7**, 157 (2016).
142. Kuru, E., Tekkam, S., Hall, E., Brun, Y. V. & Van Nieuwenhze, M. S. Synthesis of fluorescent D-amino acids and their use for probing peptidoglycan synthesis and bacterial growth in situ. *Nat. Protoc.* **10**, 33–52 (2015).
143. Bascomb, S. & Manafi, M. Use of enzyme tests in characterization and identification of aerobic and facultatively anaerobic gram-positive cocci. *Clinical Microbiology Reviews* **11**, 318–340 (1998).
144. Zachos, N. C. *et al.* Human enteroids/colonoids and intestinal organoids functionally recapitulate normal intestinal physiology and pathophysiology. *Journal of Biological Chemistry* **291**, 3759–3766 (2016).
145. Han, J. & Burgess, K. Fluorescent indicators for intracellular pH. *Chem. Rev.* **110**, 2709–2728 (2010).
146. Wencel, D., Abel, T. & McDonagh, C. Optical chemical pH sensors. *Analytical Chemistry* **86**, 15–29 (2014).
147. Bas, T. & Augenlicht, L. H. Real time analysis of metabolic profile in Ex vivo mouse intestinal crypt organoid cultures. *J. Vis. Exp.* e52026 (2014). doi:10.3791/52026
148. Zakharova, M. *et al.* Multiplexed blood-brain barrier organ-on-chip. *Lab Chip* **20**, 3132–3143 (2020).
149. Gaver, D. P. & Kute, S. M. A theoretical model study of the influence of fluid stresses on a cell adhering to a microchannel wall. *Biophys. J.* **75**, 721–733 (1998).
150. Kihara, T., Ito, J. & Miyake, J. Measurement of Biomolecular Diffusion in Extracellular Matrix Condensed by Fibroblasts Using Fluorescence Correlation Spectroscopy. *PLoS One* **8**, e82382 (2013).
151. Zhuang, G. & Kutter, J. P. Anti-stiction coating of PDMS moulds for rapid microchannel fabrication by double replica moulding. *J. MICROMECHANICS MICROENGINEERING J. Micromech. Microeng* **21**, 105020–105026 (2011).
152. Zhao, Y. Stiction and anti-stiction in MEMS and NEMS. *Acta Mech. Sin. Xuebao* **19**, 1–10 (2003).
153. Shyamala, K., Yanduri, S., Girish, H. C. & Murgod, S. Neural crest: The fourth germ layer. *J. Oral Maxillofac. Pathol.* **19**, 221–229 (2015).
154. Barber, K., Studer, L. & Fattahi, F. Derivation of enteric neuron lineages from human

pluripotent stem cells. *Nat. Protoc.* **14**, 1261–1279 (2019).

155. Chen, G. *et al.* Chemically defined conditions for human iPSC derivation and culture. *Nat. Methods* **8**, 424–429 (2011).
156. Li, W. *et al.* Characterization and transplantation of enteric neural crest cells from human induced pluripotent stem cells. *Mol. Psychiatry* **23**, 499–508 (2018).
157. Bernd, P. Appearance of nerve growth factor receptors on cultured neural crest cells. *Dev. Biol.* **112**, 145–156 (1985).
158. Huang, M. *et al.* Generating trunk neural crest from human pluripotent stem cells. *Sci. Rep.* **6**, 1–9 (2016).
159. Menendez, L., Yatskievych, T. A., Antin, P. B. & Dalton, S. Wnt signaling and a Smad pathway blockade direct the differentiation of human pluripotent stem cells to multipotent neural crest cells. *Proc. Natl. Acad. Sci. U. S. A.* **108**, 19240–19245 (2011).
160. Heppt, M. V. *et al.* MSX1-Induced Neural Crest-Like Reprogramming Promotes Melanoma Progression. *J. Invest. Dermatol.* **138**, 141–149 (2018).
161. Binder, E. *et al.* Enteric Neurospheres Are Not Specific to Neural Crest Cultures: Implications for Neural Stem Cell Therapies. *PLoS One* **10**, e0119467 (2015).

Appendix

Table 1. Markers for various cell phenotypes

Cell type	Gene	Specific function/subtype
Pluripotent stem cells	OCT-4 NANOG	
Intestinal stem cells	LGR5 OLFM4	
	Sox2 PDX1	Foregut
	Sox9 CDX2	Hindgut
Enterocytes	OCLN ZO-1 CLDN1 CDH1	Tight junction
	f-actin VIL1 EZR	Intestinal brush border
	PEPT1 MDR1 SLC2A2 SLC5A1	Intestinal transporter
	LYZ DEFA5 MMP7	Paneth cells
	MUC2 MUC5 TFF-3 TFF-1	Goblet cells
	NGN3 CHGA GLP-1R PYY GAST GHRL	Enteroendocrine cells

	GIP SCT MLN CCK THP1	
Neural crest cells	p75 HNK1 SOX10 EDNRB	
	TRKC PHOXB2 HOXB2-5	Vagal neural crest
Neurons	HuC/D TUBB3 MAP2 5-HT NOS GABA ChAT	 Immature neuron Mature Neuron Serotoninergic neuron Nitric oxide producing neuron Gabaergic Cholinergic neuron
Glia	GFAP S100β IBA-1	

The compilation of genes shown in this table was obtained from references [39,79,84,86,88,90,117].

Figure 1. Detailed schematics for "rough" MGBA chip.

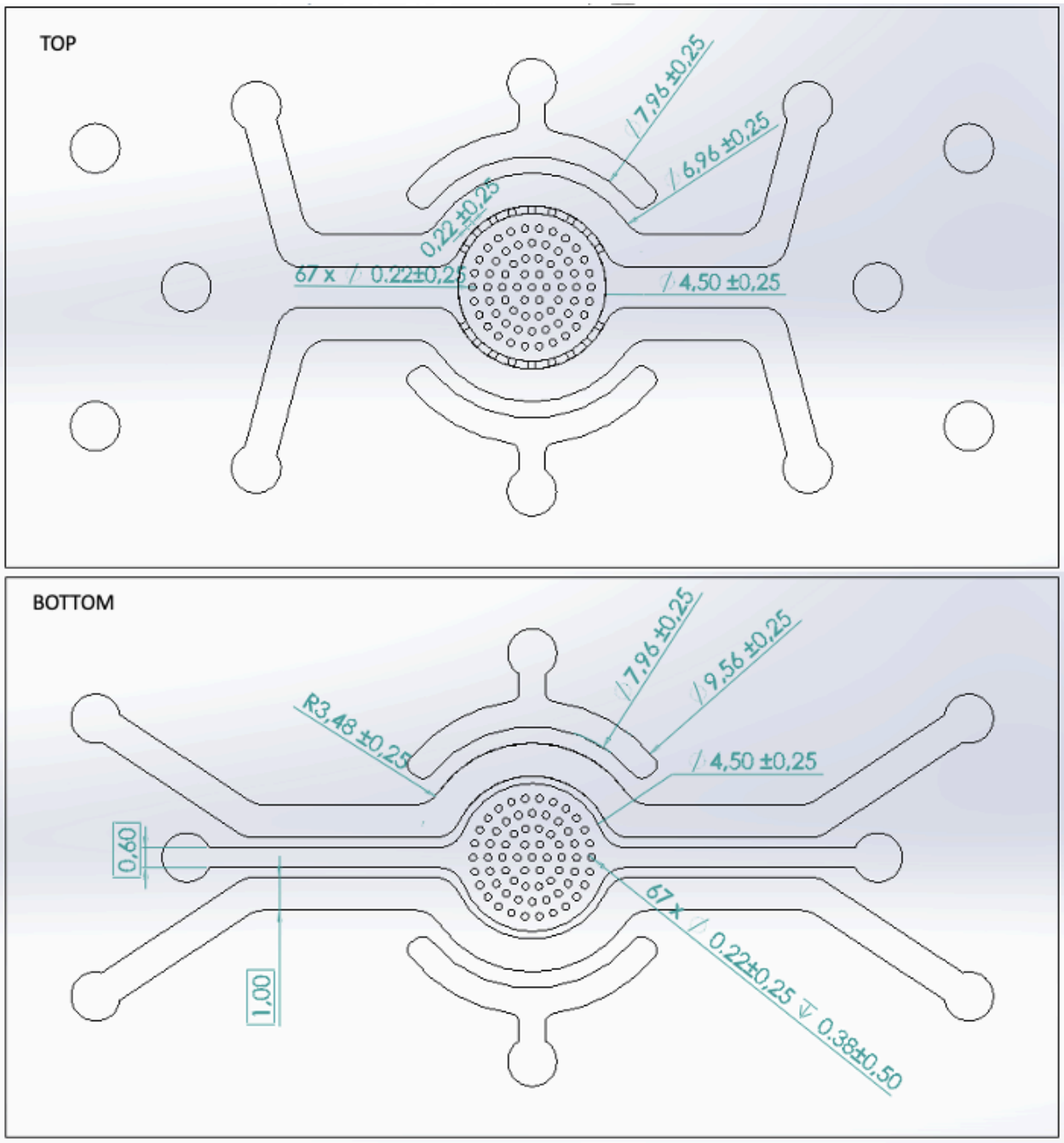

Figure 2. Detailed schematics for clean room fabricated MGBA chip.

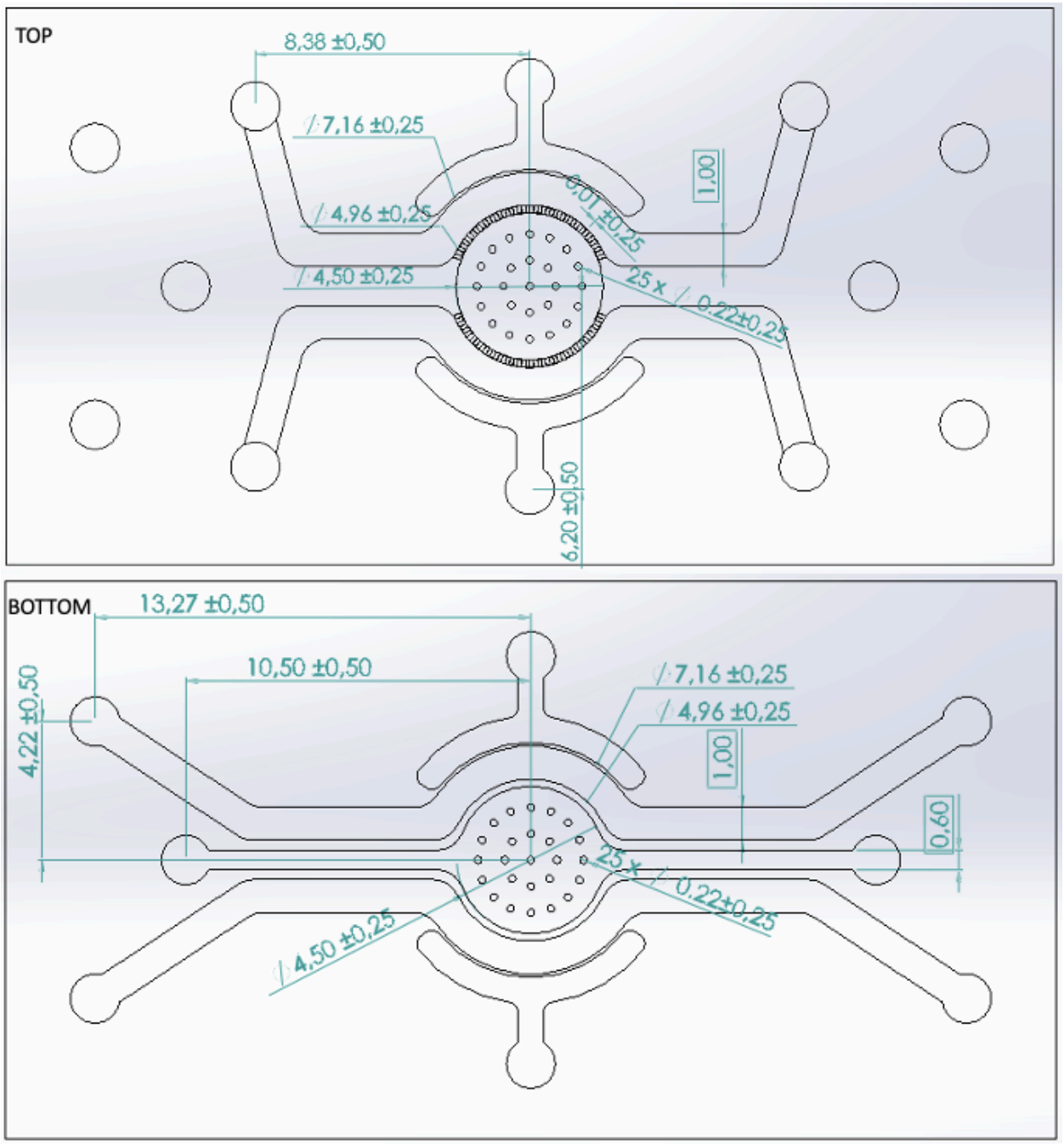

Figure 3. Zoomed-out view of the mechanical deformation test on clean room fabricated MGBA chip.

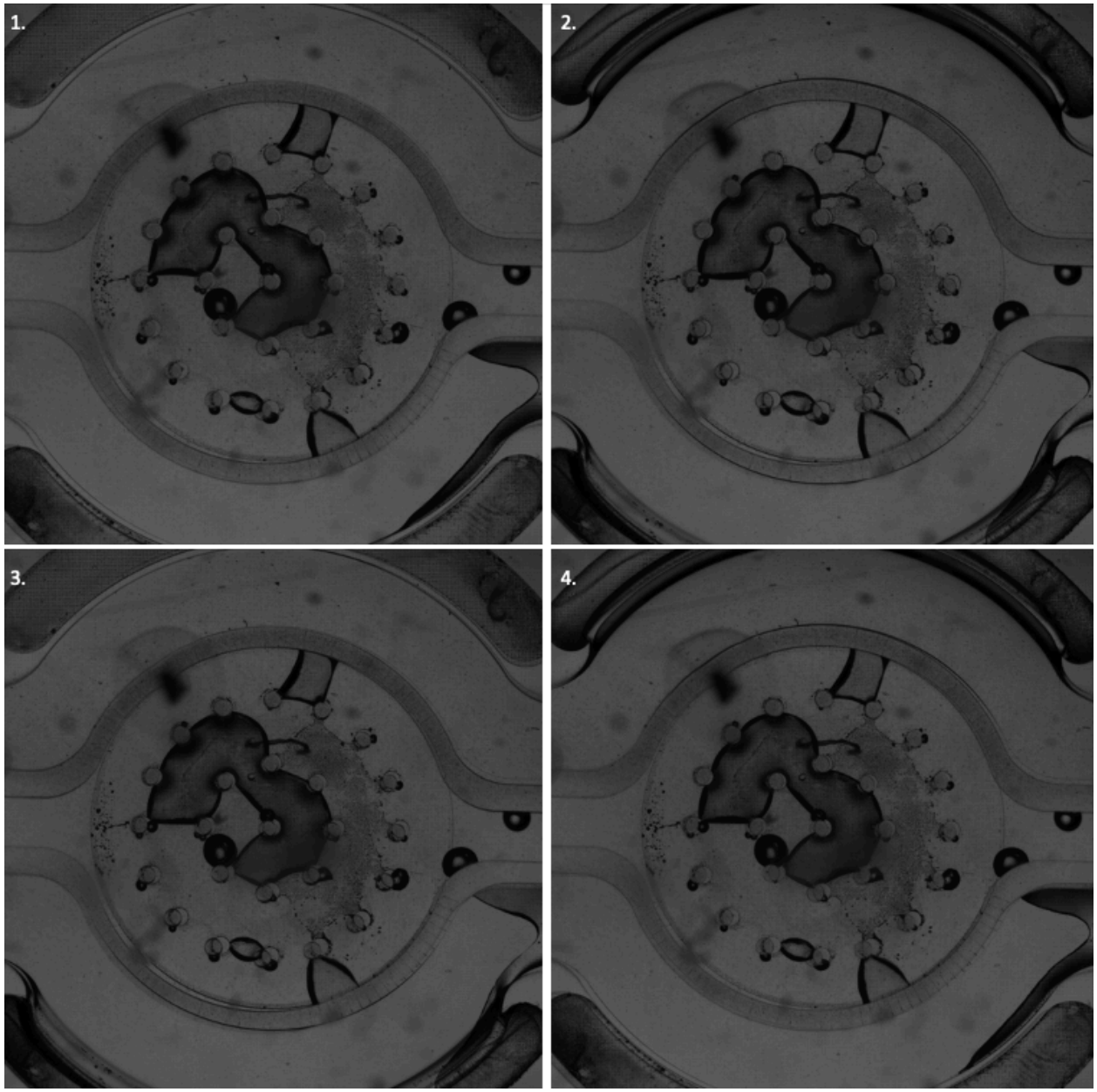

Mechanical deformation test on clean room fabricated MGBA chip. **1**. View of the chip without any vacuum chamber activated. **2**.View of the chip with both vacuum chambers activated, a stretching of the membrane on both sides can be observed. **3.** View of the chip with the bottom vacuum chamber activated. **4.** View of the chip with the top vacuum chamber activated.

Table 2. Primary and secondary antibodies used for immunofluorescent staining.

Primary antibody	**Catalog number**	**Source**	**host**	**dillution**
Nestin	MAB1259	R&D systems	mouse	1:500
β-III tubulin	sc-80005	Santa cruz	mouse	1:500
MAP2	ab32454	Abcam	rabbit	1:500
Synapsin 1/2	106004	Synaptic systems	guinea pig	1:500
GFAP	-	BIOS	mouse	1:200
HNK1 (anti CD57)	359614	Biolegend	mouse	1:200
p75 (CD271(	345106	Biolegend	mouse	1:200
Secondary antibody	**Catalog number**	**Source**	**Dillution**	
Goat anti mouse-488	A11001	Invitrogen	1:1000	
Goat anti rabbit-647	A21244	Invitrogen	1:1000	

Figure 4. Additional flow cytometry analysis results of cells at D12 of NC induction.

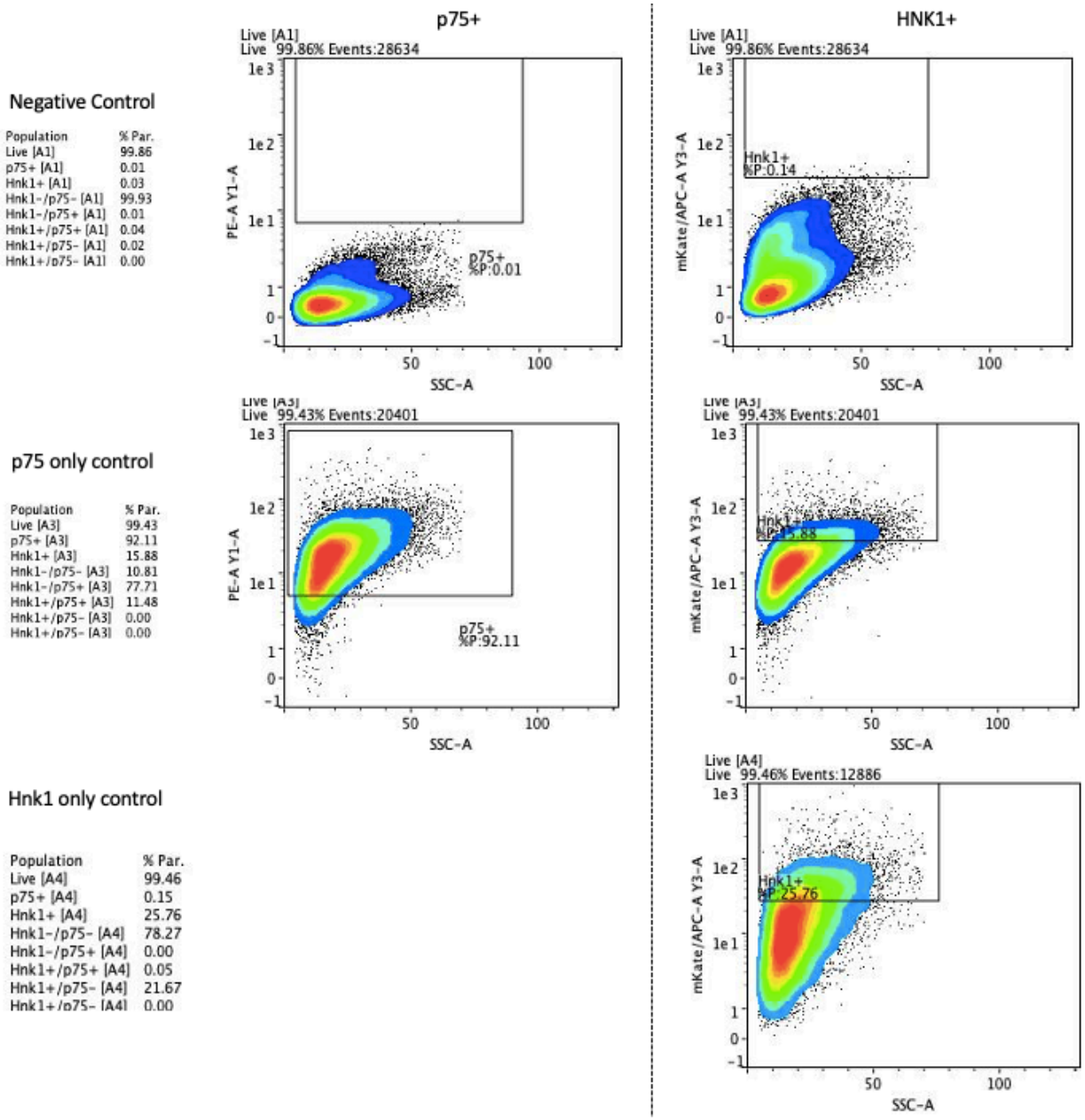

Different controls for HNK1/p75 flow cytometry analysis. Negative control shows a clear lack of signal for p75 laser however there is a wider signal distribution for the HNK1 laser. Control stained with only p75 antibody shows a population of ~90% positively stained cells however there is some signal detected in the HNK1 laser given that 15.88% appear as HNK1 positive. Control stained with only HNK1 antibody shows a very small population of cells (25%) that were stained with HNK1.

Figure 5. Comparison of flow cytometry results after 40 min and overnight incubation.

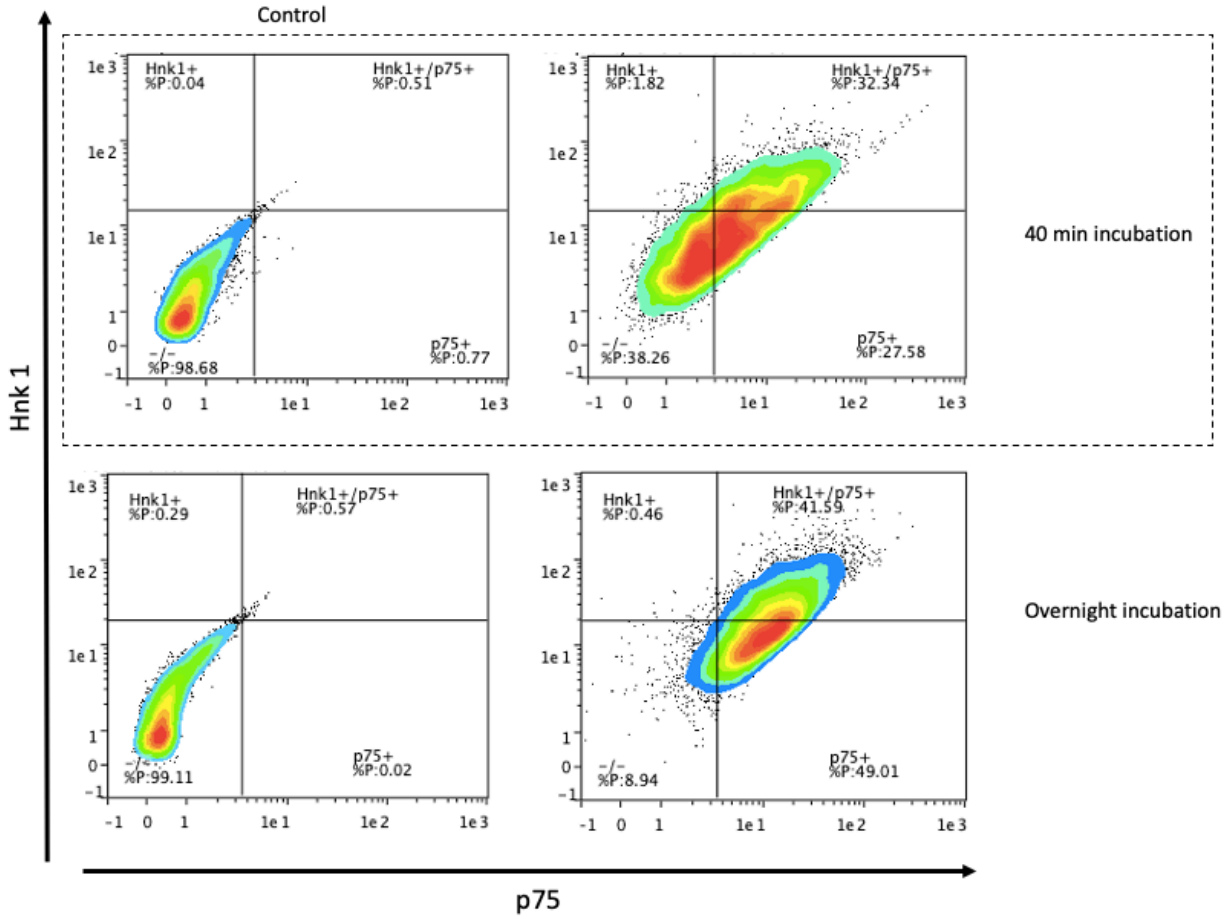

At induction day 12 cells were dissociated and stained with p75 and HNK1 fluorescently conjugated antibodies. Samples were incubated at 4ºC for either 40 min or over night. Samples that were incubated overnight had a 41.5% HNK1/p75 double positive population while those incubated for 40 min had a 32.3% HNK1/p75 double positive population.

Figure 6. Preliminary results of neuron integration into chips.

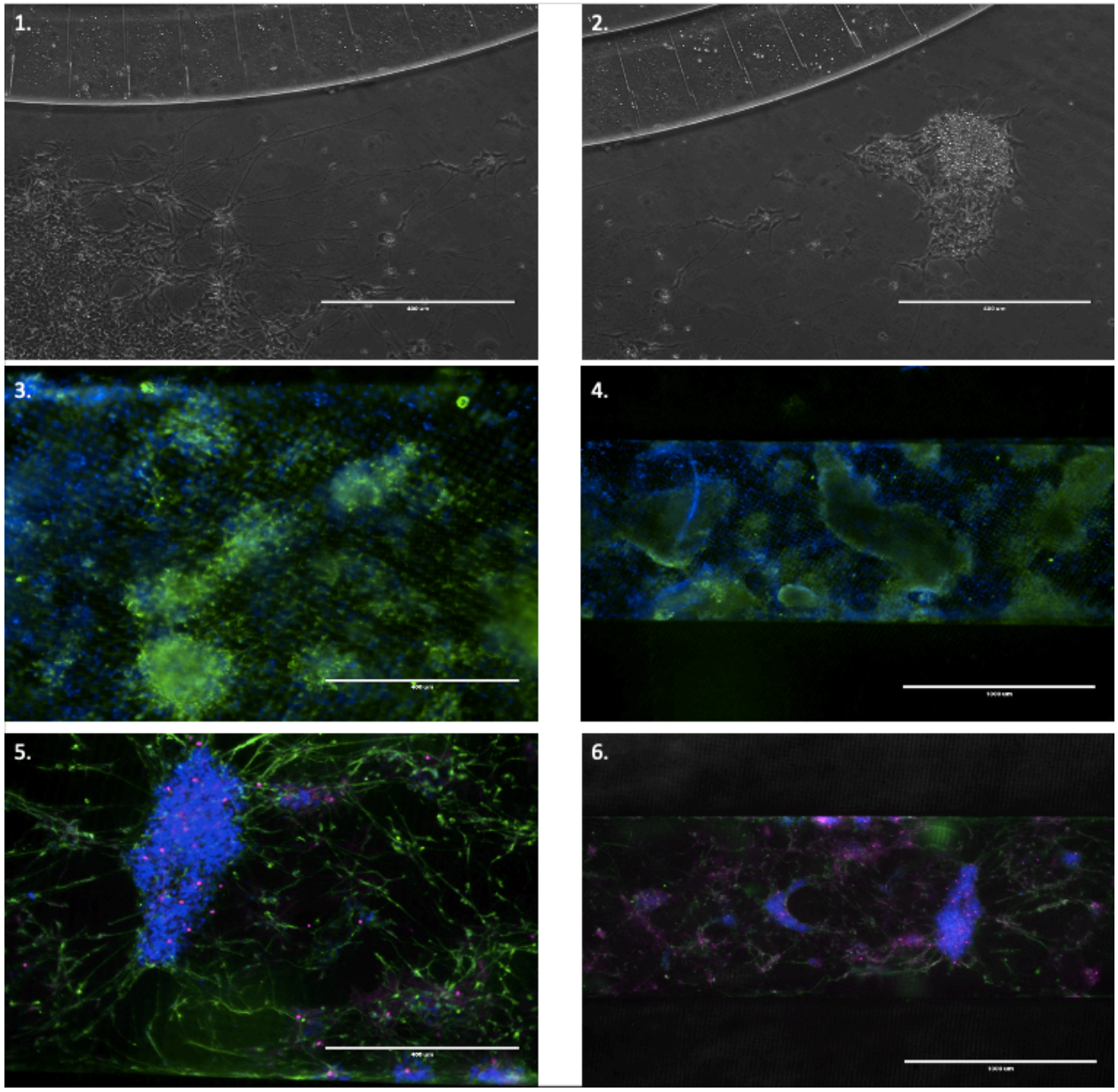

1. and **2.** ENS-derived neurons after 5 days of maturation on the glass-bonded top layer of the MGBA chip. Scale bar 400µm. **3.** and **4.** ENS-derived neurons stained with Nestin (green) after 10 days of maturation on a two-channel PDMS chip. Scale bar 400µm (3.) and 1,000µm (4.)
5. and **6.** ENS-derived neurons stained with β-III tubulin (green), and Phalloidin (magenta) after 10 days of maturation on a two-channel PDMS chip. Scale bar 400µm (5.) and 1,000µm (6.).